Méthodes d'identification approchée de cibles sondées par ondes impulsives

Armand Wirgin

METHODES D'IDENTIFICATION APPROCHEE DE CIBLES SONDEES PAR ONDES IMPULSIVES [1]

Armand Wirgin [2]

October 22, 2005

[1]Course of the Ecole d'Eté, sponsored by the GDR ONDES, entitled *Méthodologies de l'Inversion des Ondes et Modèles Directs*, given at SUPELEC, Gif/Yvette on 7 September 2005.

[2]Laboratoire de Mécanique et d'Acoustique, UPR 7051 du CNRS, 31 chemin Joseph Aiguier, 13009 Marseille, France, wirgin@lma.cnrs-mrs.fr.

Contents

Chapter 1

General Introduction

1.1 Traitement approché des problèmes directs et inverses

L'identification d'une cible (i.e., milieu ou ensemble de milieux, objet ou ensemble d'objets homogène ou hétérogène) signifie: trouver sa position, et/ou orientation, et/ou taille, et/ou forme et/ou composition. En 3D, la position comporte trois paramètres, l'orientation deux paramètres de plus, la taille trois paramètres de plus, et la composition encore au moins trois paramètres ou fonctions (e.g., densité, parties réelle et imaginaire de l'indice de réfraction). Enfin, la description de la forme peut nécessiter un nombre important (i.e., au moins une douzaine en 3D) de paramètres.

Nous supposons que l'identification se fera par traitement de l'information contenue dans la réponse de la cible à une (des) onde(s). La quantité d'information nécessaire pour réussir l'identification est d'autant plus grande que les paramètres à rechercher sont plus nombreux. On a donc intérêt, notamment dans les cas où, pour des raisons de temps d'acquisition courts (e.g., cas d'un diagnostic médical) et d'accessibilité limitée (e.g., cas où la cible ne peut être sondée que dans un secteur angulaire restreint), à disposer du maximum

d'information a priori sur quelques-uns, ou sur la totalité, des paramètres à identifier. Il faut, même dans le cas où le temps d'acquisition des données et l'accessibilité de la cible à l'onde de sondage ne posent pas de problèmes, disposer d'autant que possible d'information a priori afin de rendre stable et unique la solution du problème inverse.

L'information a priori sur la cible est généralement moins précise et moins complète que l'information que l'on essaie de récupérer par traitement des données, sinon point besoin de résoudre le problème inverse (toutefois, le cas où l'on peut se contenter d'une solution très approchée du problème inverse est assez courant puisque l'on n'a pas toujours besoin d'identifier précisément la cible).

Disposer d'information a priori peut requérir la résolution de manière approchée du problème inverse de départ, ou d'un problème inverse quelque peu similaire au problème inverse de départ. Il est même courant que la résolution plus précise d'un problème inverse se fasse par une méthode reposant sur l'emploi d'une solution initiale assez imprécise, laquelle solution est affinée itérativement.

Ce cours est dédié à l'obtention de ces solutions approchées, lesquelles ont pour fonction de servir, soit de solution tout court du problème inverse, soit de solution initiale dans une méthode itérative, soit de source d'information pour une régularisation rationnelle.

Le sondage se fait par l'envoi d'une ou plusieurs ondes sur la cible ; nous supposons disposer d'un générateur d'impulsions, de sorte que le signal pour chacune des ondes, couvre une assez large bande pas-

sante dans le domaine fréquentiel. Les sources sont supposées proches (cas d'onde cylindrique ou sphérique incidentes) ou très distantes (cas d'ondes plane incidente) de la cible.

Nous supposons que l'acquisition du champ sonore diffracté se fait, soit en zone proche, soit en zone lointaine, i.e., les capteurs sont proches ou distantes de la cible.

Les solutions approchées du problème inverse seront obtenues (parfois simultanément) dans les cadres simplifiés suivants :

- problème 3D traité comme un problème 2D ;
- acoustique ou viscoacoustique, i.e., lorsque les vitesses des ondes de cisaillement dans les milieux sont très basses (ce cadre trouve son équivalent dans certaines configurations impliquant des ondes électromagnétiques);
- densité (ou perméabilité) constante, i.e., la densité de la cible est égale à celle du milieu-hôte et est partout constant ;
- milieux hétérogènes traités comme des milieux homogénéisés ;
- basses fréquences, i.e., lorsque la (ou les) dimension(s) caractéristique(s) de la cible est(sont) très inférieure(s) à la longueur d'onde dans le milieu-hôte ou dans la cible;
- hautes fréquences, i.e., lorsque la (ou les) dimension(s) caractéristique(s) de la cible est(sont) très supérieure(s) à la longueur d'onde dans le milieu-hôte ou dans la cible;
- faible contraste des célérités, i.e., le rapport entre la célérité

moyenne du milieu remplissant la cible et la célérité du milieu-hôte est voisin de 1 ;

- faible écart de forme par rapport à une forme canonique, i.e., la forme de la cible est proche de celle e.g., d'un plan ou d'un cylindre circulaire.

Ainsi, seront examinés les méthodes d'identification suivantes :

1. la méthode de séries de Born faisant appel à différentes fonctions de Green;
2. la méthode de Rayleigh ;
3. la méthode de perturbation pour des faibles écarts de forme ;
4. la méthode basses/hautes fréquences pour des cibles de forme presque canonique ;
5. la méthode ICBA.

Des références utiles: [1], [2], [3], [4], [5], [6], [7] [8], [9].

1.2 Formes opérationnelles des problèmes directs

Les trois problèmes directs (tout est connu a priori [1] sauf le champ acoustique) sous-jacents aux problèmes inverses que nous allons aborder dans ce cours sont: i) la prédiction du champ rayonné par une source , ii) la prédiction du champ diffracté par un objet (région borné ou non borné d'un milieu que nous chercherons à caractériser et que nous pouvons appeler "cible"), lequel champ est supposé exister au

[1] le matériau de l'objet est généralement hétérogène aux échelles microscopique, mésoscopique, et macroscopique, et n'est pas, de ce fait réellement "connu"; en ce cas, il faut résoudre un problème inverse (de caractérisation matérielle) avant d'attaquer le problème direct, et mieux vaut le faire sur une éprouvette de forme standard (e.g., plaque ou barreau).

sein et/ou sur l'objet, iii) la prédiction de la propagation du champ depuis l'objet jusqu'au lieu où est mesuré le champ (figs. 1.2.1, 1.2.2, 1.2.3).

Les différentes étapes que nous venons d'évoquer se mettent sous forme d'équations opérationnelles que nous appelons: équation de rayonnement **c=Ks**, équation de diffraction **Ea=c**, et équation de propagation **Ha=d**, dans lesquelles **c** est lié au champ rayonné, **K** un opérateur intégrant les paramètres géométriques du domaine dans lequel on cherche à résoudre le problème ainsi que les paramètres physiques du milieu remplissant ce domaine (hormis ceux de l'objet), **s** lié à la densité de sources, **a** lié au champ diffracté, **d** lié au champ propagé (le symbole **d** provient du fait qu'il désignera les données du problème inverse), **E** et **H** des opérateurs intégrant à la fois : i) les paramètres géométriques et physiques du domaine et milieu hors de l'objet et ii) le domaine et milieu de l'objet (figs. 1.3.1-1.3.2).

S'agissant du problème direct du rayonnement seul, **s** et **K** étant connus, on obtient **c** par un simple produit opérationnel. S'agissant d'un problème direct de rayonnement suivi de diffraction et propagation, la marche à suivre est (dans l'ordre) : i) trouver **c** de **c=Ks**, ii) trouver **a** de **Ea=c**, iii) trouver **d** de **Ha=d** ou, si l'on préfère (en termes formelles) : trouver **d** de $\mathbf{d} = \mathbf{H}\mathbf{E}^{-1}\mathbf{K}\mathbf{s}$, ce qui montre, en passant, qu'il y a une similarité formelle entre le problème direct de rayonnement et le problème direct de rayonnement/diffraction/propagation puisque $\mathbf{d} = (\mathbf{H}\mathbf{E}^{-1}\mathbf{K})\mathbf{s}$ est de la même forme que **c=Ks**.

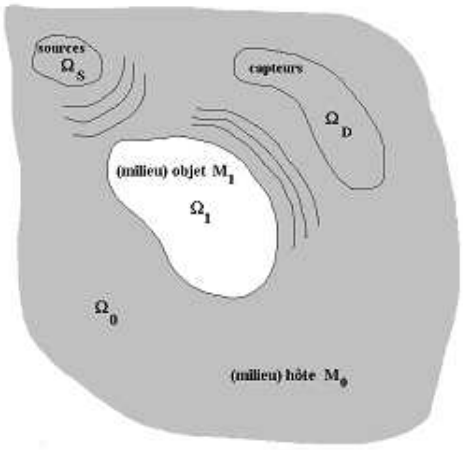

Figure 1.2.1: Rayonnement par une source, suivi de diffraction par une cible compacte, et propagation vers les capteurs.

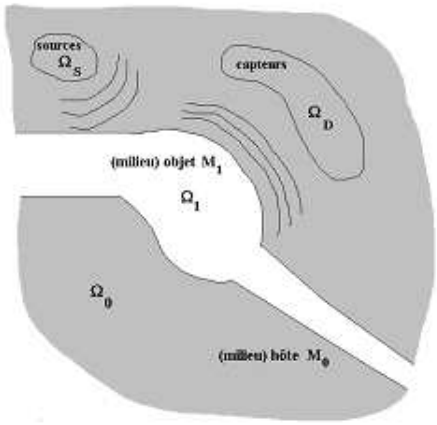

Figure 1.2.2: Rayonnement par une source, suivi de diffraction par une cible non-compacte, et propagation vers les capteurs.

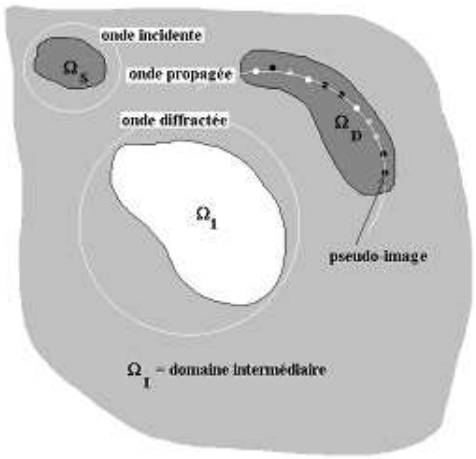

Figure 1.2.3: Rayonnement par une source, suivi de diffraction par une cible, et propagation vers les capteurs. Le champ, ou quelque chose le ressemblant, au niveau des capteurs, constitue la *pseudo image* de la source et/ou de la cible.

Ce qu'il importe de souligner, c'est que **c=Ks** est linéaire en termes de l'inconnue **c**, **Ea=c** est linéaire en termes de l'inconnue **a**, et **Ha=d** est linéaire en termes de l'inconnue **d**. On peut donc dire que les problèmes directs (e.g., de l'acoustique linéaire) sont linéaires. De plus, dans presque tous les cas, ils sont bien posés en ce sens que l'existence d'au moins une solution est assurée, cette solution est unique, et des petites perturbations sur **K, E, H**, ou **s** n'engendrent pas de gros changements dans les solutions **c**, **a** et **d**. Nous verrons plus loin que toute autre est la situation pour les problèmes inverses.

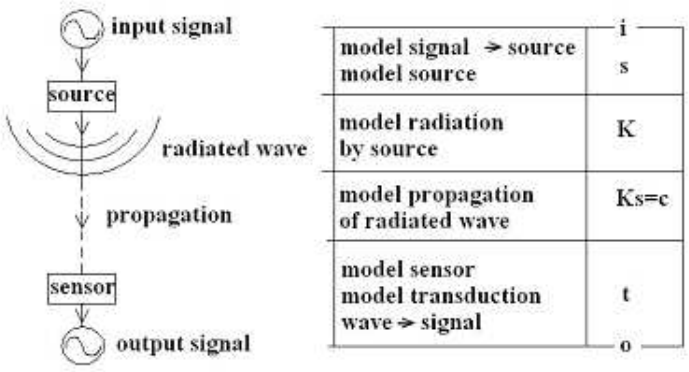

Figure 1.3.1: Rayonnement par une source.

1.3 Formes opérationnelles des problèmes inverses

Le problème inverse de sources est de déterminer **s** à partir de l'équation **c=Ks** (que nous appelons: équation de rayonnement inverse) sous l'hypothèse que l'on connaît **K** et **c**. Formellement, il semblerait que le problème soit du même type que celui de déterminer **a** à partir de **Ea=c** dans le contexte des problèmes directs. Ceci n'est généralement pas vrai car le support de **s** et **c** sont disjoints dans le problème inverse de sources alors que le support de **a** et **c** sont identiques dans le problème direct de diffraction.

Ainsi le problème inverse de sources est généralement mal posé, tout en étant linéaire lorsque l'on connaît a priori le milieu dans lequel sont situées les sources puisque l'opérateur **K** ne dépend pas de l'inconnue

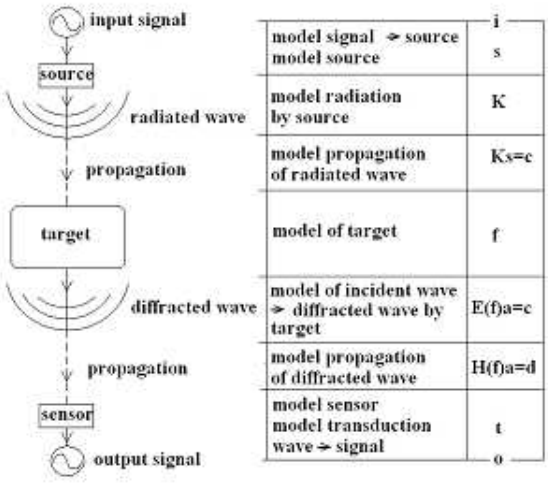

Figure 1.3.2: Rayonnement à partir de sources, et diffraction par une cible du champ rayonné, suivie de la propagation du champ diffracté vers des capteurs

$\mathbf{s}$ (nous n'abordons pas ici le problème, pourtant courant, comme en acoustique sous-marine, de détermination de $\mathbf{s}$ lorsque l'on ne connaît pas le milieu).

Le problème plus difficile est celui de la reconstruction d'un milieu-objet (supposé à support spatial borné ou non-borné et appelé "cible" à partir de maintenant) connaissant l'onde $\mathbf{c}$ (et donc le $\mathbf{s}$ dont elle est issue) qui le sollicite ainsi que le milieu qui l'entoure (dit milieu hôte). Cet objet est décrit par les paramètres de géométrie (position, orientation, forme, taille) et ses paramètres physiques (distribution spatiale de densité, vitesse, etc.) que l'on peut regrouper dans le vecteur $\mathbf{f}$. Le but est de trouver un, plusieurs, ou des combinaisons des entrées du vecteur $\mathbf{f}$ à partir des données relatifs au champ acoustique propagé $\mathbf{d}$.

Rappelons que $\mathbf{c}$ est, par hypothèse, indépendant de l'existence ou non de l'objet. Il n'en est pas de même des opérateurs $\mathbf{E}$ et $\mathbf{H}$ de sorte que $\mathbf{E}$=$\mathbf{E}(\mathbf{f})$ et $\mathbf{H}$=$\mathbf{H}(\mathbf{f})$. Les équations de diffraction et de propagation ont maintenant les formes $\mathbf{E}(\mathbf{f})\mathbf{a}(\mathbf{f})$=$\mathbf{c}$ et $\mathbf{H}(\mathbf{f})\mathbf{a}(\mathbf{f})$=$\mathbf{d}(\mathbf{f})$, équations que nous appelons, pour rappeler qu'il s'agit d'un problème inverse : équation de diffraction inverse et équation de rayonnement inverse.

Traiter le problème inverse consiste à extraire $\mathbf{f}$ de ces deux équations, qui sont non-linéaires en termes de $\mathbf{f}$. On note que $\mathbf{a}(\mathbf{f})$ est la deuxième inconnue de ces deux équations; on peut l'éliminer, lorsque $\mathbf{E}^{-1}(\mathbf{f})$ existe, en ramenant les deux équations en une seule: $\mathbf{H}(\mathbf{f})\mathbf{E}^{-1}(\mathbf{f})\mathbf{c}(\mathbf{f}) = \mathbf{d}(\mathbf{f})$. Celle-ci s'appelle l'équation de cou-

plage.

Hormis la non-linéarité des équations inverses de diffraction et de propagation, il se pose la question de l'existence, unicité et stabilité de leurs "solutions". La logique voudrait que l'on commence par traiter l'équation de propagation inverse. Du fait que les données sont généralement recueillies dans un domaine autre que celui de l'objet, chercher $\mathbf{f}$ (ou même $\mathbf{a}$) à partir de cette équation devient un problème mal posé (se traduisant numériquement par le mauvais conditionnement de l'opérateur $\mathbf{H}$). Il en sera de même pour l'équation de couplage de sorte que le problème de reconstruction de l'objet est un problème mal posé. C'est pourquoi on ne "résout" pas ce problème. Par contre, on peut tenter de le "traiter".

Dans la suite, et compte tenu de ces difficultés, on essaiera de trouver, par des approximations appropriées, une solution explicite de $\mathbf{E}(\mathbf{f})\mathbf{a}(\mathbf{f})=\mathbf{c}$ et même une expression explicite de $\mathbf{f}$.

Chapter 2

Homogénéisation électrostatique

2.1 Permittivité effective d'un ensemble de M cylindres circulaires diélectriques par la méthode de Wagner

2.1.1 Position du problème

☐ Méthode de Wagner en (1914) pour trouver la permittivité effective d'un ensemble de M cylindres circulaires diélectriques (fig. 2.1.1).

☐ M cylindres diélectriques identiques (dont les axes sont tous parallèles à l'axe des z d'un repère cartésien $Oxyz$, l'origine O étant située près du barycentre de l'ensemble des cylindres), de rayon a et de permittivité (électrique) ε_d, sont plongés dans l'espace libre rempli d'un milieu diélectrique de permittivité ε_c.

☐ L'ensemble est soumis à un champ électrique constant $\mathbf{E}^i$ dirigé dans le sens $\mathbf{i}_x$ (vecteur unitaire de l'axe des x).

☐ Problème est donc 2D et peut être examiné dans plan de section droite $x - y$ (voir la fig. 2.1.1).

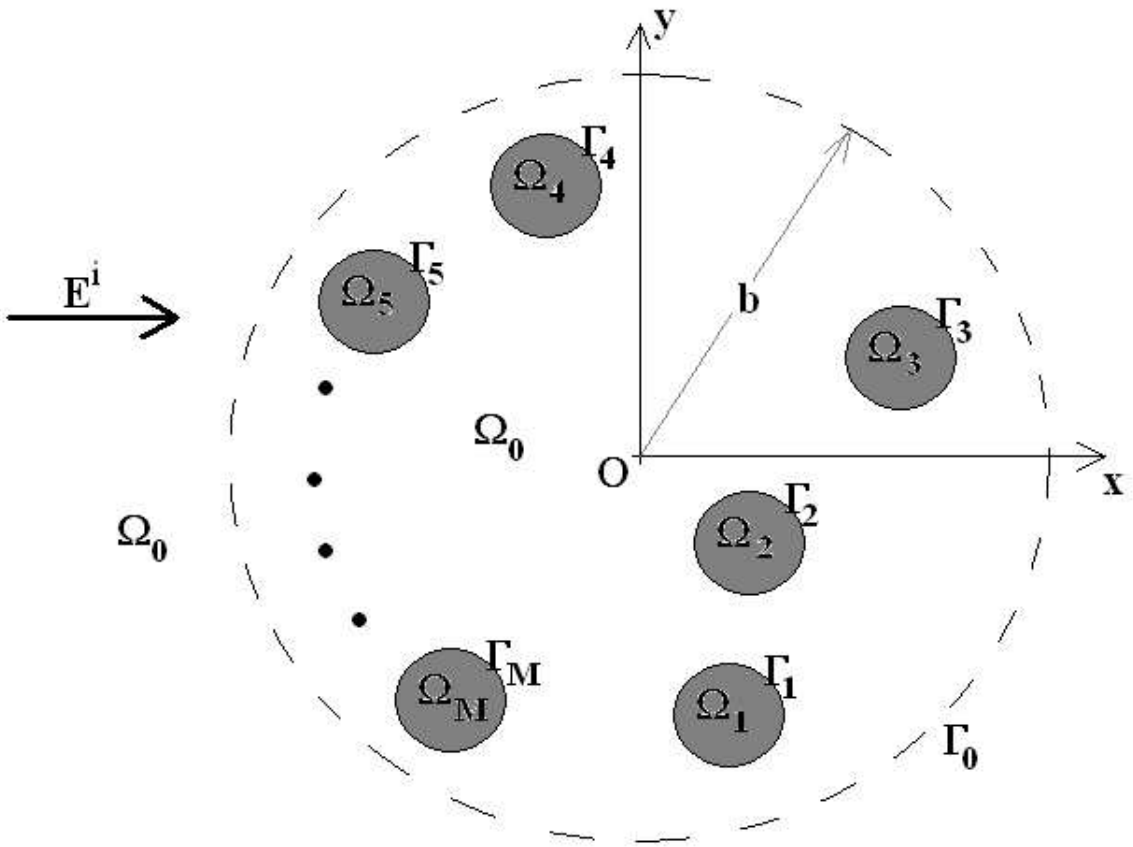

Figure 2.1.1: Vue en coupe de la configuration de M cylindres diélectriques de permittivité ε_d soumis à un champ électrique $\mathbf{E}^i$. Le milieu ambiant est un diélectrique de permittivité ε_c.

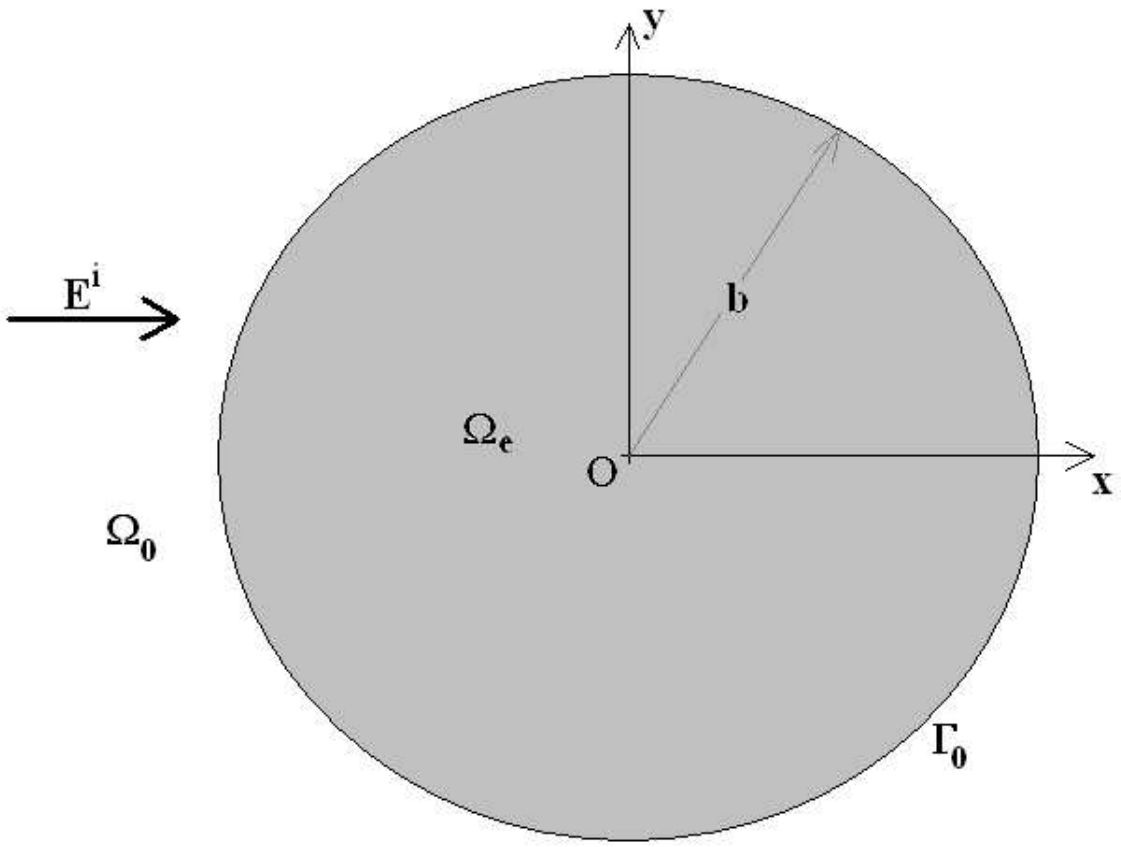

Figure 2.1.2: Vue en coupe de la configuration du "cylindre effectif" de permittivité ε_e et centré en $O_m = O$, soumis à un champ électrique $\mathbf{E}^i$. Le milieu ambiant est un diélectrique de permittivité ε_c.

□ On suppose que configuration (dans le plan $x - y$) peut être contenue dans un cercle Γ_0 dont le rayon minimal est b et le centre en O

■ Problème est de trouver le cylindre de rayon b et de permittivité constante ε_e (dite *permittivité effective)* qui donne lieu au même potentiel électrostatique loin de O que l'ensemble des M cylindres d'origine lorsque les deux configurations sont soumis au même champ électrique $\mathbf{E}^i$.

□ Ω_m,Γ_m sont le domaine et la frontière respectivement du $m^{\text{ième}}$ cylindre. Le domaine extérieur à l'ensemble des M cylindres est Ω_0, tandis que le domaine intérieur à Γ_0 est Ω_e lorsque ce domaine est rempli du milieu homogène de permittivité ε_e (voir la fig. 2.1.2).

□ Le potentiel total dans Ω_m ; $m = 0, 1, 2, ..., M$ est ϕ_m. Le potentiel associé à $\mathbf{E}^i$ est ϕ^i.

□ Les équations qui gouvernent l'ensemble des problèmes électrostatiques considérés:

$$\mathbf{E}^i(\mathbf{x}) = -\nabla\phi^i(\mathbf{x}) = E^i\mathbf{i}_x \iff$$

$$\phi^i(\mathbf{x}) = -E^i x = -E^i r\cos\theta \ \ ; \ \ \mathbf{x} \in \mathbb{R}^2 \ , \quad (2.1.1)$$

$$\nabla^2\phi_m(\mathbf{x}) = 0 \ \ ; \ \ \mathbf{x} \in \Omega_m \ , \ m = 0, 1, 2, ..., M \ , \quad (2.1.2)$$

$$\phi_m(\mathbf{x}) - \phi_0(\mathbf{x}) = 0 \ \ ; \ \ \mathbf{x} \in \Gamma_m \ , \ m = 1, 2, ..., M \ , \quad (2.1.3)$$

$$\varepsilon_d\partial_{\nu_m}\phi_m(\mathbf{x}) - \varepsilon_c\partial_{\nu_m}\phi_0(\mathbf{x}) = 0 \ ; \ \mathbf{x} \in \Gamma_m \ , \ m = 1, 2, ..., M \ , \quad (2.1.4)$$

$$\phi_m(\mathbf{x}) < \infty \ \ ; \ \ \mathbf{x} \in \Omega_m \ , \ m = 1, 2, ..., M \ , \quad (2.1.5)$$

$$\phi_0(\mathbf{x}) - \phi^i(\mathbf{x}) = o(r^{-1}) \;\; ; \;\; r \to \infty \;,\; \mathbf{x} \in \Omega_0 \;, \tag{2.1.6}$$

où $\mathbf{x} = (x, y)$ et $\partial_{\nu_m} = \boldsymbol{\nu_m} \cdot \nabla$ est dérivée normale et $\boldsymbol{\nu_m}$ le vecteur unitaire normale à la courbe-frontière Γ_m.

2.1.2 Solution du problème direct d'un seul cylindre centré en $O_m = O$ et soumis au champ électrique $\mathbf{E}^i$

☐ Problème est décrit de manière figurative dans la fig. 2.1.3. O_m est à la fois centre du cylindre (celui-ci étant supposé exister seul dans l'espace) et origine du repère $O_m x_m y_m z_m$.

☐ Pour distinguer ce problème de ceux qui suivront, adjoignons une indice supérieure '1' sur les potentiels et coefficients. De plus, pour souligner fait qu'un seul (le m-ième) cylindre est en jeu, remplaçons $\mathbf{x}$ par $\mathbf{x}_m = (x_m, y_m)$ dans formules relatives au potentiel.

☐ Séparation de variables ⇒

$$\phi_0^{(1)}(\mathbf{x}_m) = \phi^i(\mathbf{x}_m) + \sum_{n=0}^{\infty} B_n^{(1)} r_m^{-n} \cos(n\theta_m) =$$

$$\sum_{n=0}^{\infty} \left(-\delta_{n1} E^i r_m^n + B_n^{(1)} r_m^{-n} \right) \cos(n\theta_m) \;\; ; \;\; \mathbf{x}_m \in \Omega_0 \;, \tag{2.1.7}$$

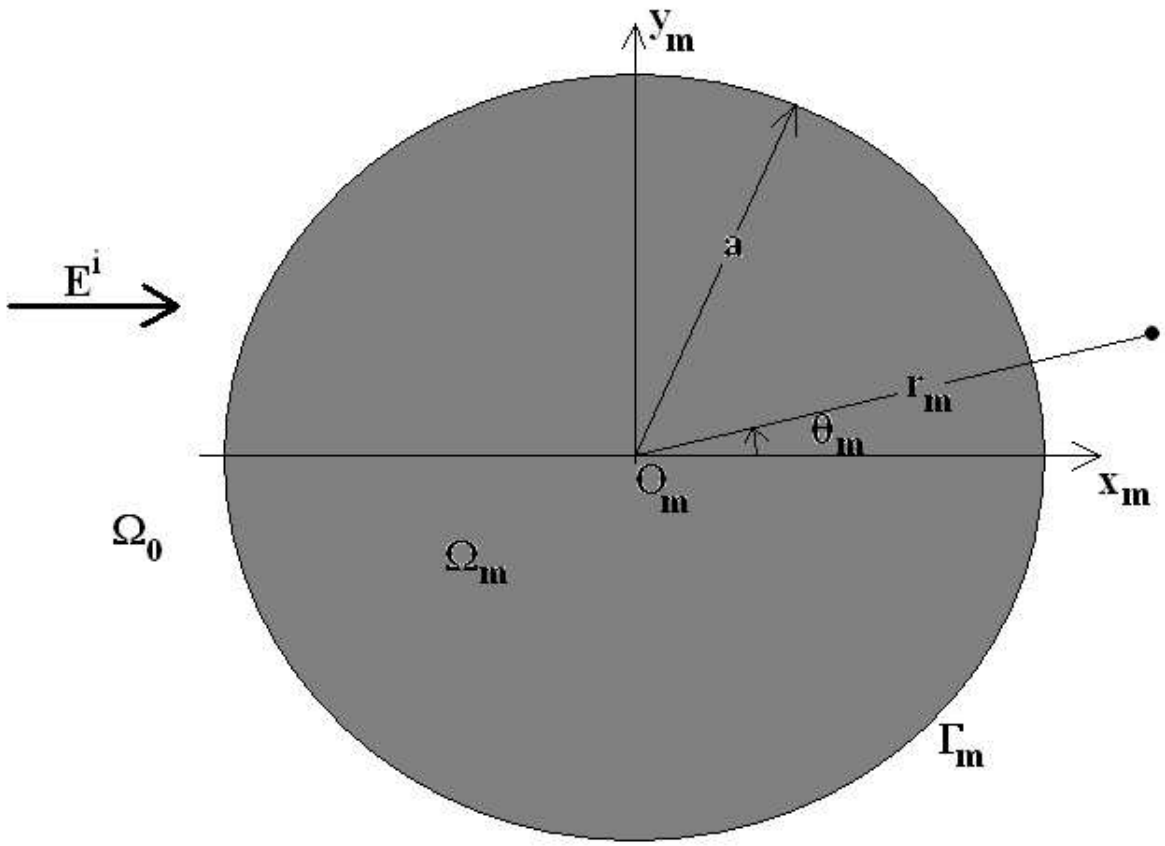

Figure 2.1.3: Vue en coupe de la configuration du m-ième cylindre diélectrique de permittivité ε_d et centré en $O_m = O$, soumis à un champ électrique $\mathbf{E}^i$. Le milieu ambiant est un diélectrique de permittivité ε_c.

$$\phi_m^{(1)}(\mathbf{x}_m) = \sum_{n=0}^{\infty} A_n^{(1)} r_m^n \cos(n\theta_m) \quad ; \quad \mathbf{x}_m \in \Omega_m \ , \ m = 1, 2, ..., M \ , \tag{2.1.8}$$

où $\epsilon_0 = 1, \ \epsilon_{n>0} = 2, \ \delta_{nn} = 1 \ , \delta_{nm\neq n} = 0.$

□ Conditions aux limites ⇒

$$B_n^{(1)} = E^i \frac{a^2}{2} \left(\frac{\varepsilon_d - \varepsilon_c}{\varepsilon_d + \varepsilon_c} \right) \delta_{n1} \quad ; \quad n = 0, 1, 2, ..., . \tag{2.1.9}$$

■ Ainsi

$$\phi_0^{(1)}(\mathbf{x}_m) = -E^i r_m \cos\theta_m + E^i \frac{a^2}{2r_m} \left(\frac{\varepsilon_d - \varepsilon_c}{\varepsilon_d + \varepsilon_c} \right) \cos\theta_m \quad ; \quad \mathbf{x}_m \in \Omega_0 \ . \tag{2.1.10}$$

2.1.3 Solution du problème direct d'un seul cylindre centré en $O_m \neq O$ et soumis au champ électrique $\mathbf{E}^i$

□ Problème direct (dit "problème 2") est même sauf que maintenant centre du cylindre O_m ne se confond plus avec origine O du repère. Pour souligner fait qu'un seul (m-ième) cylindre est en jeu, remplaçons $\mathbf{x}$ par $\mathbf{x}_m$ dans les formules relatives au potentiel.

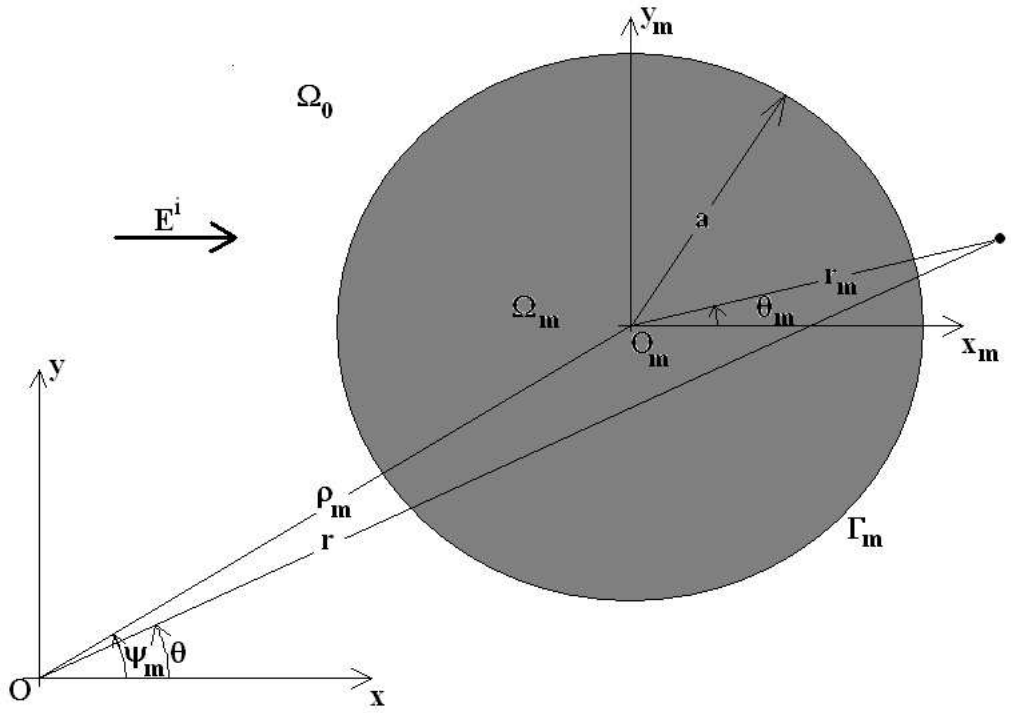

Figure 2.1.4: Vue en coupe de la configuration du m-ième cylindre diélectrique de permittivité ε_d et centré en $O_m \neq O$, soumis à un champ électrique $\mathbf{E}^i$. Le milieu ambiant est un diélectrique de permittivité ε_c.

□ On considère cas où distance ρ_m entre O_m et O est faible par rapport à la distance r entre le point d'observation et O (voir la fig. 2.1.4).

$$\delta_m := \frac{\rho_m}{r} << 1 \quad ; \quad m = 1, 2, \ldots . \tag{2.1.11}$$

$\Rightarrow$

$$r_m = r\left[1 - \delta_m \cos(\psi_m - \theta) + \mathcal{O}(\delta_m^2)\right] \approx r \quad ,$$

$$r_m^{-1} = r^{-1}\left[1 + \delta_m \cos(\psi_m - \theta) + \mathcal{O}(\delta_m^2)\right] \approx r^{-1} \quad ;$$

$$\delta_m \to 0 \quad ; \quad m = 1, 2, \ldots . \tag{2.1.12}$$

□ Pour points d'observation loin de O,

$$\cos\psi_m \approx \cos\theta \quad ; \quad m = 1, 2, \ldots , \quad \Rightarrow \tag{2.1.13}$$

■

$$\phi_0(\mathbf{x}_m) \approx \phi_0^{(2)}(\mathbf{x}_m) = -E^i r\cos\theta + E^i \frac{a^2}{2r}\left(\frac{\varepsilon_d - \varepsilon_c}{\varepsilon_d + \varepsilon_c}\right)\cos\theta \quad ;$$

$$\delta_m \to 0 \quad ; \quad \mathbf{x}_m \in \Omega_0 \ . \tag{2.1.14}$$

2.1.4 Solution du problème direct de M cylindres non- interagissants et soumis au champ électrique $\mathbf{E}^i$

□ Retour au problème de départ (fig. 2.1.1). Ce problème direct (dit "problème 3") est même que dans la section précédente sauf que

maintenant M cylindres au lieu d'un.

□ Concentrons attention sur cas où distance ρ_m entre O_m et O est faible par rapport à la distance r entre le point d'observation et O (voir la fig. 2.1.4), et ce pour tout $M = 1, 2, \ldots$.

□ Supposons que distances entre cylindres sont tellement grandes et contraste de permittivité est tellement faible pour que les cylindres n'interagissent pas entre eux lorsqu'ils sont soumis au champ incident.

■ $\Rightarrow$

$$\phi_0(\mathbf{x}) \approx \phi_0^{(3)}(\mathbf{x}) = \phi^i(\mathbf{x}) + \sum_{m=1}^{M} \left[\phi_0^{(2)}(\mathbf{x}_m) - \phi^i(\mathbf{x}_m) \right] =$$

$$- E^i r \cos\theta + E^i M \frac{a^2}{2r} \left(\frac{\varepsilon_d - \varepsilon_c}{\varepsilon_d + \varepsilon_c} \right) \cos\theta \quad ; \quad \mathbf{x} \in \Omega_0 \ . \quad (2.1.15)$$

□ Ceci constitue solution (approchée) du problème direct de M cylindres soumis au champ électrique $\mathbf{E}^i$.

2.1.5 Solution du problème direct du "cylindre effectif" soumis au champ électrique $\mathbf{E}^i$

□ Considérons problème direct (fig. 2.1.2) d'un cylindre de rayon b et de permittivité ε_e, dit "cylindre effectif", soumis au champ électrique $\mathbf{E}^i$.

□ Ce problème direct (dit "problème 4") est même que problème 1 à ceci près que b remplace a et ε_e remplace ε_d $\Rightarrow$

■

$$\phi_0(\mathbf{x}) = \phi_0^{(4)}(\mathbf{x}) = -E^i r\cos\theta + E^i \frac{b^2}{2r}\left(\frac{\varepsilon_e - \varepsilon_c}{\varepsilon_e + \varepsilon_c}\right)\cos\theta \;\; ; \;\; \mathbf{x} \in \Omega_0 \; . \tag{2.1.16}$$

Cette solution est aussi valable lorsque point d'observation est loin de O.

2.1.6 Solution du problème "inverse" de recherche du "cylindre effectif" qui donne même réponse en zone lointaine que l'ensemble des M cylindres lorsque les deux configurations sont soumis au même champ électrique $\mathbf{E}^i$

■ Retour au probléme "inverse": trouver "cylindre effectif" qui donne la même réponse en zone lointaine que l'ensemble des M cylindres lorsque les deux configurations sont soumis au même champ électrique $\mathbf{E}^i$. Traduction mathématique de cette phrase est

$$\phi_0^{(4)}(\mathbf{x}) = \phi_0^{(3)}(\mathbf{x}) \;\; ; \;\; \mathbf{x} \in \Omega_0 \; , \tag{2.1.17}$$

$\Rightarrow$

$$-E^i r\cos\theta + E^i \frac{b^2}{2r}\left(\frac{\varepsilon_e - \varepsilon_c}{\varepsilon_e + \varepsilon_c}\right) =$$

$$-E^i r\cos\theta + E^i M\frac{a^2}{2r}\left(\frac{\varepsilon_d - \varepsilon_c}{\varepsilon_d + \varepsilon_c}\right) \; . \tag{2.1.18}$$

□ $A_b = \pi b^2$ l'aire du disque de rayon b et $A_a = \pi a^2$ l'aire du disque de rayon a.
⇒
Rapport de l'aire totale occupé par les M cylindres à l'aire du disque qui les contient est

$$\frac{M}{A_b} A_a = N A_a = M \frac{a^2}{b^2} := f \ , \tag{2.1.19}$$

où N est le nombre de cylindres par unité d'aire, et f est *fraction surfacique* d'inclusions cylindriques de permittivité ε_d dans une aire représentative remplie (en l'absence des inclusions) de matériau de permittivité ε_c.
⇒

$$\left(\frac{\varepsilon_e - \varepsilon_c}{\varepsilon_e + \varepsilon_c} \right) = f \left(\frac{\varepsilon_d - \varepsilon_c}{\varepsilon_d + \varepsilon_c} \right) \quad \Rightarrow \ . \tag{2.1.20}$$

■

$$\varepsilon_e = \varepsilon_c \left[\frac{(\varepsilon_d + \varepsilon_c) + f(\varepsilon_d - \varepsilon_c)}{(\varepsilon_d + \varepsilon_c) - f(\varepsilon_d - \varepsilon_c)} \right] \ . \tag{2.1.21}$$

□ Cette formule est "plausible" car $\varepsilon_e = \varepsilon_c$ lorsque $f = 0$ et $\varepsilon_e = \varepsilon_d$ lorsque $f = 1$.

□ Cependant, pas licite de l'employer pour des facteurs de remplissage importants du fait qu'en ce cas l'approximation de cylindres non-interagissants ne tient plus.

☐ Formule de Wagner est identique à celle de Maxwell-Garnett obtenue par une toute autre technique.

☐ Dans la communauté de l'Optique, le contexte est "dynamique", et on emploie la formule de Wagner en remplaçant ε_c par $\varepsilon_c(\omega)$ et ε_d par $\varepsilon_d(\omega)$, sachant que ω est la fréquence angulaire, et que $\varepsilon_c(\omega)$ et $\varepsilon_d(\omega)$ sont les permittivités dynamiques, décrites par un modèle qui est typiquement celui de Lorentz et/ou Drude (voir ci-après). Cette démarche est criticable car la formule de Wagner a été conçue dans un contexte d'électrostatique et non d'électrodynamique.

2.2 Permittivité effective d'un ensemble de M sphères diélectriques par la méthode de Wagner

2.2.1 Position du problème

☐ Ici, des sphères de rayon a remplacent les cylindres de rayon a et une "sphère effective" de rayon b remplace le "cylindre effectif" de rayon b.

2.2.2 Solution du problème "inverse" de la recherche de "sphère effective" qui donne même réponse en zone lointaine que l'ensemble des M sphères lorsque les deux configurations sont soumises au même champ électrique $\mathbf{E}^i$

☐ Démarche est même que pour les cylindres et conduit à

$$\varepsilon_e = \varepsilon_c \left[\frac{(\varepsilon_d + 2\varepsilon_c) + 2f(\varepsilon_d - \varepsilon_c)}{(\varepsilon_d + 2\varepsilon_c) - f(\varepsilon_d - \varepsilon_c)} \right] \ , \qquad (2.2.22)$$

où f est maintenant *fraction volumique* d'inclusions sphèriques de

permittivité ε_d dans un volume représentatif rempli (en l'absence des inclusions) de matériau de permittivité ε_c.

Chapter 3

Homogénéisation acoustique

3.1 Nombre d'onde acoustique effectif d'un ensemble de M patatoïdes fluides contenu dans une lame virtuelle plongée dans une autre fluide: méthode de Urick-Ament

□ Abordons ici une méthode mise au point par Urick et Ament en 1949 pour trouver le nombre d'ondes effectif d'un ensemble de M patatoïdes (corps 3D) fluides contenu dans une lame virtuelle plongée dans un autre fluide lorsque l'ensemble est sollicité par une onde plane acoustique (fig. 3.1.1).

3.2 Position du problème

□ M patatoïdes fluides identiques de composition quelconque sont contenues dans, ce qui est départ est une boîte virtuelle (de largeur α, longueur β et épaisseur γ), et qui deviendra plus tard une lame virtuelle (à faces parfaitement planes et parallèles), et sont immergés dans un autre fluide. Cette boîte est la plus petite de son espèce pouvant contenir toutes les inclusions patatoïdes.

□ L'origine O d'un repère cartésien $Oxyz$ est située sur face hor-

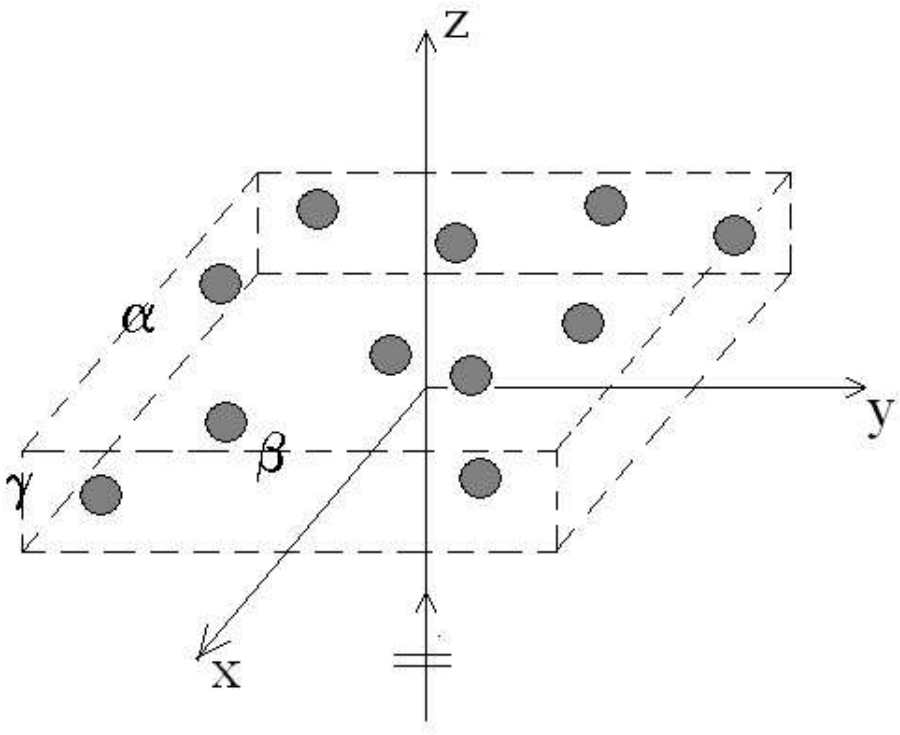

Figure 3.1.1: Vue 3D de la configuration de l'ensemble de M inclusions patatoïdes fluides contenu dans une lame virtuelle plongée dans un autre fluide lorsque l'ensemble est sollicité par une onde plane acoustique.

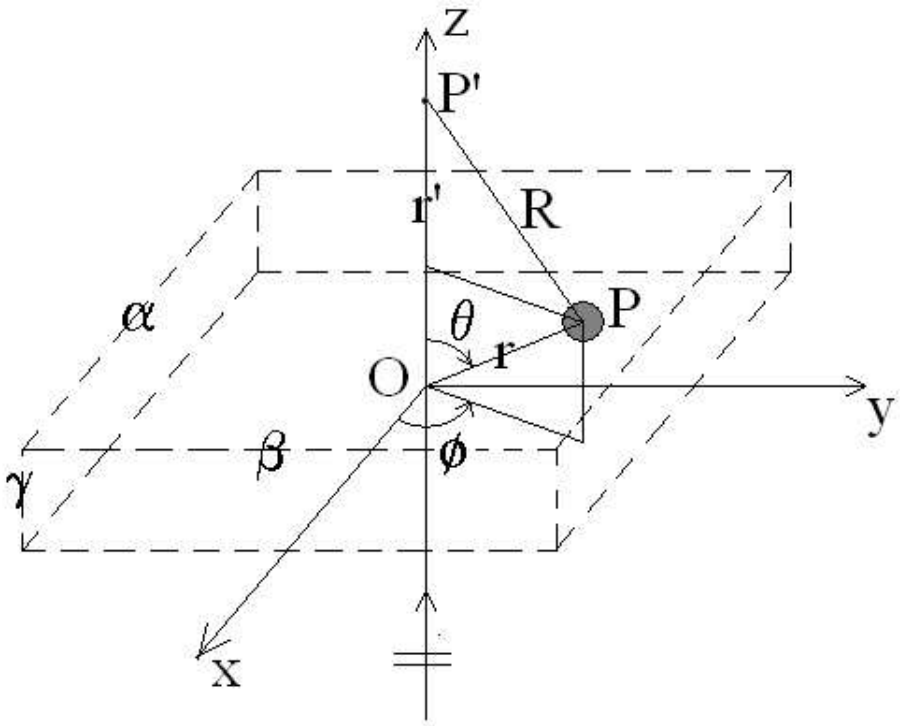

Figure 3.2.1: Vue 3D de la configuration de la m-ième inclusion patatoïde fluide contenu dans une lame virtuelle plongée dans un autre fluide lorsque l'ensemble des inclusions est sollicité par une onde plane acoustique. Les nombres d'ondes dans le fluide-hôte et dans les patatoïdes sont k_c et k_d respectivement. Les patatoïdes sont identiques et acoustiquement mous, durs, ou plus généralement pénétrables.

izontale inférieure de la boîte, l'axe des z étant perpendiculaire aux faces horizontales de la boîte (voir la fig. 3.2.1).

□ Le nombre d'ondes dans le fluide hôte (i.e., hors de la boîte, et dans espaces entre inclusions) est k_c et nombre d'onde dans chaque inclusion est k_d.

□ Cet ensemble de patatoïdes est soumis à une onde plane acoustique se propageant dans le direction $+z$.

□ Le problème est 3D.

□ On considère aussi un autre problème depeint dans la fig. 3.2.2. Cette fois-ci, la boîte est remplacée par une lame "effective" (résultat des opérations $\alpha \to \infty$, $\beta \to \infty$, γ étant comme dans le premier problème), et le contenant de la boîte est un fluide homogène (nombre d'onde constant k_e) du fait de l'absence des inclusions. Le nombre d'onde (k_c) du milieu-hôte et la solicitation (onde plane acoustique se dirigenant vers $+z$) sont les mêmes que dans le premier problème.

■ Le problème est de trouver le nombre d'onde effectif dans la lame d'épaisseur γ qui donne lieu à la même pression acoustique transmise loin de O que l'ensemble des M inclusions d'origine lorsque les deux configurations sont soumises à la même onde plane acoustique.

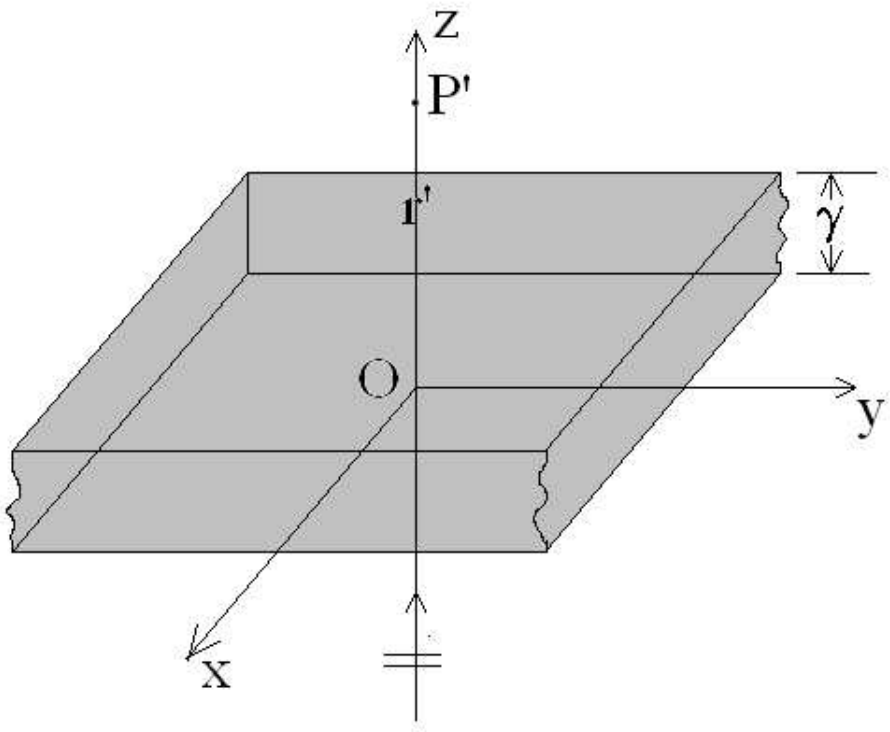

Figure 3.2.2: Vue en coupe de la configuration de la "lame effective fluide" dans laquelle le nombre d'ondes est k_e. Cette lame est soumise à une onde plane acoustique en incidence verticale. Le milieu ambient est un autre fluide en lequel le nombre d'onde est k_c.

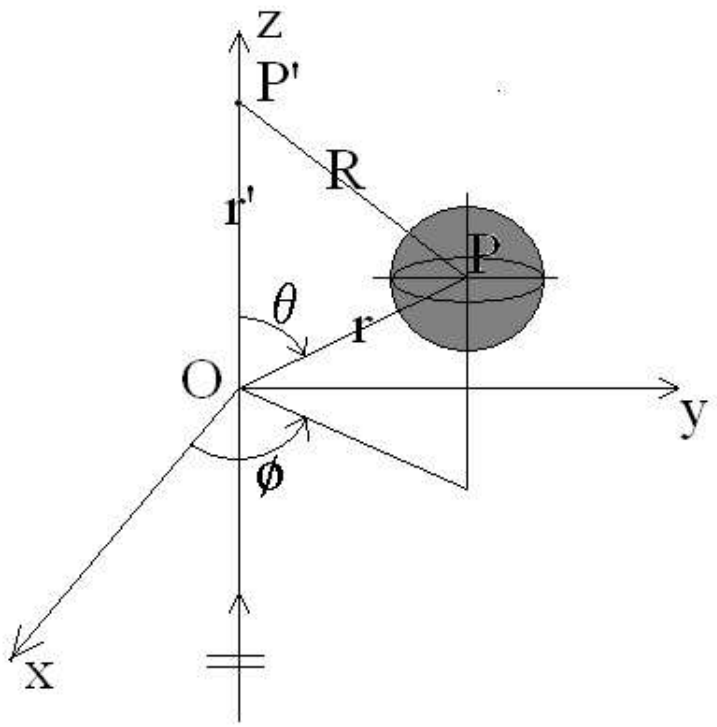

Figure 3.3.1: Vue de la configuration du m-ième inclusion en l'espace libre. Les nombres d'onde dans et hors de l'inclusion sont k_d et k_c respectivement.

3.3 Diffraction par une inclusion isolée

☐ On considère un autre problème (direct, contrairement au problème précédent lequel est inverse) qui est celui de la détermination au point $P = (x', y', z') = (r', 0, 0)$ éloigné de l'origine O du champ de pression diffracté résultant de l'action d'une onde plane acoustique sur un objet 3D patatoïde localisé en $P = (x, y, z) = (r, \theta, \phi)$ (ce point étant dans le voisinage de O) (voir la fig. 3.3.1).

☐ Le nombre d'onde dans le fluide remplissant l'inclusion est k_d alors que le nombre d'onde dans le fluide remplissant l'espace en dehors de l'inclusion est k_c.

□ Abordons ce problème dans cadre espace-fréquence. Les équations régissant le phénomène sont: l'eq́uation de Helmholtz homogène, conditions aux limites, caractère borné du champ de pression dans l'inclusion et condition de rayonnement.

□ Celle-ci prend la forme (dans le référentiel situé en O

$$p^d(\mathbf{x}') := p(\mathbf{x}') - p^i(\mathbf{x}') \sim S(\theta', \phi', z)\frac{i}{k_c R}e^{ik_c R} \;\; ; \;\; k_c R \to \infty \;, \tag{3.3.1}$$

où $p^d(\mathbf{x}')$, $p(\mathbf{x}')$ sont les champs diffracté et total au point d'observation P' très éloigné de O, $S(\theta', \phi', z)$ est la fonction complexe de diffusion (qui dépend de z du fait de la dépendance de S sur l'onde incidente), $\mathbf{x}' = (x', y', z') = (r', \theta', \phi') = (z', \theta', \phi')$, $\mathbf{x} = (x, y, z) = (r, \theta, \phi)$, $\mathbf{R} = \mathbf{x}' - \mathbf{x}$, $|\mathbf{x}'| = r'$, $|\mathbf{x}| = r$, $R = |\mathbf{R}|$ et $p^i(\mathbf{x}')$ le champ incident en P' qui, du fait qu'il s'agit d'une onde plane homogène, prend la forme

$$p^i(\mathbf{x}) = A^i e^{ik_c z} \;. \tag{3.3.2}$$

□ En combinant (4.5.45) et (3.3.2) et en remplaçant le signe $\sim$ par $=$ du fait qu'il est implicite que P' est très loin de P, il vient

$$p^d(\mathbf{x}') = p^i(\mathbf{x}')S(\theta', \phi', z)\frac{i}{k_c R}e^{ik_c(R-z')} \;. \tag{3.3.3}$$

□ Ainsi, le champ total prend la forme

$$p(\mathbf{x}') = p^i(\mathbf{x}') \left[1 + S(\theta', \phi', z) \frac{i}{k_c R} e^{ik_c(R-z')} \right] . \tag{3.3.4}$$

□ Or,

$$R = \sqrt{(x'-x)^2 + (y'-y)^2 + (z'-z)^2} = \sqrt{x^2 + y^2 + (z'-z)^2} = |z'-z| \sqrt{1 + \frac{x^2+y^2}{(z'-z)^2}} . \tag{3.3.5}$$

de sorte que

$$p(\mathbf{x}') = p^i(\mathbf{x}') \left[1 + S(\theta', \phi', z) \frac{i}{k_c |z'-z|} \frac{e^{ik_c \left[-z' + |z'-z| \sqrt{1 + \frac{x^2+y^2}{(z'-z)^2}} \right]}}{\sqrt{1 + \frac{x^2+y^2}{(z'-z)^2}}} \right] . \tag{3.3.6}$$

3.4 Réponse d'un ensemble de M inclusions à l'onde plane

□ La réponse de la m-ième inclusion isolée est donnée par (3.3.6) dans laquelle on remplace $x,\ y,\ z$ par $x_m,\ y_m,\ z_m$.

■ La réponse (i.e., champ diffracté) de *l'ensemble des M inclusions*, *en supposant que ces inclusions n'interagissent pas entre elles*, est la somme des réponses de chaque inclusion isolée, ce qui

s'exprime par

$$p(\mathbf{x}') = p^i(\mathbf{x}')\times$$
$$\left[1+\sum_{m=1}^{M} S_m(\theta'_m,\phi'_m,z_m)\frac{i}{k_c|z'-z_m|}\frac{e^{ik_c\left[-z'+|z'-z_m|\sqrt{1+\frac{x_m^2+y_m^2}{(z'-z_m)^2}}\right]}}{\sqrt{1+\frac{x_m^2+y_m^2}{(z'-z_m)^2}}}\right] . \tag{3.4.7}$$

3.5 Réponse d'un continuum d'inclusions à l'onde plane

■ Soit N le nombre d'inclusions par unité de volume dans la boîte englobant de côtés $\alpha,\ \beta,\ \gamma$.

□ Soit f une fonction attachée au m-ième inclusion.

□ Alors, la transition entre un ensemble discret d'inclusions vers un continuum d'inclusions s'effectue, en ce qui concerne f, au moyen de

$$\sum_{m=1}^{M} \ \rightarrow \ \int_0^{\gamma} dz \int_{-\frac{\beta}{2}}^{\frac{\beta}{2}} dy \int_{-\frac{\alpha}{2}}^{\frac{\alpha}{2}} dx N f(x,y,z) \ . \tag{3.5.8}$$

□ Pour $r >> \gamma$, on a $\theta \approx 0$, de sorte que

$$S(\theta',\phi',z) \approx S(0)e^{ik_c z} \ , \tag{3.5.9}$$

où $S(0)$ est la *fonction complexe de diffusion vers l'avant.*

□ Il s'ensuit

$$p(\mathbf{x}') = p^i(\mathbf{x}')\Big[1 + N\int_0^{\gamma} dz \int_{-\frac{\beta}{2}}^{\frac{\beta}{2}} dy \int_{-\frac{\alpha}{2}}^{\frac{\alpha}{2}} dx \times S(\theta', \phi', z)\frac{i}{k_c|z'-z|}\frac{e^{ik_c\left[-(z'-z)+|z'-z|\sqrt{1+\frac{x^2+y^2}{(z'-z)^2}}\right]}}{\sqrt{1+\frac{x^2+y^2}{(z'-z)^2}}}\Big] \ . \quad (3.5.10)$$

□ Mais (voir fig. 3.2.1) $|z'-z| = z'-z$, et comme $r' >> \gamma$, alors $\frac{x^2+y^2}{(z'-z)^2} << 1$, ce qui signifie que

$$\sqrt{1+\frac{x^2+y^2}{(z'-z)^2}} \approx 1 + \frac{1}{2}\frac{x^2+y^2}{(z'-z)^2} \ . \quad (3.5.11)$$

■ Comme phase est plus sensible à des erreurs que l'amplitude, on garde les deux termes dans formule précédente pour phase et premier terme pour l'amplitude, de façon a réduire (3.5.10) à

$$p(\mathbf{x}') = p^i(\mathbf{x}')\left[1 + \frac{iNS(0)}{k_c}\int_0^{\gamma} dz \int_{-\frac{\beta}{2}}^{\frac{\beta}{2}} dy \int_{-\frac{\alpha}{2}}^{\frac{\alpha}{2}} dx \frac{e^{i\frac{k_c}{2}\frac{x^2+y^2}{(z'-z)^2}}}{z'-z}\right] \ . \quad (3.5.12)$$

□ Considérons l'intégrale double

$$I(\alpha,\beta)=\int_{-\frac{\beta}{2}}^{\frac{\beta}{2}}dy\int_{-\frac{\alpha}{2}}^{\frac{\alpha}{2}}dx\frac{e^{i\frac{k_c}{2}\frac{x^2+y^2}{(z'-z)^2}}}{z'-z}=\frac{4}{z'-z}J(\alpha)J(\beta)\ , \quad (3.5.13)$$

où

$$J(\zeta):=\int_0^{\frac{\zeta}{2}}e^{i\frac{k_c}{2}\frac{\chi^2}{(z'-z)^2}}d\chi=\sqrt{\frac{\pi(z'-z)}{k_c}}\int_0^{\frac{\zeta}{2\sqrt{\frac{\pi(z'-z)}{k_c}}}}e^{i\frac{\pi}{2}\tau^2}d\tau\ . \quad (3.5.14)$$

□ Employant des résultats connus ⇒

$$J(\zeta)=\sqrt{\frac{\pi(z'-z)}{k_c}}\left[\mathcal{S}\left(\frac{\zeta}{2\sqrt{\frac{\pi(z'-z)}{k_c}}}\right)+i\mathcal{C}\left(\frac{\zeta}{2\sqrt{\frac{\pi(z'-z)}{k_c}}}\right)\right]\ , \quad (3.5.15)$$

où $\mathcal{S}$ et $\mathcal{C}$ sont intégrales de Fresnel.

□ Par conséquent

$$I(\alpha,\beta)=4\frac{\pi}{k_c}\left[\mathcal{S}\left(\frac{\alpha}{2\sqrt{\frac{\pi(z'-z)}{k_c}}}\right)+i\mathcal{C}\left(\frac{\alpha}{2\sqrt{\frac{\pi(z'-z)}{k_c}}}\right)\right]\times \left[\mathcal{S}\left(\frac{\beta}{2\sqrt{\frac{\pi(z'-z)}{k_c}}}\right)+i\mathcal{C}\left(\frac{\beta}{2\sqrt{\frac{\pi(z'-z)}{k_c}}}\right)\right]\ , \quad (3.5.16)$$

□ Du fait que voulons que notre boîte devienne une lame d'extension

latérale infinie, devons prendre la limite $\lim_{\alpha\to\infty}\lim_{\beta\to\infty}$, ce qui donne, en employant résultats connus,

$$\lim_{\alpha\to\infty}\lim_{\beta\to\infty} I(\alpha,\beta) \;=\; 4\frac{\pi}{k_c}\left[\frac{1}{2}+i\frac{1}{2}\right]\left[\frac{1}{2}+i\frac{1}{2}\right] \;=\; i\frac{\pi}{k_c}\;. \quad (3.5.17)$$

■ Ainsi:

$$p(\mathbf{x}') = p^{(1)}(\mathbf{x}') = p^{i}(\mathbf{x}')\left[1-\frac{\pi\gamma N}{k_c^2}S(0)\right]\;. \quad (3.5.18)$$

où avons introduit l'indice $^{(1)}$ sur pression afin de distinguer celle-ci du résultat qui suit.

3.6 Unfinished business: the exact solution of diffraction of a plane wave by a homogeneous fluid layer

□ Changeons de langue (ce matériel ayant été écrit en anglais).

□ Term "diffraction" here means (somewhat abusively) the response of layer to incident wave.

□ Before treating the problem described in fig. 3.2.2, we shall solve more general problem depicted (in a cross section view, which corresponds to our problem with the associations $x_2 \leftrightarrow -z$, $x_1 \leftrightarrow y$) in fig. 3.6.1.

□ Field representations for the layer incorporating the radiation conditions:

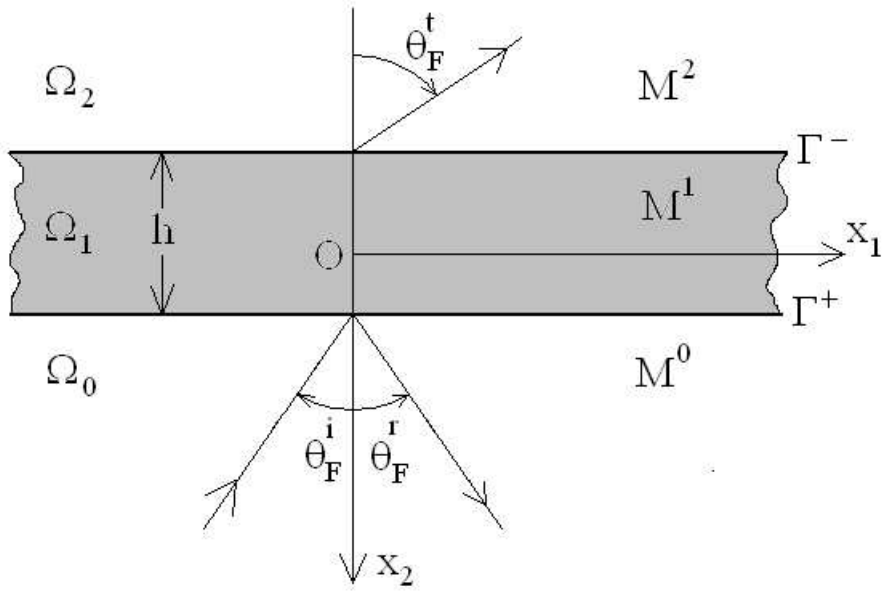

Figure 3.6.1: Cross section view of the configuration for a P plane wave striking a homogeneous, planar, horizontal fluid layer located between two half spaces occupied below by a fluid and above by another fluid.

$$p^0(\mathbf{x}) = \int_{-\infty}^{\infty} \left[A^0(k_1)\exp(i\mathbf{k}^{0-}\cdot\mathbf{x}) + B^0(k_1)\exp(i\mathbf{k}^{0+}\cdot\mathbf{x})\right] dk_1 \ , \tag{3.6.19}$$

$$p^1(\mathbf{x}) = \int_{-\infty}^{\infty} [A^1(k_1)\exp(i\mathbf{k}^{1-}\cdot\mathbf{x}) + B^1(k_1)\exp(i\mathbf{k}^{1+}\cdot\mathbf{x})] dk_1 \ , \tag{3.6.20}$$

$$p^2(\mathbf{x}) = \int_{-\infty}^{\infty} A^2(k_1)\exp(i\mathbf{k}_F^{2-}\cdot\mathbf{x}) dk_1 \ , \tag{3.6.21}$$

wherein:

$$\mathbf{k}^{j\pm} = (k_1,\ k_2^{j\pm})\ ,\ k_2^{j\pm} = \pm\sqrt{(k^j)^2 - (k_1)^2}\ ,\ \Re k_2^{j+} \geq 0\ ,\ \Im k_2^{j+} \geq 0\ . \tag{3.6.22}$$

and

$$A^0(k_1) = A^i \delta(k_1 - k_1^i)\ , \tag{3.6.23}$$

with $\delta(\ .\ )$ the Dirac distribution.

$\square$ Transmission boundary conditions:

$$p^0(\mathbf{x},\omega) - p^1(\mathbf{x},\omega) = 0\ ;\ \forall \mathbf{x} \in \Gamma^+\ , \tag{3.6.24}$$

$$\frac{1}{\rho^0} p^0_{,2}(\mathbf{x},\omega) - \frac{1}{\rho^1} p^1_{,2}(\mathbf{x},\omega) = 0\ ;\ \forall \mathbf{x} \in \Gamma^+\ , \tag{3.6.25}$$

$$p^2(\mathbf{x},\omega) - p^1(\mathbf{x},\omega) = 0\ ;\ \forall \mathbf{x} \in \Gamma^-\ , \tag{3.6.26}$$

$$\frac{1}{\rho^2} p^2_{,2}(\mathbf{x},\omega) - \frac{1}{\rho^1} p^1_{,2}(\mathbf{x},\omega) = 0\ ;\ \forall \mathbf{x} \in \Gamma^-\ . \tag{3.6.27}$$

$\square$ Introduction of field representations into these transmission conditions $\Rightarrow$

$$B^0(k_1) = A^i\delta(k_1 - k_1^i)e^{-2ik_2^{0+}h^+}\times$$
$$\left[\frac{\left(\frac{k_2^{0+}}{\rho^0} - \frac{k_2^{1+}}{\rho^1}\right)\left(\frac{k_2^{1+}}{\rho^1} + \frac{k_2^{2+}}{\rho^2}\right)e^{-ik_2^{1+}h} + \left(\frac{k_2^{0+}}{\rho^0} + \frac{k_2^{1+}}{\rho^1}\right)\left(\frac{k_2^{1+}}{\rho^1} - \frac{k_2^{2+}}{\rho^2}\right)e^{ik_2^{1+}h}}{\left(\frac{k_2^{0+}}{\rho^0} + \frac{k_2^{1+}}{\rho^1}\right)\left(\frac{k_2^{1+}}{\rho^1} + \frac{k_2^{2+}}{\rho^2}\right)e^{-ik_2^{1+}h} + \left(\frac{k_2^{0+}}{\rho^0} - \frac{k_2^{1+}}{\rho^1}\right)\left(\frac{k_2^{1+}}{\rho^1} - \frac{k_2^{2+}}{\rho^2}\right)e^{ik_2^{1+}h}}\right]$$
$$:= A^i\delta(k_1 - k_1^i)R^0(k^1)\ , \quad (3.6.28)$$

$$A^1(k_1) = A^i\delta(k_1 - k_1^i)e^{-i\left(k_2^{0+}h^+ - k_2^{1+}h^-\right)}\times$$
$$\left[\frac{2\frac{k_2^{0+}}{\rho^0}\left(\frac{k_2^{1+}}{\rho^1} + \frac{k_2^{2+}}{\rho^2}\right)}{\left(\frac{k_2^{0+}}{\rho^0} + \frac{k_2^{1+}}{\rho^1}\right)\left(\frac{k_2^{1+}}{\rho^1} + \frac{k_2^{2+}}{\rho^2}\right)e^{-ik_2^{1+}h} + \left(\frac{k_2^{0+}}{\rho^0} - \frac{k_2^{1+}}{\rho^1}\right)\left(\frac{k_2^{1+}}{\rho^1} - \frac{k_2^{2+}}{\rho^2}\right)e^{ik_2^{1+}h}}\right],$$
$$:= A^i\delta(k_1 - k_1^i)T^1(k^1) \quad (3.6.29)$$

$$B^1(k_1) = A^i\delta(k_1 - k_1^i)e^{-i\left(k_2^{0+}h^+ + k_2^{1+}h^-\right)}\times$$
$$\left[\frac{2\frac{k_2^{0+}}{\rho^0}\left(\frac{k_2^{1+}}{\rho^1} - \frac{k_2^{2+}}{\rho^2}\right)}{\left(\frac{k_2^{0+}}{\rho^0} + \frac{k_2^{1+}}{\rho^1}\right)\left(\frac{k_2^{1+}}{\rho^1} + \frac{k_2^{2+}}{\rho^2}\right)e^{-ik_2^{1+}h} + \left(\frac{k_2^{0+}}{\rho^0} - \frac{k_2^{1+}}{\rho^1}\right)\left(\frac{k_2^{1+}}{\rho^1} - \frac{k_2^{2+}}{\rho^2}\right)e^{ik_2^{1+}h}}\right],$$
$$:= A^i\delta(k_1 - k_1^i)R^1(k^1) \quad (3.6.30)$$

$$A^2(k_1) = A^i\delta(k_1 - k_1^i)e^{-i\left(k_2^{0+}h^+ - k_2^{2+}h^-\right)}\times$$
$$\left[\frac{4\frac{k_2^{0+}}{\rho^0}\frac{k_2^{1+}}{\rho^1}}{\left(\frac{k_2^{0+}}{\rho^0} + \frac{k_2^{1+}}{\rho^1}\right)\left(\frac{k_2^{1+}}{\rho^1} + \frac{k_2^{2+}}{\rho^2}\right)e^{-ik_2^{1+}h} + \left(\frac{k_2^{0+}}{\rho^0} - \frac{k_2^{1+}}{\rho^1}\right)\left(\frac{k_2^{1+}}{\rho^1} - \frac{k_2^{2+}}{\rho^2}\right)e^{ik_2^{1+}h}}\right].$$
$$:= A^i\delta(k_1 - k_1^i)T^2(k^1) \quad (3.6.31)$$

3.7 La pression transmise par la lame effective

□ Retournons à la langue française.

□ Rappelons que lame effective était plongée dans un fluide M^0 (qui remplit donc Ω_0 et Ω_2 dans la notation du problème de la section précédente.

□ Ainsi, avons $k^2 = k^0$ et devons prendre $k_2^{2\pm} = k_2^{0\pm}$ dans formules de section précédente.

□ De plus, comme seul le champ transmis nous intéresse, nous ne nous occuperons que du facteur de transmission T du fait que

$$p^2(\mathbf{x}) = \int_{-\infty}^{\infty} A^2(k_1)\exp[i(k_1x_1 - k_2^{2+})]dk_1 = \int_{-\infty}^{\infty} A^iT(k_1)\delta(k_1 - k_1^i)\exp[i(k_1x_1 - k_2^{0+})]dk_1 = A^iT(k_1^i)\exp[i(k_1x_1 - k_2^{0i+})] = T(k_1^i)p^i(\mathbf{x})\ . \quad (3.7.32)$$

□ On montre, à partir de (3.6.31) et au cas $k_2^{2+} = k_2^{0+}$, que:

$$T(k_1) = \frac{4e^{i(k_2^{1+}-k_2^{0+})h}}{2\left(1+e^{2ik_2^{1+}h}\right)+\left(\frac{k_2^{0+}\rho^1}{k_2^{1+}\rho^0}+\frac{k_2^{1+}\rho^0}{k_2^{0+}\rho^1}\right)\left(1-e^{2ik_2^{1+}h}\right)} \ . \tag{3.7.33}$$

□ Rappelons aussi que nous supposions que l'onde plane frappe lame en incidence normale, ce qui signifie que $k_2^{j+} = k^j$, de sorte que

$$T(k_1) = \frac{4e^{i(k^1-k^{0+})h}}{2\left(1+e^{2ik^1h}\right)+\left(\frac{k^0\rho^1}{k^1\rho^0}+\frac{k^1\rho^0}{k^0\rho^1}\right)\left(1-e^{2ik^1h}\right)} \ . \tag{3.7.34}$$

□ Nous supposons que fréquence est assez basse et/ou l'indice de réfraction de la lame n'est pas trop grande, et/ou l'épaisseur h de la lame assez faible pour que

$$\|2k^1h\| << 1 \quad \Rightarrow \ . \tag{3.7.35}$$

□

$$T(k_1) \approx e^{i(k^1-k^0)h} \ , \tag{3.7.36}$$

ce qui veut dire que la lame agit comme *un objet de phase* dans le langage des opticiens.

□ Nous supposons enfin que nombre d'onde (effective) dans la lame est suffisamment proche de celui du milieu-hôte pour que

$$\|(k^1 - k^0)h\| << 1 \quad \Rightarrow \ , \tag{3.7.37}$$

□

$$T(k_1) \approx 1 + i(k^1 - k^0)h \ . \tag{3.7.38}$$

■ Ceci se traduit, au niveau du champ transmis, par (on remplace désormais $\approx$ par $=$, k_1 par k_e, k_0 par k_c, h et par γ):

$$p(0,0,z') = p^{(2)}(0,0,z') = p^i(0,0,z')[1 + i(k_e - k_c)\gamma] \ , \tag{3.7.39}$$

formule dans laquelle nous avons ajouté l'indice $^{(2)}$ pour distinguer solution de ce problème de celui de l'ensemble d'inclusions.

3.8 Obtention du nombre d'onde effectif par comparaison de $p^{(1)}$ et $p^{(2)}$

■ Comme indiqué plus haut, méthode d'Urick-Ament répose sur l'égalisation des champs transmis d'une part par l'ensemble d'inclusions, et d'autre part par la lame effective, i.e.,

$$p^{(1)}(0,0,z') = p^{(2)}(0,0,z') \ . \tag{3.8.40}$$

□ Ceci se traduit par

$$1 - \frac{\pi N \gamma}{k_c^2} S(0) = 1 + i(k_e - k_c)\gamma \quad \Rightarrow \tag{3.8.41}$$

■

$$\frac{k_e}{k_c} = 1 + i\frac{\pi N}{k_c^3} S(0) \ . \tag{3.8.42}$$

□ Ce résultat (nommé formule U-A) appelle un certain nombre de rappels et de remarques:

- Le nombre d'inclusions par unité de volume est $N = \frac{\phi}{V}$, où V est le volume d'une inclusion, et ϕ le facteur de remplissage dans un élément de volume représentatif (= 1 si les inclusions remplissent totalement l'EVR),

- $S(0)$ est la fonction complexe de diffusion par une inclusion isolée dans la direction de diffusion vers l'avant; cette fonction est facile à obtenir pour sphère, moins facile pour inclusions ayant d'autres formes canoniques, et possible numériquement pour objets de forme autre,

- il semblerait que dimensions caractéristiques, nombre d'onde, et densités des milieu-hôte et du matériau des inclusions soient *absents* dans la formule U-A, mais, en réalité tous ces paramètres sont *présents* à travers $S(0)$,

- k_e dépend de la fréquence angulaire ω même si k_c et k_d n'en dépendent pas, du fait que $S(0)$ dépend de ω; autrement dit, *le milieu effectif est dispersif*, même si le milieu hôte et le matériau des inclusions ne sont pas dispersifs,

- k_e est généralement complexe, même si le milieu-hôte est non-dissipatif (i.e., k_c est réel) et le milieu remplissant chaque inclusion est non-dissipatif (i.e., k_d est réel); cette *dissipation du milieu effectif* provient du fait que la présence des inclusions engendre de la diffusion se traduisant par de l'énergie de l'onde incidente partant non seulement dans les directions prises par l'onde spéculairement réfléchie et l'onde spéculairement transmise par la lame, mais aussi dans d'autres directions (ceci constituant véritablement la "diffraction"), et, étant donné que le modèle de lame effective ne tient pas explicitement compte de cette diffusion (du fait qu'elle est homogène et a faces planes et parallèles), le modèle U-A compense pour cet "oubli" (i.e., l'énergie perdue par diffusion) par l'introduction d'une dissipation fictive au sein de la lame,

- la formule U-A n'est vraisemblablement pas valable pour des concentrations élevées d'inclusions (i.e., proches l'une de l'autre), et des inclusions qui diffractent fortement (ce qui se traduit par k_e très différent de k_c); il est même probable que le modèle U-A, comme tout modèle *d'homogénéisation*, ne soit valable qu'aux basses fréquences,

- lorsque les inclusions sont des fibres (cylindres de section quelconque) mutuellement parallèles et parallèles à l'axe des y, on montre que la formule U-A prend la forme

$$\frac{k_e}{k_c} = 1 + i\frac{2N}{k_c^2} S(0) \ . \tag{3.8.43}$$

où $N = \phi/A$, ϕ est le facteur de remplissage surfacique, et A

l'aire dans sa section droite d'un cylindre.

3.9 Vitesse de phase et atténuation au sens d'Urick et Ament

□ La formule U-A peut s'écrire

$$k_e = k_c + i\frac{\pi N}{k_c^2} S(0) := \frac{\omega}{c_e} + i\alpha_e \ , \tag{3.9.44}$$

où c_e est la *vitesse de phase effective*, et α_e *l'atténuation effective* données (obtenues en prenant les parties réelle et imaginaire de (3.8.43)) par:

$$c_e = \left[1 - \frac{\pi N}{k_c^3} \Im S(0)\right]^{-1} \ , \tag{3.9.45}$$

$$\alpha_e = \frac{\pi N}{k_c^2} \Re S(0) \ . \tag{3.9.46}$$

□ En principe, il est possible de déterminer ϕ, les dimensions caractéristiques de l'inclusion-type et les paramètres matériels de celui-ci, à partir de la connaissance de $\alpha_e(\omega)$ et/ou $c_e(\omega)$. Ces fonctions s'obtiennent (i.e., résolution d'un problème inverse) à partir de données expérimentales portant sur $R(k_1^i, \omega)$ et/ou $T(k_1^i, \omega)$ du matériau hétérogène contenue dans une lame (ou plaque).

Chapter 4

Dispersion and dissipation

4.1 Acoustic/elastic/electromagnetic response of materials due to their microscopic (electronic, molecular,...) properties

☐ Subject: acoustic/electromagnetic response of materials that are macroscopically- and mesoscopically-homogeneous.

☐ Here, microscopic scale deals with electronic, atomic and molecular constituents of matter, mesoscopic scale with matter that contains inclusions of dimensions an order of magnitude (or more) greater than dimensions of molecules, and macroscopic scale is that of matter that is either homogeneous on scale of specimen, or contains inclusions that are of length scale of specimen.

■ All materials, even those qualified as homogeneous, are inhomogeneous at microscopic length scale.

☐ We show that this microscopic heterogeneity gives rise to phenomena, in response to wave-like solicitations (see, e.g. fig. 4.1.1, relative to an experiment in which a slab or layer specimen of material is submitted to a pulse-like or variable-frequency plane wave

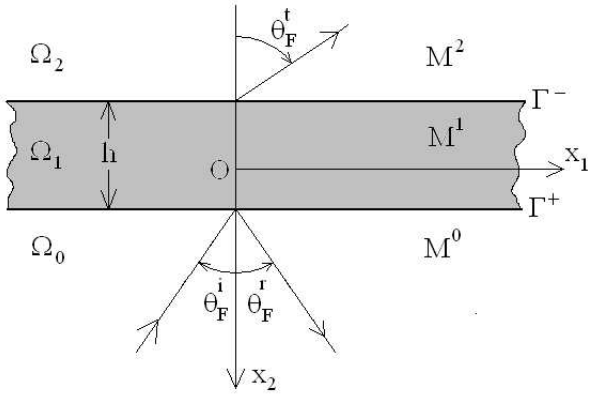

Figure 4.1.1: Cross section view of configuration for a plane wave striking a layer or slab specimen of a macroscopically- and mesoscopically-homogeneous material.

and response (reflectance, transmittance) of latter is measured either in direction taken by specularly-reflected or specularly-transmitted wave in time domain or as a function of frequency), that are in many respects similar to those in materials that are either mesoscopically- or macroscopically-heterogeneous.

■ The phenomena that we are most concerned with are *dispersion* and *dissipation*.

4.2 Electromagnetic (more specifically, optical) constitutive properties of materials

4.2.1 Introduction

□ Optical (i.e., electromagnagnetic (EM)) properties (which manifest themselves by phenomena such as dispersion, i.e., refractive indices that vary with frequency, giving rise, in some materials, to distinctive color when viewed in reflection) of solids (insulators, semiconductors and metals), are predominantly determined by outer (valence or con-

duction) electrons.

☐ Before this was known, Maxwell, and independently Sellmeyer, proposed a simple mechanical model to explain dispersion.

☐ Lorentz extended this theory by viewing material as a fine-grained assembly of molecular oscillators (i.e., dynamical systems possessing natural free periods and which are excited by incident field (to which is associated a force) which enabled him to account at least qualitatively for many electrical and optical phenomena.

☐ Lorentz assumed molecular systems to obey laws of classical dynamics; it is now known that they are in fact governed by laws of quantum mechanics.

4.2.2 Basics of Lorentz theory

☐ Classical (and quantum) theories of EM dispersion seek to calculate displacement of charge from center of gravity of an atomic system as a function of frequency and intensity of solicitation.

☐ Averaging over atoms contained within an appropriately-chosen volume element $\Rightarrow$ expression of $\mathbf{P} = \mathbf{D} - \varepsilon_0 \mathbf{E}$ of medium, i.e., dipole moment per unit volume.

☐ Classical result, i.e., that of a single-degree-of-freedom (SDOF) mechanical system (has same form as quantum mechanical form and) leads, in many cases, to an adequate representation of way index of refraction varies with frequency.

4.2.3 Basics of SDOF (mechanical/electrical) dynamical systems

Differential equation of SDOF model

□ $x(t)$=time history of displacement, t =time variable.

■ SDOF model:

$$M\ddot{x}(t) + C\dot{x}(t) + Kx = F(t) \ , \tag{4.2.1}$$

wherein M, C and K are real, positive constants, and $F(t)$ is the solicitation.

□ $x(t)$ and $F(t)$ are real functions of t, $\dot{x} = \frac{dx}{dt}$ is the velocity, and $\ddot{x} = \frac{d^2x}{dt^2}$ the acceleration.

Solicitation

Sinusoidal solicitation:

$$F(t) = A\sin(\varpi t + \varphi) \ , \tag{4.2.2}$$

wherein A is the amplitude A and φ the phase.

Transformation from time domain to frequency domain

$$x(t) = \int_{-\infty}^{\infty} x(\omega)e^{-i\omega t}d\omega \ \ , \ \ F(t) = \int_{-\infty}^{\infty} F(\omega)e^{-i\omega t}d\omega \ , \tag{4.2.3}$$

wherein ω is (real) angular frequency variable.

□ Since $x(t)$ and $F(t)$ are real

$$x(t) = 2\Re \int_0^\infty x(\omega) e^{-i\omega t} d\omega \quad , \quad F(t) = 2\Re \int_0^\infty F(\omega) e^{-i\omega t} d\omega \ . \tag{4.2.4}$$

Also

$$\int_{-\infty}^{\infty} \left[\left(-M\omega^2 - i\omega C + K \right) x(\omega) - F(\omega) \right] e^{-i\omega t} d\omega = 0 \ , \tag{4.2.5}$$

whence, by Fourier inversion

$$\left(-M\omega^2 - i\omega C + K \right) x(\omega) - F(\omega) = 0 \ . \tag{4.2.6}$$

Complex eigenfrequencies

□ Eigenfrequencies of system are obtained by removing solicitation ⇒

$$-M\omega^2 - i\omega C + K = 0 \ . \tag{4.2.7}$$

□ When system is dissipationless, $C = 0$ ⇒

$$\lim_{C \to 0} \omega = \sqrt{\frac{K}{M}} := \Omega \ . \tag{4.2.8}$$

Ω is real eigenfrequency of dissipationless system.

□ In presence of dissipation, complex eigenfrequency is

$$\omega = \sqrt{\Omega^2 - \frac{C^2}{4M^2}} - i\frac{C}{2M} \ . \tag{4.2.9}$$

General solution of frequency domain differential equation

☐ Solution of (4.2.6):

$$x(\omega) = \frac{F(\omega)}{-M\omega^2 - i\omega C + K} = \frac{-M^{-1}F(\omega)}{\omega^2 - \Omega^2 + i\frac{\omega C}{M}} \ . \tag{4.2.10}$$

☐ Denominator of frequency-domain response function cannot vanish for real (physical) ω in a physically-realistic system in which there is dissipation.

4.2.4 More on Lorentz theory

☐ Lorentz theory makes use of SDOF model to relate electrical polarization $\mathbf{P}$ to applied electric field $\mathbf{E}$.

$$\mathbf{P} = \mathbf{D} - \varepsilon_0\mathbf{E} = \left(\frac{\varepsilon}{\varepsilon_0} - 1\right)\varepsilon_0\mathbf{E} = (\kappa_e - 1)\varepsilon_0\mathbf{E} \ , \tag{4.2.11}$$

wherein $\varepsilon,\ \varepsilon_0$ are electrical inductive capacities of material and free space respectively and κ_e is specific electrical inductive capacity (also called the dielectric constant) of the material.

☐ Lorentz transposes the dynamical variables and constants to electrical variables and constants by associating x with $\mathbf{P}$, F with $\varepsilon\mathbf{E}$, M with a^2 (a constant proportional to number of oscillators per unit volume whose *resonant frequency* is ω_0 related to Ω by $\Omega^2 = \omega_0^2 - \frac{a^2}{3}$)

and $\frac{C}{M}$ with g (which takes account of dissipative, quasi-frictional forces introduced by collisions of molecules) the *damping factor*. g is often designated by $\Gamma = 1/\tau$, wherein τ is the relaxation time (or mean collision time for conducting electrons)

■ Constants ω_0 and g, just like $K,\ C,\ M$ in classical dynamical model, must be determined from experimental data concerning response of system (to $\mathbf{E}$ in electrical phenomena, and to F in dynamical system phenomena).

□ ⇒

$$\mathbf{P} = (\kappa_e(\omega) - 1)\,\varepsilon_0\mathbf{E} = \frac{a^2}{\omega_0^2 - \omega^2 - i\omega g}\varepsilon_0\mathbf{E}\ , \tag{4.2.12}$$

⇒

$$\kappa_e(\omega) = 1 - \frac{a^2}{\omega^2 - \omega_0^2 + i\omega g}\ . \tag{4.2.13}$$

Consequences of complex, frequency-dependent nature of κ_e on electrical field wave equation derived from Maxwell's equations

□ Wave equation takes form (in a non-conducting material and in absence of applied currents and charges)

$$\nabla^2 u(\mathbf{x}, t) - \varepsilon\mu\partial_t^2 u(\mathbf{x}, t) = 0\ , \tag{4.2.14}$$

wherein $\mathbf{x} = (x, y, z)$, $u = E_x$, $u = E_y$ or $u = E_z$.

□ If material is assumed to be homogeneous and to fill all of space,

a solution of this equation is

$$u(\mathbf{x},t) = \Re\{A\exp[i\mathbf{k}\cdot\mathbf{x} - i\omega t)]\} \ , \tag{4.2.15}$$

wherein A is a constant, $\mathbf{k} = k\hat{\mathbf{k}} = (k_x, k_y, k_z)$ and

$$\mathbf{k}\cdot\mathbf{k} = k^2 = \omega^2\varepsilon\mu = \omega^2\varepsilon_0\mu_0\kappa_e\kappa_m \ , \tag{4.2.16}$$

and $\kappa_m = \frac{\mu}{\mu_0}$.

□ If (as is often case in dielectric materials) $\kappa_m \approx 1$, then

$$k = \omega\sqrt{\varepsilon_0\mu_0}\sqrt{\kappa_e} = \frac{\omega}{c_0}\sqrt{\kappa_e} = \frac{\omega}{c_0}\eta \ , \tag{4.2.17}$$

wherein $c_0 = \frac{1}{\sqrt{\varepsilon_0\mu_0}}$ is speed of light in vacumn, and η is index of refraction of the material.

□ κ_e a complex function of frequency ⇒ the wavenumber k and the index of refraction η are complex functions of angular frequency ω ⇒

$$k(\omega) = \frac{\omega}{c_0}\sqrt{\kappa_e(\omega)} = k'(\omega) + ik"(\omega) \ , \tag{4.2.18}$$

$$\eta(\omega) = \sqrt{\kappa_e(\omega)} = \eta'(\omega) + i\eta"(\omega) \ . \tag{4.2.19}$$

■ Index of refraction depends on frequency and is complex ⇔ the

material is *dispersive and dissipative.*

□ To discern more clearly dissipative aspect, introduce (4.2.18) into (4.2.15)

$$u(\mathbf{x},t) = \Re\{A\exp[i\hat{\mathbf{k}}\cdot\mathbf{x}(k' + ik") - i\omega t)]\} = \exp(-k"\hat{\mathbf{k}}\cdot\mathbf{x})\Re\{A\exp[i\hat{\mathbf{k}}\cdot\mathbf{x}k' - i\omega t)]\}\ , \quad (4.2.20)$$

whereby is seen that wave is *attenuated* as it progresses in the material, this attenuation being synonymous with fact that material is *dissipative.*

4.2.5 Optical response

Spectral character of optical response of insulators

□ Consider (electrically-) insulating materials which are ionically - bonded such as alkali-halides (e.g., KCl). In these materials, valence electrons are strongly localized at negative ion (for KCl, this would be Cl atom), and hence optical spectrum contains some atomic-like features, with many resonances. This can be seen in reflectance spectrum for KCl shown in fig. 4.2.1. It is apparent that *single oscillator Lorentz model of material does not give quantitatively-accurate results for ionic materials.*

■ This shows, that most real materials must, at very least (i.e., not taking into account quantum-mechanical effects), be thought of as a *collection of Lorentz oscillators with different frequencies.*

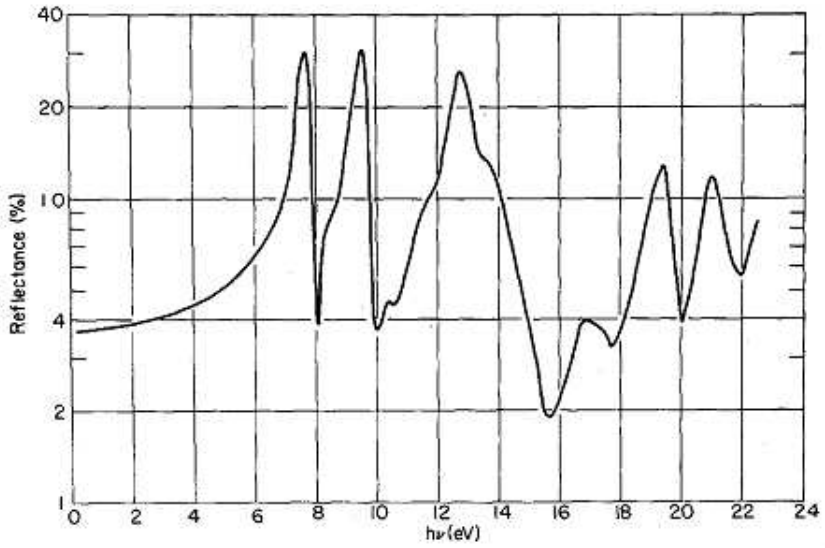

Fig. 3.6 The spectral dependence of the reflectance of KCl. The region of transparency extends to about 7 eV. Above 7 eV, there are a number of sharp peaks related to narrow energy bands and excitons. [From H. R. Philipp and H. Ehrenreich, *Phys. Rev.* **131**, 2016 (1963).]

Figure 4.2.1: Dispersive properties of KCl as manifested in graph of reflectance versus frequency (more specifically, $\hbar\nu$ in electron-volts).

□ Lorentz theory, as described previously, sought to account for behavior of wavenumber in neighborhood of a *single resonance frequency*. In reality, a molecule is a complicated dynamical system with many degrees of freedom, and therefore possessing many natural frequencies, each affecting reaction of molecule to impressed field.

■ Location of these natural frequencies cannot be determined by classical theory. In fact this is an *inverse problem* that has to be solved by comparing a theoretical multiple degree of freedom (MDOF) model of response to experimental data concerning response of material to a pulse or a sinusoidal wave of varying frequency over a wide range of frequencies. Such a MDOF model could take form

$$\kappa_e(\omega) = 1 - \sum_{l=1}^{L} \frac{a_l^2}{\omega^2 - \omega_l^2 + i\omega g_l} \ . \tag{4.2.21}$$

Spectral character of optical response of semiconductors

□ Semiconductors are covalently-bonded materials where electrons are shared between neighboring atoms. (Some insulators are covalently bonded, too.) Thus, electrons are smeared out into broader bands and their resonance frequencies are lower than for ionically-bonded materials.

□ Often, these materials can be described by single energy gap and single broad absorption band above energy gap. Example of silicon (Si) is shown in fig. 4.2.2. Si appears as a grayish reflector throughout visible spectrum. ($\sim$1.7-3.2 eV) due to fact that reflectance has

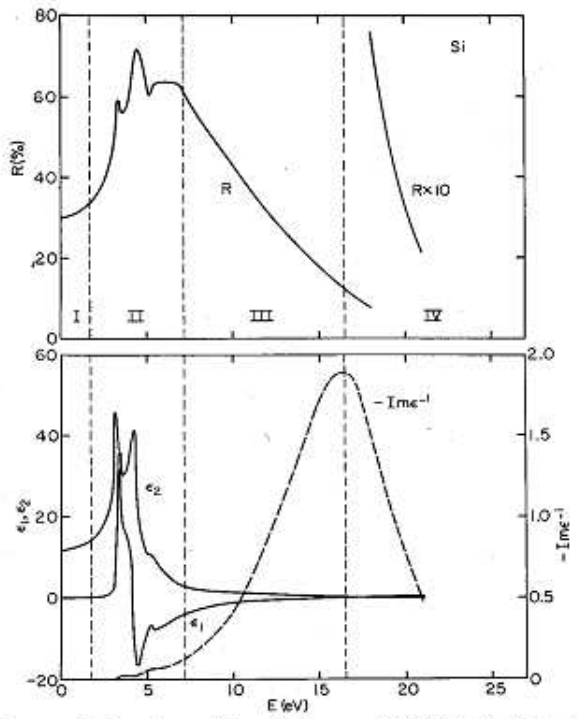

Fig. 3.7 The spectral dependence of the reflectance and dielectric functions of Si. Regions I, II, III, and IV correspond to the regions with the same designation shown in Figs. 3.1, 3.3, and 3.4. [H. R. Philipp and H. Ehrenreich, *Phys. Rev.* **129**. 1550 (1963).]

Figure 4.2.2: Dispersive properties of Si as manifested in graph of reflectance versus frequency (more specifically, $\hbar\nu$ in electron-volts) top, and real (ϵ_1) and imaginary (ϵ_2) parts of dielectric constant (in optical notation).

no pronounced absorption troughs or peaks in this frequency band.

Spectral character of optical response of metals and the Drude model

☐ Optical properties of metals are dominated by *conduction electrons*. Lorentz model applies equally well to metals, in which case, since electrons are unbound or "free", they experience zero restoring force and hence resonance frequency ω_0 is also zero. This is known as the *Drude model*.

☐ Drude model amounts to

$$\kappa_e(\omega) = 1 - \frac{\omega_p^2}{\omega^2 + i\Gamma\omega} \ , \tag{4.2.22}$$

(wherein Γ is the electron collision rate, which is the inverse of the mean electron collision time τ, and ω_p is the *plasma frequency*) $\Rightarrow$

$$\Re\kappa_e(\omega) = \kappa_e'(\omega) = 1 - \frac{\omega_p^2}{\omega^2 + \Gamma^2} = 1 - \frac{\omega_p^2\tau^2}{1 + \omega^2\tau^2} \ , \tag{4.2.23}$$

$$\Im\kappa_e(\omega) = \kappa_e{}''(\omega) = \omega_p^2 \frac{\Gamma/\omega}{\omega^2 + \Gamma^2} = \frac{\omega_p^2\tau}{\omega(1 + \omega^2\tau^2)} \ . \tag{4.2.24}$$

☐ Thus, *Drude model predicts dispersion and dissipation for metals.*

☐ Drude model implies that only plasma frequency should dictate appearance of metals. This works for many metals, e.g., zinc, but

does not explain why copper is red, gold is yellow and silver is colorless. In fact, appearance of these metals is characterized by an edge in reflectance spectrum, similar to that predicted by Drude model, but problem is that these three metals have same number of valence electrons. Also, calculated plasma frequency for all three should lie at about 9 eV, well outside visible region, so *the plasma frequency cannot in itself account for colors of Cu and Au.*

☐ Need *additional Lorentz oscillator* to account for their behavior.

☐ Combined effects of free electrons (Drude model) and bound electrons (Lorentz model) can account for reflectance properties of metal.

☐ Hence, $\kappa_e = \kappa_e^{free} + \kappa_e^{bound}$, wherein κ_e^{free} is described by Drude model (i.e., $\omega_0 = 0$ and κ_e^{bound} is described by Lorentz single oscillator model.

4.3 Acoustic/Elastic constitutive properties of materials

☐ Many materials respond to acoustic/elastic wave fields in much same way as they do to electromagnetic waves. This means that they are dissipative and exhibit dispersion.

☐ Since Lorentz theory was inspired by dynamic behavior of mechanical systems, it is not surprising that microscopic acoustic/elastic wave response of materials can be described by a generalized Lorentz model.

□ For instance, dynamic (e.g., shear) modulus $\mathcal{M}$ often exhibits multiple resonance/relaxation phenomena and can be represented by

$$\frac{\mathcal{M}(\omega)}{\mathcal{M}_R} = 1 - \sum_{l=1}^{L} \frac{b_l}{\omega^2 - \omega_l^2 + i\omega\Gamma_l} \ , \tag{4.3.25}$$

wherein $\mathcal{M}_R$ is a relaxed shear modulus, b_l a mode participation coefficient, ω_l the natural frequency of an "eigenmode", and $\Gamma_l = \frac{1}{\tau_l}$, τ_l the damping factor and relaxation time respectively of the l-th eigenmode.

■ Usually, it is difficult to determine b_l, ω_l and Γ_l from first principles, so that these parameters have to be reconstructed (i.e., *an inverse problem has to be solved*) by comparing (4.3.25) to experimental data concerning spectral properties of some response function such as particle displacement, velocity, or acceleration. A possible way of doing this for a SDOF model is described hereafter.

4.4 A method for solving inverse problem of determination of parameters of a SDOF system model

4.4.1 Statement of problem

□ In SDOF model, appear three parameters M, K and C which we propose to determine by processing data concerning, for instance, the acceleration.

□ As previously, mechanical system is driven by sinusoïdal function, i.e.,

$$F(t) = A\sin(\varpi t + \varphi) \ , \tag{4.4.26}$$

wherein *driving frequency ϖ is assumed to be known*, whereas *amplitude A and phase φ may be unknown* a priori.

□ Important to underline this point, as it is very often assumed, or implied, that, on contrary, solicitation is completely known.

■ Thus, determination of certain aspects of solicitation is also a part of inverse problem.

□ This solicitation produces a response embodied in time history of acceleration

$$\mathcal{H} := \{\ddot{x}(t) \ ; \ 0 \leq t \leq T\} \ , \tag{4.4.27}$$

wherein T is (known) duration of record. $\mathcal{H}$ is *data of inverse problem.*

4.4.2 Time history of displacement and acceleration for general solicitation

Recall:

$$x(\omega) = \frac{F(\omega)}{-M\omega^2 - i\omega C + K} = \frac{-M^{-1}F(\omega)}{\omega^2 - \Omega^2 + i\frac{\omega C}{M}} \ . \tag{4.4.28}$$

wherein

$$G(\omega) := -M\left(\omega^2 - \Omega^2 + i\frac{\omega C}{M}\right) \ . \tag{4.4.29}$$

$\Rightarrow$

$$x(t) = 2\Re\int_0^\infty \frac{F(\omega)}{G(\omega)}e^{-i\omega t}d\omega \ , \tag{4.4.30}$$

$$\ddot{x}(t) = -2\Re\int_0^\infty \omega^2\frac{F(\omega)}{G(\omega)}e^{-i\omega t}d\omega \ . \tag{4.4.31}$$

4.4.3 Spectrum of sinusoidal solicitation

$\square$ Spectrum of solicitation $F(t)$:

$$F(\omega) = \frac{1}{2\pi}\int_{-\infty}^{\infty} F(t)e^{i\omega t}dt \ , \tag{4.4.32}$$

so that, for sinusoidal excitation:

$$F(\omega) = \frac{A}{2i}\left[\delta(\omega+\varpi)e^{i\varphi} - \delta(\omega-\varpi)e^{-i\varphi}\right] \ , \tag{4.4.33}$$

wherein $\delta(\ )$ is delta distribution, so that (since $\varpi \geq 0$)

$$F(\omega) = -\frac{A}{2i}\delta(\omega-\varpi)e^{-i\varphi} \ \ ; \ \ \omega \geq 0 \ . \tag{4.4.34}$$

4.4.4 Time history of acceleration for a sinusoidal solicitation

□ Introduction of (4.4.34) into (4.4.31) ⇒

$$\ddot{x}(t) = \Re\frac{A}{i}\int_0^\infty \omega^2 \frac{\delta(\omega-\varpi)e^{-i\varphi}}{G(\omega)} e^{-i\omega t} d\omega =$$
$$-A\Re i\varpi^2 \frac{e^{-i(\varpi t+\varphi)}}{G(\varpi)} = -A\frac{\varpi^2}{\|G\|^2}[G_r \sin(\varpi t+\varphi)+G_i\cos(\varpi t+\varphi)] \ , \tag{4.4.35}$$

wherein

$$G_r = -M\left(\varpi^2-\Omega^2\right) \ , \ G_i = -M\frac{\varpi C}{M} = -\varpi C \ , \ \|G\|^2 = G_r^2+G_i^2 \ . \tag{4.4.36}$$

⇒

$$\ddot{x}(t) = \frac{A}{M}\frac{\varpi^2}{\left[\left(\varpi^2-\Omega^2\right)^2+\left(\frac{\varpi C}{M}\right)^2\right]}\times$$
$$\left[\left(\varpi^2-\Omega^2\right)\sin(\varpi t+\varphi)+\left(\frac{\varpi C}{M}\right)\cos(\varpi t+\varphi)\right] \ , \tag{4.4.37}$$

□ Thus, seen that $\ddot{x}(t)$ is function of *internal parameters* C/M, $\Omega^2 = K/M$, and *external parameters* ϖ, A/M and φ. Since ϖ assumed to be known, $\ddot{x}(t)$ is function of *four unknown parameters*, i.e.,

$$\ddot{x}(t) = \ddot{x}(t;\varpi;C/M,K/M,A/M,\varphi) \ . \tag{4.4.38}$$

■ $\ddot{x}(t)$ is *nonlinear* function of three parameters C/M, K/M, φ and *linear* function of remaining parameter A/M. Means that will probably be easier to retrieve A/M than C/M, K/M, φ.

4.4.5 Particular features of time history of displacement for a sinusoidal solicitation

□ Refer to sect. 4.4.4: displacement time history for a sinuosoidal solicitation is:

$$x(t) = \frac{A}{M} \frac{1}{\left[\left(\varpi^2 - \Omega^2 \right)^2 + \left(\frac{\varpi C}{M} \right)^2 \right]} \times \left[- \left(\varpi^2 - \Omega^2 \right) \sin(\varpi t + \varphi) - \left(\frac{\varpi C}{M} \right) \cos(\varpi t + \varphi) \right] \ , \quad (4.4.39)$$

Define *three asymptotic regimes*:

1. $\varpi << \Omega$,
2. $\varpi \approx \Omega$,
3. $\varpi >> \Omega$,

that correspond to driving frequencies that are low, resonance and high respectively.

□ *low frequency* (L) asymptotic form of $x(t)$:

$$x(t) \sim x_L(t) := \frac{A}{M} \frac{1}{\Omega^2} \sin(\varpi t + \varphi) = \frac{F(t)}{M\Omega^2} \quad ; \quad \varpi << \Omega \ , \quad (4.4.40)$$

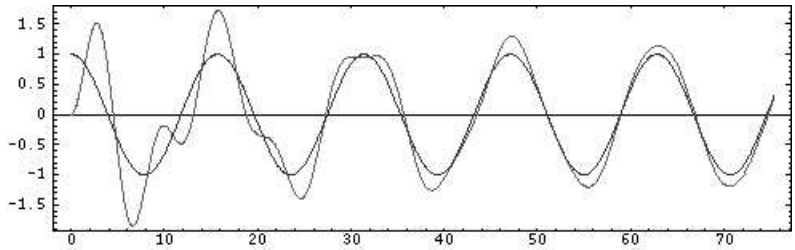

Figure 4.4.1: Time history of displacement in low frequency regime. Ordinates represent x and abcissas t. Black (sinusoidal) curve corresponds to solicitation and grey curve to displacement response.

which shows that in L regime, displacement response tends to be *in phase* with solicitation for relatively-large t. This is confirmed in numerical result depicted in fig. 4.4.1. Note also that in L regime, displacement response is independent of C, and is all the larger the smaller is M, for large-enough t.

□ In *resonance* (R) regime , $x(t)$ is of form:

$$x(t) \sim x_R(t) := \frac{A}{\Omega C} \cos(\varpi t + \varphi) \quad ; \quad \varpi \approx \Omega \ , \tag{4.4.41}$$

which shows that in R regime, displacement response tends to be out of phase by $\pi/2$ with solicitation for relatively-large t. This is confirmed in numerical result depicted in fig. 4.4.2. Note also that in R regime, displacement response is independent of M, and is all the larger the smaller is C, for large-enough t.

□ In *high frequency* (H) regime, $x(t)$ is of form:

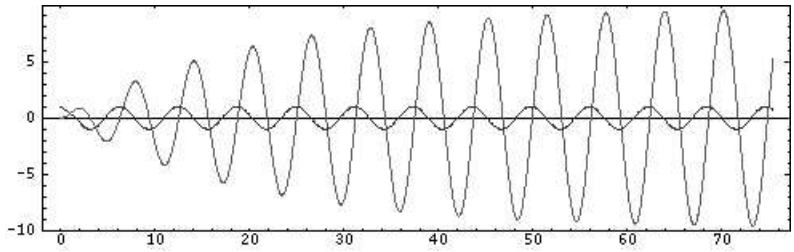

Figure 4.4.2: Time history of displacement in near-resonant frequency regime. Ordinates represent x and abcissas t. Black (sinusoidal) curve corresponds to solicitation and grey curve to displacement response.

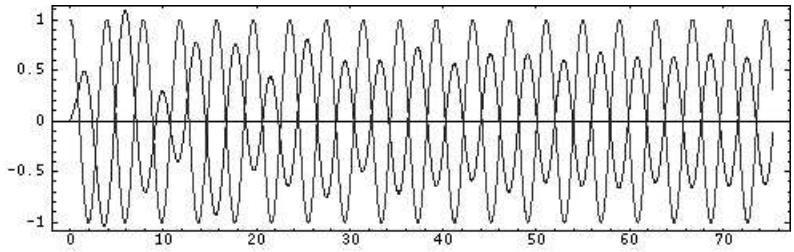

Figure 4.4.3: Time history of displacement in high frequency regime. Ordinates represent x and abcissas t. Black (sinusoidal) curve corresponds to solicitation and grey curve to displacement response.

$$x(t) \sim x_H(t) := -\frac{A}{M\varpi^2}\sin(\varpi t + \varphi) = \frac{-1}{M\varpi^2}F(t) \quad ; \quad \varpi >> \Omega \ , \tag{4.4.42}$$

which shows that in H regime, displacement response tends to be out of phase by π with solicitation for relatively-large t. This is confirmed in numerical result depicted in fig. 4.4.3. Note also that in H regime, displacement response is independent of C, and is all the larger the smaller is M, for large-enough t.

□ Same type of asymptotic forms apply to acceleration response and phase relations of latter to solicitation are same as for displacement

response.

4.4.6 Retrieval of C/M, K/M, A and φ from data pertaining to time history of acceleration

☐ Term *estimator* designates theoretical model of data that is employed for comparison to actual data during reconstruction of unknown parameters.

☐ Let $\tilde{\ddot{x}}(t;\varpi;c/m,k/m,a,\phi)$ be estimator for *trial values* c/m, k/m, a, ϕ of C/M, K/M, A/M and φ respectively.

☐ Let $\hat{\ddot{x}}(t;\varpi;C/M,K/M,A/M,\varphi)$ be *measured data* for the *actual values* of the four parameters C/M, K/M, A and φ respectively.

☐ Possible manner of obtaining C/M, K/M, A/M and φ is by varying *trial parameters* c/m, k/m, a/m, ϕ so as to *minimize cost function*

$$J_1(T,\varpi;C/M,K/M,A/M,\varphi) = \int_0^T \Big|\hat{\ddot{x}}(t;\varpi;C/M,K/M,A/M,\varphi) - \tilde{\ddot{x}}(t;\varpi;c/m,k/m,a/m,\phi)\Big|^2 dt \ , \quad (4.4.43)$$

it being understood that when J attains a (relative or absolute) minimum, current values of c/m, k/m, a/m, ϕ constitute a possible solution of problem, i.e., are possibly close to C/M, K/M, A/M, φ.

☐ This strategy might not be sufficient to obtain a stable, unique solution.

☐ Another strategy is to increase amount of data by exciting system with sinuoïds having a variety of *known frequencies* ϖ_1, ϖ_2, ..., ϖ_N. Then, this second manner for obtaining C/M, K/M, A/M and φ is by varying trial parameters c/m, k/m, a/m, ϕ so as to minimize cost function

$$J_N(T, \varpi; C/M, K/M, A_1/M, \varphi_1, A_2/M, \varphi_2, ..., A_N/M, \varphi_N) = \sum_{n=1}^{N} \int_0^T \left| \hat{\ddot{x}}(t; \varpi_n; C/M, K/M, A_n/M, \varphi_n) - \tilde{\ddot{x}}(t; \varpi_n; c/m, k/m, a_n/M, \phi_n) \right|^2 dt \ . \quad (4.4.44)$$

☐ Success of inversion by *minimization of cost function* depends not only on N but also on duration T of measured signal.

☐ Fact of increasing number of realizations (from 1 to $N > 1$) also increases number of unknowns A_n/M and φ_n so that not obvious that this will make reconstruction of C/M, K/M more stable and unique.

☐ Interesting question: to what extent reconstruction of C/M, K/M becomes more stable and unique with increased a priori knowledge

of Ω and/or C/M and/or A/M and/or φ?

□ As a general rule, the closer are the initial values of c/m, k/m, a/m, ϕ to actual values of C/M, K/M, A/M, φ, the greater are the chances of obtaining convergence of iterative scheme, inherent in reconstruction process, to correct values of unknown parameters.

4.4.7 Retrieval of K,M and C from data pertaining to time histories of displacement response for low, resonance, and high frequency solicitations

□ Inversion methods outlined in previous section are subject to all pitfalls of numerical minimization schemes and have disadvantage of being purely numerical in nature, this meaning that they do not take account of salient mathematical features of response of system.

□ Idea: make use of such features and thereby carry out inversion in simple, explicit manner.

■ Done by employing asymptotic forms $x_L(t)$, $x_R(t)$ and $x_H(t)$ (given in sect. 4.4.5) of displacement in response to low, resonance, and high frequency solicitations $F_L(t)$, $F_R(t)$ and $F_H(t)$ respectively.

4.5 Use of microscopic dynamic response functions as well as homogeneization in direct problems of diffraction by targets

4.5.1 Introduction

□ For a large class of bounded 3D targets, diffracted field far from target expressed by

$$p^d(\mathbf{x}) := p(\mathbf{x}) - p^i(\mathbf{x}) \sim S(\theta,\phi)\frac{i}{k_c r}e^{ik_c r} \quad ; \quad k_c r \to \infty \ , \quad (4.5.45)$$

wherein k_c is wavenumber in host medium, r the radial distance from origin located near the barycenter of target to observation point, and $\theta,\ \phi$ the angular variables in spherical coordinate system.

☐ All material and geometrical parameters concerning target are contained in complex far-field scattering function $S(\theta,\phi)$, so that to solve *direct* scattering problem (i.e., that of predicting far-field response of target to an incident wave), one must specify these parameters.

☐ If one assumes target to be linear, isotropic, and *homogeneous*, one of material parameters will surely be wavenumber k_d of medium inside target. As most real materials are dispersive and dissipative, something like Lorentz (SDOF or MDOF) theory will have to be employed to provide this wavenumber.

☐ Prior to this, parameters that enter into Lorentz theory will have to be identified (i.e., an inverse problem will have to be solved) by processing experimentally-observed response of material of target, obtained by employing a suitably-chosen specimen form (e.g., slab or layer).

☐ If, on other hand, target is linear, isotropic, and *inhomogeneous*, and choice is made to homogenize this medium, then *effective wavenumber* k_e will have to be employed to compute $S(\theta,\phi)$.

☐ Assuming that heterogeneity is characterized by an assembly of small inclusions in which wavenumber is k_d, located within a medium in which wavenumber is k_c, homogenization procedure will provide an expression for k_e in terms of k_d and k_c, and at least one other parameter ϕ which is concentration (i.e., volume fraction) of inclusions.

☐ Assuming k_c is known a priori, there remains (inverse) problem of identifying k_d and ϕ. Once again, this can be done by processing experimentally-observed response of material of target, obtained by employing a suitably-chosen specimen form (e.g., slab or layer).

☐ In optics community, very common to employ an expression for $k_e = \omega(\mu\varepsilon)^{1/2} = \frac{\omega}{c_0}(\varepsilon_e\varepsilon_m)^{1/2} \approx \frac{\omega}{c_0}(\varepsilon_e)^{1/2}$ derived from ε_e obtained from Maxwell-Garnett (M-G) theory.

☐ This is questionable procedure, since optics is dynamical phenomenon, whereas Maxwell-Garnett theory is based on a static (electromagnetic) theory.

☐ Better choice: replace Maxwell-Garnett theory by Urick-Ament (U-A) theory which applies to dynamical regime.

☐ Whether one chooses M-G, U-A or other theories to derive expression for k_e, there remains problem of introducing suitable values for k_d in dynamical regime constituted by optics (similar problem arises in acoustics and elastodynamics).

□ Once again, can be done by using Lorentz description, and again one is faced with inverse problem of obtaining parameters of this description by processing response data of a suitable specimen of material of which are composed the inclusions (a similar problem would occur if k_c were not known a priori).

4.5.2 Homogeneous and inhomogeneous targets

■ Thus, for *direct* diffraction problems in dynamical regime involving a macroscopic, dispersive and dissipative (as is usually case) target:

- *if target is homogeneous* at chosen scale of observation, one first has to determine $k_d(\omega)$ by employing Lorentz-like model, parameters of which have to be determined by (solving an inverse problem) processing response data for suitable specimen (often slab-shaped (fig. 4.1.1)) of material of which target is composed,
- *if target is inhomogeneous* at chosen scale of observation, one first has to determine $k_e(\omega)$ (which replaces $k_d(\omega)$ of previous configuration) by employment of an effective medium theory such as ones of M-G or U-A. In these theories, at least two parameters $k_d(\omega)$ (wavenumber in inclusions) and ϕ (concentration of inclusions) appear which have to be identified beforehand. As for $k_d(\omega)$, this can be done, first by employing a Lorentz-like theory, and then by identifying parameters of this theory by (solving another inverse problem) processing response data for suitable specimen (often slab-shaped (fig. 4.1.1)) of material of which inclusions are composed.

Chapter 5

Acoustic identification of a rough interface between two fluid-filled half spaces

5.1 Features of inverse problem

□ Object: 2D fluid acoustical inverse problem illustrated in fig. 5.1.1.

□ In absence of roughness, configuration is that of a half space domain $\overline{\Omega}_1$ filled with a known homogeneous fluid M^1 with (spatially-constant) acoustic parameters (k^1, ρ^1), separated by flat, horizontal interface $\overline{\Gamma} = \Gamma^g \cup \Gamma^0 \cup \Gamma^d$ (wherein Γ^g, Γ^0, Γ^d are flat, horizontal segments) from half-infinite domain $\overline{\Omega}_0$ filled with a known homogeneous fluid M^0 with (spatially-constant) acoustic parameters (k^0, ρ^0).

■ *In presence of roughness*, localized in domain Γ^c described by parametric equation $x_2 = f(x_1)$, interface is $\Gamma = \Gamma^g \cup \Gamma^c \cup \Gamma^d$.

■ Problem is to identify Γ^c from measurements of pressure field in subdomains of Ω_0^{d1}, Ω_0^{d2},..., $\Omega_0^{dM_0}$ of Ω_0 when configuration is probed by cylindrical waves radiated by cylindrical sources having supports

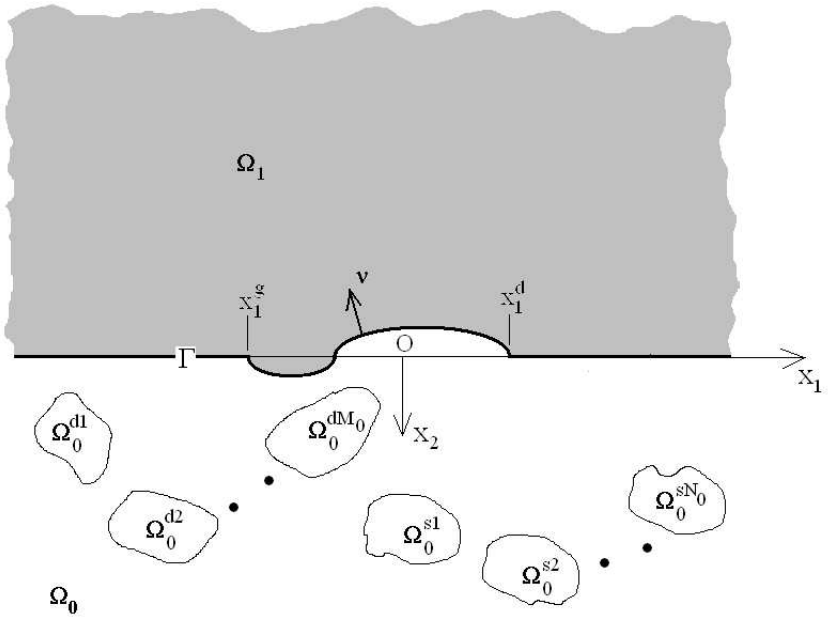

Figure 5.1.1: Configuration, in cross-section plane, corresponding to inverse problem of identification of rough interface between two homogeneous fluid-like half spaces, probed by waves radiated by a set of cylindrical sources located in lower half space.

Ω_0^{s1}, Ω_0^{s2},..., $\Omega_0^{sN_0}$ in Ω_0.

☐ Γ separates half-infinite domain $\Omega_0 \supset \overline{\Omega}_0$ filled with a known homogeneous fluid M^0 with (spatially-constant) acoustic parameters (k^0, ρ^0) from half-infinite domain $\Omega_1 \supset \overline{\Omega}_1$ filled with a known homogeneous fluid M^1 with (spatially-constant) acoustic parameters (k^1, ρ^1).

☐ Note that each experimental realization is conducted with only one source radiating at a time and measurements of pressure field are made in any or all of subdomains Ω_0^{d1}, Ω_0^{d2},..., $\Omega_0^{dM_0}$ of Ω_0 for n_0-th incident-wave-in-Ω_0 realization.

5.2 Governing equations for scattering from a rough interface separating a homogeneous half space separated from another half space, probed by a cylindrical wave radiated by a cylindrical source whose support is $\Omega_0^{sn_0}$

☐ Governing equations for pressure field:

$$\left[\triangle + \left(k^0\right)^2\right] p^{0n}(\mathbf{x}, \omega) = -s^{0n}(\mathbf{x}) \;\; ; \;\; \mathbf{x} \in \Omega_0 \;, \tag{5.2.1}$$

$$\left[\triangle + \left(k^1\right)^2\right] p^{1n}(\mathbf{x}, \omega) = 0 \;\; ; \;\; \mathbf{x} \in \Omega_1 \;, \tag{5.2.2}$$

$$p^{0n}(\mathbf{x}, \omega) - p^{1n}(\mathbf{x}, \omega) = 0 \;\; ; \;\; \mathbf{x} \in \Gamma \;, \tag{5.2.3}$$

$$\frac{1}{\rho^0}\boldsymbol{\nu}(\mathbf{x})\cdot\nabla p^{0n}(\mathbf{x},\omega)-\frac{1}{\rho^1}\boldsymbol{\nu}(\mathbf{x})\cdot\nabla p^{1n}(\mathbf{x},\omega)=0\ \ ;\ \ \mathbf{x}\in\Gamma\ , \tag{5.2.4}$$

$$p^{0n}(\mathbf{x},\omega)\sim\text{outgoing waves}\ ,\ \mathbf{x}\in\Omega_0\ ,\ \|\mathbf{x}\|\to\infty\ , \tag{5.2.5}$$

$$p^{1n}(\mathbf{x},\omega)\sim\text{outgoing waves}\ ,\ \mathbf{x}\in\bar{\Omega}_1\ ,\ \|\mathbf{x}\|\to\infty\ , \tag{5.2.6}$$

(wherein $n=n_0$) and $\boldsymbol{\nu}$ is unit vector normal to Γ). Note that there are N_0 of these sets of equations for realizations $n_0=1,2,...,N_0$.

5.3 Governing equations for specific Green's function

□ Governing equations:

$$\left[\triangle+\left(K(\mathbf{x})\right)^2\right]g(\mathbf{x},\mathbf{z},\omega)=-\delta(\mathbf{x}-\mathbf{z})\ \ ;\ \ \mathbf{x}\in\mathbb{R}^2\ ,\ \mathbf{z}\in\mathbb{R}^2\ , \tag{5.3.7}$$

$$K(\mathbf{x})=\begin{cases}k^0\ \ ;\ \mathbf{x}\in\overline{\Omega}_0\\ k^1\ \ ;\ \mathbf{x}\in\overline{\Omega}_1\end{cases}\ , \tag{5.3.8}$$

$$g(\mathbf{x},\mathbf{z},\omega)=\begin{cases}g^0(\mathbf{x},\mathbf{z},\omega)\ \ ;\ \mathbf{x}\in\overline{\Omega}_0\\ g^1(\mathbf{x},\mathbf{z},\omega)\ \ ;\ \mathbf{x}\in\overline{\Omega}_1\end{cases}\ , \tag{5.3.9}$$

$$g^0(\mathbf{x},\mathbf{z},\omega) - g^1(\mathbf{x},\mathbf{z},\omega) = 0 \;\; ; \;\; \mathbf{x} \in \overline{\Gamma} \; , \tag{5.3.10}$$

$$\frac{1}{\rho^0}\boldsymbol{\nu}(\mathbf{x})\cdot\nabla g^0(\mathbf{x},\mathbf{z},\omega) - \frac{1}{\rho^1}\boldsymbol{\nu}(\mathbf{x})\cdot\nabla g^1(\mathbf{x},\mathbf{z},\omega) = 0 \; ; \; \mathbf{x} \in \overline{\Gamma} \, , \tag{5.3.11}$$

$$g(\mathbf{x},\mathbf{z},\omega) \sim \text{outgoing waves} \; , \; \mathbf{x} \in \overline{\Omega}_0 \; , \; \|\mathbf{x}\| \to \infty \; . \tag{5.3.12}$$

$$g(\mathbf{x},\mathbf{z},\omega) \sim \text{outgoing waves} \; , \; \mathbf{x} \in \overline{\Omega}_1 \; , \; \|\mathbf{x}\| \to \infty \; . \tag{5.3.13}$$

□ Henceforth we drop ω dependence of various field quantites.

5.4 Towards an integral representation of pressure field in Ω_0 for n-th realization

□ In obvious short-hand notation, we obtain from previous governing equations:

$$g^0 \left[\Delta + \left(k^0\right)^2\right] p^{0n} = -g^0 s^{0n} \;\; ; \;\; \text{in } \Omega_0 \; , \tag{5.4.14}$$

$$p^{0n} \left[\Delta + \left(k^0\right)^2\right] g^0 = -p^{0n}\delta \;\; ; \;\; \text{in } \Omega_0 \; , \tag{5.4.15}$$

so that after use of Green's theorem and sifting property of δ function:

$$\int_{\Gamma}(g^0\partial_\nu p^{0n} - p^{0n}\partial_\nu g^0)d\gamma + \int_{\Omega_0} g^0 s^{0n} d\varpi = \mathcal{H}_{\Omega_0}(\mathbf{z})p^{0n}(\mathbf{z}) \ , \quad (5.4.16)$$

wherein $\partial_\nu \mathcal{F} := \boldsymbol{\nu}(\mathbf{x})\cdot\nabla\mathcal{F}(\mathbf{x})$, $d\gamma$ is differential element of arc length, and $d\varpi$ differential element of area.

□ From fact that Γ is composite

$$\frac{\rho^1}{\rho^0}\int_{\Gamma^g+\Gamma^d}(g^0\partial_\nu p^{0n} - p^{0n}\partial_\nu g^0)d\gamma + \frac{\rho^1}{\rho^0}\int_{\Gamma^c}(g^0\partial_\nu p^{0n} - p^{0n}\partial_\nu g^0)d\gamma + \frac{\rho^1}{\rho^0}\int_{\Omega_0} g^0 s^{0n} d\varpi = \frac{\rho^1}{\rho^0}\mathcal{H}_{\Omega_0}(\mathbf{z})p^{0n}(\mathbf{z}) \ . \quad (5.4.17)$$

5.5 Towards an integral representation of pressure field in Ω_1 for n-th realization

□ In obvious short-hand notation, we obtain from previous governing equations:

$$g^1\left[\Delta + \left(k^1\right)^2\right]p^{1n} = 0 \ \ ; \ \ \text{in } \Omega_1 \ , \quad (5.5.18)$$

$$p^{1n}\left[\Delta + \left(k^1\right)^2\right]g^1 = -p^{1n}\delta \ \ ; \ \ \text{in } \Omega_1 \ , \quad (5.5.19)$$

so that after use of Green's theorem and sifting property of δ function:

$$-\int_{\Gamma}(g^1\partial_\nu p^{1n}-p^{1n}\partial_\nu g^1)d\gamma=\mathcal{H}_{\Omega_1}(\mathbf{z})p^{1n}(\mathbf{z})\ . \tag{5.5.20}$$

□ On account of transmission conditions (5.2.3)-(5.2.4), we can write

$$-\int_{\Gamma}\left(g^1\frac{\rho^1}{\rho^0}\partial_\nu p^{0n}-p^{0n}\partial_\nu g^1\right)d\gamma=\mathcal{H}_{\Omega_1}(\mathbf{z})p^{1n}(\mathbf{z})\ . \tag{5.5.21}$$

□ From fact that Γ is composite, we have

$$\begin{aligned}-\int_{\Gamma^g+\Gamma^d}\left(g^1\frac{\rho^1}{\rho^0}\partial_\nu p^{0n}-p^{0n}\partial_\nu g^1\right)d\gamma-\\ \int_{\Gamma^c}\left(g^1\frac{\rho^1}{\rho^0}\partial_\nu p^{0n}-p^{0n}\partial_\nu g^1\right)d\gamma=\mathcal{H}_{\Omega_1}(\mathbf{z})p^{1n}(\mathbf{z})\ ,\end{aligned} \tag{5.5.22}$$

or, after use of transmission conditions(5.3.10)-(5.3.11),

$$\begin{aligned}-\frac{\rho^1}{\rho^0}\int_{\Gamma^g+\Gamma^d}\left(g^0\frac{\rho^1}{\rho^0}\partial_\nu p^{0n}-p^{0n}\partial_\nu g^0\right)d\gamma-\\ \int_{\Gamma^c}\left(g^1\frac{\rho^1}{\rho^0}\partial_\nu p^{0n}-p^{0n}\partial_\nu g^1\right)d\gamma=\mathcal{H}_{\Omega_1}(\mathbf{z})p^{1n}(\mathbf{z})\ ,\end{aligned} \tag{5.5.23}$$

5.6 Integral representations, without boundary terms on $\Gamma^g + \Gamma^d$, of pressure fields in Ω_0 and Ω_1 for n-th realization

□ Addition of (5.4.16) and (5.5.23) gives

$$\int_{\Gamma^c} \left[\frac{\rho^1}{\rho^0}(g^0 - g^1) - \left(\frac{\rho^1}{\rho^0}\partial_\nu p^{0n} - \partial_\nu g^1 \right) p^{0n} \right] d\gamma + \frac{\rho^1}{\rho^0} \int_{\Omega_0} g^0 s^{0n} d\varpi = \frac{\rho^1}{\rho^0}\mathcal{H}_{\Omega_0}(\mathbf{z}) p^{0n}(\mathbf{z}) + \mathcal{H}_{\Omega_1}(\mathbf{z}) p^{1n}(\mathbf{z}) \ , \quad (5.6.24)$$

or

$$\mathcal{H}_{\Omega_0}(\mathbf{z}) p^{0n}(\mathbf{z}) + \frac{\rho^0}{\rho^1}\mathcal{H}_{\Omega_1}(\mathbf{z}) p^{1n}(\mathbf{z}) = \int_{\Omega_0} g^0 s^{0n} d\varpi + \int_{\Gamma^c} \left[(g^0 - g^1)\partial_\nu p^{0n} - p^{0n} \left(\partial_\nu g^{0n} - \frac{\rho^0}{\rho^1}\partial_\nu g^1 \right) \right] d\gamma \ , \quad (5.6.25)$$

from which it ensues, on account of properties of domain Heaviside function:

$$p^{0n}(\mathbf{z}) = \int_{\Omega_0} g^0 s^{0n} d\varpi + \int_{\Gamma^c} \left[(g^0 - g^1)\partial_\nu p^{0n} - p^{0n} \left(\partial_\nu g^{0n} - \frac{\rho^0}{\rho^1}\partial_\nu g^1 \right) \right] d\gamma \quad ; \quad \mathbf{z} \in \Omega_0 \ , \quad (5.6.26)$$

$$p^{1n}(\mathbf{z}) = \frac{\rho^1}{\rho^0}\int_{\Omega_0} g^0 s^{0n} d\varpi + \frac{\rho^1}{\rho^0}\int_{\Gamma^c}\left[(g^0-g^1)\partial_\nu p^{0n} - p^{0n}\left(\partial_\nu g^{0n} - \frac{\rho^0}{\rho^1}\partial_\nu g^1\right)\right] d\gamma \quad ; \quad \mathbf{z}\in\Omega_1 \ . \tag{5.6.27}$$

■ Note that it is use of a specific Green's function that has enabled elimination of bothersome boundary terms on half-infinite segments Γ^g and Γ^d (which appear in final expressions of field in method employing free-space Green's functions G^0 and G^1).

□ Another advantage of use of specific Green's function is that zeroth-order Kirchhoff (ZOK) approximations, obtained by neglecting integral over Γ^c in (5.6.26)-(5.6.27), are certainly better approximations than ZOK approximations arising from use of G^0 and G^1 due to fact that latter contain no information about basic configuration (flat interface separating M^0 from M^1), whereas g^0 does contain this information.

5.7 State equations for N_0 incident wave realizations

□ Recall that a given realization is characterized by an incident wave radiated by a source in Ω_0. Thus, from (5.6.25) we get:

$$\frac{1}{2}\left(p^{0n}(\mathbf{z})+\frac{\rho^0}{\rho^1}p^{1n}(\mathbf{z})\right)=\int_{\Omega_0}g^0s^{0n}d\varpi+\int_{\Gamma^c}(g^0-g^1)\partial_{\nu_x}p^{0n}d\gamma-$$
$$pv\int_{\Gamma^c}p^{0n}\left(\partial_{\nu_x}g^{0n}-\frac{\rho^0}{\rho^1}\partial_{\nu_x}g^1\right)d\gamma\ \ ;\ \ \mathbf{z}\in\Gamma^c\ \ ;\ n_0=1,2,...,N_0\ , \tag{5.7.28}$$

wherein pv designates a Cauchy principal value.

□ After use of boundary condition (5.2.3) we find

$$\frac{1}{2}\left(1+\frac{\rho^0}{\rho^1}p^{0n}(\mathbf{z})\right)=\int_{\Omega_0}g^0s^{0n}d\varpi+\int_{\Gamma^c}(g^0-g^1)\partial_{\nu_x}p^{0n}d\gamma-$$
$$pv\int_{\Gamma^c}p^{0n}\left(\partial_{\nu_x}g^{0n}-\frac{\rho^0}{\rho^1}\partial_{\nu_x}g^1\right)d\gamma\ \ ;\ \ \mathbf{z}\in\Gamma^c\ \ ;\ n_0=1,2,...,N_0\ . \tag{5.7.29}$$

□ Furthermore, from (5.6.25) we obtain

$$\frac{1}{2}\left(\partial_{\nu_z}p^{0n}(\mathbf{z})+\frac{\rho^0}{\rho^1}\partial_{\nu_z}p^{1n}(\mathbf{z})\right)=\int_{\Omega_0}\partial_{\nu_z}g^0s^{0n}d\varpi+$$
$$pv\int_{\Gamma^c}(\partial_{\nu_z}g^0-\partial_{\nu_z}g^1)\partial_{\nu_x}p^{0n}d\gamma-$$
$$fp\int_{\Gamma^c}p^{0n}\left(\partial_{\nu_z}\partial_{\nu_x}g^{0n}-\frac{\rho^0}{\rho^1}\partial_{\nu_z}\partial_{\nu_x}g^1\right)d\gamma\ \ ;$$
$$\mathbf{z}\in\Gamma^c\ \ ;\ n_0=1,2,...,N_0\ , \tag{5.7.30}$$

wherein fp designates a Hadamard finite part.

□ After use of boundary condition (5.2.4) we obtain

$$\partial_{\nu_z} p^{0n}(\mathbf{z}) = \int_{\Omega_0} \partial_{\nu_z} g^0 s^{0n} d\varpi + pv \int_{\Gamma^c} (\partial_{\nu_z} g^0 - \partial_{\nu_z} g^1) \partial_{\nu_x} p^{0n} - fp \int_{\Gamma^c} p^{0n} \left(\partial_{\nu_z} \partial_{\nu_x} g^{0n} - \frac{\rho^0}{\rho^1} \partial_{\nu_z} \partial_{\nu_x} g^1 \right) d\gamma \ ; \quad \mathbf{z} \in \Gamma^c \ ; \ n_0 = 1, 2, ..., N_0 \ . \quad (5.7.31)$$

□ Eqs. (5.7.29) and (5.7.31) represent a *coupled* set of $2N_0$ second-kind integral equations for unknown functions $p^{0n_0}(\mathbf{x})$; $\mathbf{x} \in \Gamma^c$; $n_0 = 0, 1, 2, ..., N_0$ and $\partial_{\nu_x} p^{0n}(\mathbf{x})$; $\mathbf{x} \in \Gamma^c$; $n_0 = 0, 1, 2, ..., N_0$.

□ Each of members of this set is called a *state equation* or *coupling equation*.

□ Note that sources were assumed to be wholly in Ω_0.

5.8 Data equations for M_0 measurement domains

□ Recall that it was assumed that data is obtained in subdomains $\Omega_0^{dm_0}$; $m_0 = 1, 2, ..., M_0$ of Ω_0 for n_0-th incident wave realization (actually, M_0, as well as locations and sizes of data-gathering domains, could conceivably vary with n_0, but we will assume that this is not case).

□ From (5.6.26) we get, for n-th (i.e., n_0-th) incident wave realization:

$$p^{0n}(\mathbf{z}) = \int_{\Omega_0} g^0 s^{0n} d\varpi + \int_{\Gamma^c} \left[(g^0 - g^1)\partial_\nu p^{0n} - p^{0n} \left(\partial_{\nu_x} g^{0n} - \frac{\rho^0}{\rho^1} \partial_{\nu_x} g^1 \right) \right] d\gamma \ ; \quad \mathbf{z} \in \Omega_0^{dm_0} \ ; \ m_0 = 1, 2, ..., M_0 \ , \quad (5.8.32)$$

which represents a set of M_0 first-kind integral equations for unknown function (i.e., parametric equation $x_2 = f(x_1)$ associated with Γ^c (latter is indicator of roughness of interface).

□ Each of members of this set is called a *data equation* or *propagation equation*.

□ Note, that to solve each such equation, we must determine functions $p^{0n_0}(\mathbf{x})$; $\mathbf{x} \in \Gamma^c$; $n_0 = 0, 1, 2, ..., N_0$ and $\partial_{\nu_x} p^{0n}(\mathbf{x})$; $\mathbf{x} \in \Gamma^c$; $n_0 = 0, 1, 2, ..., N_0$ via (5.7.29) and (5.7.31), and to solve latter, we must first determine Γ_c.

■ This goes to show that inverse problem reduces to determination of not one function (i.e., one associated with Γ_c, but rather $2N_0 + 1$ functions (i.e., Γ_c, $p^{0n_0}(\mathbf{x})$; $\mathbf{x} \in \Gamma^c$; $n_0 = 0, 1, 2, ..., N_0$ and $\partial_{\nu_x} p^{0n}(\mathbf{x})$; $\mathbf{x} \in \Gamma^c$; $n_0 = 0, 1, 2, ..., N_0$).

5.9 Zeroth- order Kirchhoff approximation in state equations

□ Each one of set of state equations (5.7.29) and (5.7.31) can, in context of forward-scattering problem, be resolved by an iterative process, but since we are here interested in solving inverse problem, we shall content ourselves with an *approximate solution of each state equation.*

■ This solution is obtained by neglecting integrals over Γ^c and is expressed by

$$p^{0n}(\mathbf{z}) = \frac{2}{\left(1+\frac{\rho^0}{\rho^1}\right)} \int_{\Omega_0} g^0 s^{0n} d\varpi \;\; ; \;\; \mathbf{z} \in \Gamma^c \;\; ; \;\; n_0 = 1, 2, ..., N_0 \; , \tag{5.9.33}$$

$$\partial_{\nu_z} p^{0n}(\mathbf{z}) = \int_{\Omega_0} \partial_{\nu_z} g^0 s^{0n} d\varpi \;\; ; \;\; \mathbf{z} \in \Gamma^c \;\; ; \;\; n_0 = 1, 2, ..., N_0 \; , \tag{5.9.34}$$

■ These will be recognized to be expression of *zeroth-order Kirchhoff (ZOK) approximation*, and are equivalent to exact solution of direct problem of scattering of a cylindrical wave arising from sources s^{0n_0} by a flat interface between two homogeneous half-spaces.

5.10 Use of zeroth-order Kirchhoff approximation in data equations

□ Introducing (5.9.33)-(5.9.34) into (5.8.32) leads to following approximations for each source in Ω_0:

$$p^{0m_0}(\mathbf{z}) \approx \int_{\Omega_0} g^0(\mathbf{x},\mathbf{z}) s^{0n}(\mathbf{x}) d\varpi(\mathbf{x}) + \int_{\Gamma^c} d\gamma(\mathbf{x}) \Big[\big((g^0(\mathbf{x},\mathbf{z}) - g^1(\mathbf{x},\mathbf{z}) \big) \int_{\Omega_0} d\varpi(\mathbf{y}) \partial_{\nu_x} g^0(\mathbf{y},\mathbf{x}) s^{0n}(\mathbf{y}) - \left(\partial_\nu g^{0n}(\mathbf{x},\mathbf{z}) - \frac{\rho^0}{\rho^1} \partial_{\nu_x} g^1(\mathbf{x},\mathbf{z}) \right) \times \frac{2}{\left(1 + \frac{\rho^0}{\rho^1}\right)} \int_{\Omega_0} d\varpi(\mathbf{y}) g^0(\mathbf{y},\mathbf{x}) s^{0n}(\mathbf{y}) \Big] \ ; \quad \mathbf{z} \in \Omega_0^{dm_0} \ ; \ m_0 = 1, 2, ..., M_0 \ , \quad (5.10.35)$$

■ These can be written in simpler form, so that for each source-in- Ω_0-realization:

$$p^{0m_0}(\mathbf{z}) \approx \int_{\Omega_0} g^0(\mathbf{x},\mathbf{z}) s^{0n}(\mathbf{x}) d\Omega(\mathbf{x}) + \int_{\Gamma^c} \mathcal{K}^n(\mathbf{x},\mathbf{z}) d\gamma(\mathbf{x}) \ ; \quad \mathbf{z} \in \Omega_0^{dm_0} \ ; \ m_0 = 1, 2, ..., M_0 \ , \quad (5.10.36)$$

with

$$\mathcal{K}^n(\mathbf{x},\mathbf{z}) := \Big((g^0(\mathbf{x},\mathbf{z}) - g^1(\mathbf{x},\mathbf{z})\Big) \int_{\Omega_0} d\varpi(\mathbf{y}) \partial_{\nu_x} g^0(\mathbf{y},\mathbf{x}) s^{0n}(\mathbf{y}) -$$
$$\left(\partial_\nu g^{0n}(\mathbf{x},\mathbf{z}) - \frac{\rho^0}{\rho^1} \partial_{\nu_x} g^1(\mathbf{x},\mathbf{z}) \right) \times$$
$$\frac{2}{\left(1 + \frac{\rho^0}{\rho^1}\right)} \int_{\Omega_0} d\varpi(\mathbf{y}) g^0(\mathbf{y},\mathbf{x}) s^{0n}(\mathbf{y}) \;\; ; \;\; n = 1, 2, ..., N \; . \quad (5.10.37)$$

■ Thus, inverse problem reduces to resolution of set of first-kind integral equations (5.10.36) for unknown function $f(\mathbf{x})$.

□ Note that $p^{0m_0}(\mathbf{z}) \;\; ; \;\; \mathbf{z} \in \Omega_0^{dm_0}$ are known functions since they are assumed to be measured. Also, specific Green's function is assumed to be known, either in analytic (case that occurs when boundary of homogeneous half space is flat) or numerical form (case of heterogeneous half spaces).

□ This means that preceding formulae apply as well to a heterogeneous half space with rough boundary and are useful as long as specific Green's function can be found without too much effort.

□ This formulation is easily extended to case in which solicitations take form of plane instead of cylindrical waves.

Chapter 6

The intersecting canonical body approximation (ICBA) for the description of scattering of a plane wave by the rough interface between two fluid media

6.1 Features of inverse problem

☐ Object: 2D fluid acoustical forward-scattering problem illustrated in fig. 6.1.1.

☐ In absence of roughness, configuration is that of half space domain $\overline{\Omega}_1$ filled with known homogeneous fluid M^1 with (spatially-constant) acoustic parameters (k^1, ρ^1), separated by flat, horizontal interface $\overline{\Gamma} = \Gamma^g \cup \Gamma^0 \cup \Gamma^d$ (wherein $\Gamma^g,\ \Gamma^0,\ \Gamma^d$ are flat, horizontal segments) from half-infinite domain $\overline{\Omega}_0$ filled with known homogeneous fluid M^0 with (spatially-constant) acoustic parameters (k^0, ρ^0).

☐ *In presence of the roughness*, localized in domain Γ^c described by parametric equation $x_2 = f(x_1)$, interface is $\Gamma = \Gamma^g \cup \Gamma^c \cup \Gamma^d$.

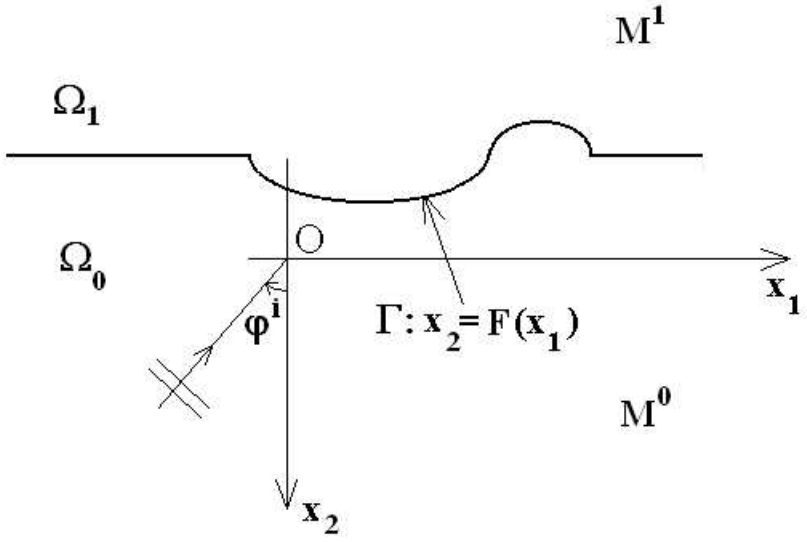

Figure 6.1.1: Configuration, in cross-section plane, corresponding to problem of scattering of acoustic plane wave from rough interface between two homogeneous fluid-like half spaces.

□ Γ separates half-infinite domain $\Omega_0 \supset \overline{\Omega}_0$ filled with known homogeneous fluid M^0 with (spatially-constant) acoustic parameters (k^0, ρ^0) from half-infinite domain $\Omega_1 \supset \overline{\Omega}_1$ filled with known homogeneous fluid M^1 with (spatially-constant) acoustic parameters (k^1, ρ^1).

■ Problem is to predict field scattered by rough interface when latter is solicited by a plane wave propagating in Ω_0.

6.2 Governing equations

□ Governing equations for pressure field:

$$\left[\triangle + \left(k^0\right)^2\right] p^0(\mathbf{x}, \omega) = 0 \;\; ; \;\; \mathbf{x} \in \Omega_0 \;, \tag{6.2.1}$$

$$\left[\triangle + \left(k^1\right)^2\right] p^1(\mathbf{x}, \omega) = 0 \;\; ; \;\; \mathbf{x} \in \Omega_1 \;, \tag{6.2.2}$$

$$p^0(\mathbf{x}, \omega) - p^1(\mathbf{x}, \omega) = 0 \;\; ; \;\; \mathbf{x} \in \Gamma \;, \tag{6.2.3}$$

$$\frac{1}{\rho^0}\boldsymbol{\nu}(\mathbf{x}) \cdot \nabla p^0(\mathbf{x}, \omega) - \frac{1}{\rho^1}\boldsymbol{\nu}(\mathbf{x}) \cdot \nabla p^1(\mathbf{x}, \omega) = 0 \;\; ; \;\; \mathbf{x} \in \Gamma \;, \tag{6.2.4}$$

$$p^0(\mathbf{x},\omega) - p^i(\mathbf{x},\omega) \sim \text{outgoing waves}\ ,\ \mathbf{x} \in \Omega_0\ ,\ \|\mathbf{x}\| \to \infty\ , \tag{6.2.5}$$

$$p^1(\mathbf{x},\omega) \sim \text{outgoing waves}\ ,\ \mathbf{x} \in \bar{\Omega}_1\ ,\ \|\mathbf{x}\| \to \infty\ , \tag{6.2.6}$$

(wherein $\boldsymbol{\nu}$ is unit vector normal to Γ), with:

$$p^i(\mathbf{x},\omega) = A^i \exp(i\mathbf{k}^i \cdot \mathbf{x})\ , \tag{6.2.7}$$

the incident plane wave,

$$\mathbf{k}^i = (k_1^i, k_2^{0i-}, 0)\ \ ,\ \ k_1^i = k^0 \sin\varphi^i\ \ , \qquad k_2^{0i\pm} = \pm\cos\varphi^i\ \ ,\ \ k^0 = \frac{\omega}{c^0}\ \ ,\ \ \mathbf{x} = (x_1, x_2)\ , \tag{6.2.8}$$

φ^i the incident angle measured clockwise from positive x_2 axis, c^0 the phase velocity of body waves in M^0, and ω the angular frequency (which is henceforth implicit).

6.3 Field representations in cartesian coordinate system

□ By separation of variables and employment of radiation condition one obtains following Rayleigh plane-wave representations of pressure field:

$$p^0(\mathbf{x}) = p^i(\mathbf{x}) + \int_{-\infty}^{\infty} B^0(k_1) \exp\left\{ i \left[k_1 x_1 + k_2^{0+} x_2 \right] \right\} dk_1 \ ; \ \mathbf{x} \in \Omega_0^+ \ , \tag{6.3.9}$$

$$p^1(\mathbf{x}) = \int_{-\infty}^{\infty} A^1(k_1) \exp\left\{ i \left[k_1 x_1 - k_2^{1+} x_2 \right] \right\} dk_1 \ ; \ \mathbf{x} \in \Omega_1^- \ . \tag{6.3.10}$$

wherein

$$k_2^{j\pm} = \sqrt{(k^j)^2 - (k_1)^2} \quad , \quad \Re k_2^{j\pm} \geq 0 \quad , \quad \Im k_2^{j\pm} \geq 0 \ . \tag{6.3.11}$$

$$\Omega_0^+ = \{ x_2 > \max_{x_1 \in \mathbb{R}} F(x_1) \ ; \ \forall x_1 \in \mathbb{R} \} \ . \tag{6.3.12}$$

$$\Omega_0^- = \{ x_2 < \min_{x_1 \in \mathbb{R}} F(x_1) \ ; \ \forall x_1 \in \mathbb{R} \} \ . \tag{6.3.13}$$

6.4 Periodic roughness

□ It proves to be useful to consider case of a *periodic* interface of period d depicted in fig. 6.4.1, i.e.,

$$F(x_1 + d) = F(x_1) \ ; \ \forall x_1 \in \mathbb{R} \ . \tag{6.4.14}$$

□ Governing equations are identical to those of previous case and

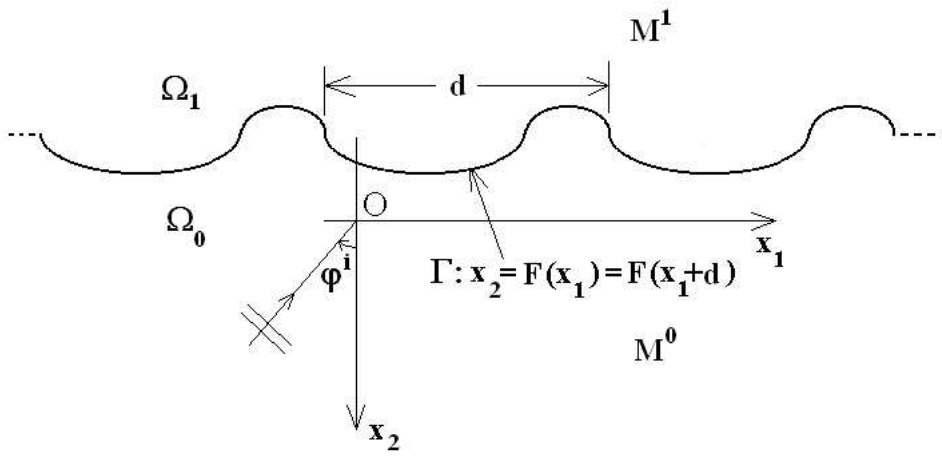

Figure 6.4.1: Configuration, in cross-section plane, corresponding to problem of scattering of an acoustic plane wave from periodically- rough interface between two homogeneous fluid-like half spaces.

from these one can deduce Floquet relation

$$p^j(x_1+d,x_2)=p^j(x_1,x_2)\exp(ik_1^id)\ ;\ \forall x_1\in\mathbb{R}\ \ ;\ \ j=0,1\ . \tag{6.4.15}$$

□ Easy to show that field representations take form:

$$p^0(\mathbf{x})=p^i(\mathbf{x})+\sum_{n=-\infty}^{\infty}B_n^0\exp\left\{i\left[k_{1n}x_1+k_{2n}^{0+}x_2\right]\right\}\ ;\ \mathbf{x}\in\Omega_0^+\ , \tag{6.4.16}$$

$$p^1(\mathbf{x})=\sum_{n=-\infty}^{\infty}A_n^1\exp\left\{i\left[k_{1n}x_1-k_{2n}^{1+}x_2\right]\right\}\ ;\ \mathbf{y}\in\Omega_1^-\ , \tag{6.4.17}$$

wherein

$$k_{1n} = k_1^i + \frac{2n\pi}{d} \ , \tag{6.4.18}$$

$$k_{2n}^{j\pm} = \sqrt{(k^j)^2 - (k_{1n})^2} \ \ , \ \ \Re k_{2n}^{j\pm} \geq 0 \ \ , \ \ \Im k_{2n}^{j\pm} \geq 0 \ . \tag{6.4.19}$$

□ Problem now reduces to computation of scattering coefficients B_n^0 and A_n^0.

6.5 Rayleigh hypothesis

□ Note that until now the Rayleigh hypothesis has not been made.

□ To do this, assume that slope of interface is everywhere small, i.e.,

$$|\dot{F}| << 1 \ \ ; \ \ \forall x_1 \in \mathbb{R} \ . \tag{6.5.20}$$

(wherein $F := F(x_1)$, $\dot{F} := \frac{dF(x_1)}{dx_1}$) which fact guarantees validity of Rayleigh hypothesis (RH).

■ Recall that RH amounts to assumption that aforementioned plane wave representations (6.4.16)-(6.4.17) can be extended *throughout* Ω_0 and Ω_1 respectively as well as *onto interface* Γ:

$$p^0(\mathbf{x}) = p^i(\mathbf{x}) + \sum_{n=-\infty}^{\infty} B_n^0 \exp\left\{i\left[k_{1n}x_1 + k_{2n}^{0+}x_2\right]\right\} \ ; \ \mathbf{x} \in \Omega_0 \cup \Gamma \ , \tag{6.5.21}$$

$$p^1(\mathbf{x}) = \sum_{n=-\infty}^{\infty} A_n^1 \exp\left\{i\left[k_{1n}x_1 - k_{2n}^{1+}x_2\right]\right\} \ ; \ \mathbf{y} \in \Omega_1 \cup \Gamma \ . \tag{6.5.22}$$

□ As previously, problem reduces to computation of scattering coefficients B_n^0 and A_n^0.

□ To do this, one introduces RH representations of field into transmission boundary conditions (6.2.4), (6.2.4), so as to give (using $\boldsymbol{\nu} \cdot \nabla p^j(\mathbf{x})|_{\mathbf{x}\in\Gamma} = \frac{(\dot{F}\partial_{x_1} - \partial_{x_2})p^j(x_1,F)}{\sqrt{\dot{F}^2+1}}$):

$$A^i \exp\left[i\left(k_1^i x_1 - k_2^{0i+}F\right)\right] + \sum_{n=-\infty}^{\infty} B_n^0 \exp\left\{i\left[k_{1n}x_1 + k_{2n}^{0+}F\right]\right\} - \sum_{n=-\infty}^{\infty} A_n^0 \exp\left\{i\left[k_{1n}x_1 - k_{2n}^{1+}F\right]\right\} = 0 \ ; \ \forall x_1 \in \mathbb{R} \ , \tag{6.5.23}$$

$$A^i \frac{i}{\rho^0} \left(\dot{F} k_1^i + k_2^{i+} \right) \exp \left[i \left(k_1^i x_1 - k_2^{i+} f \right) \right] +$$
$$\sum_{n=-\infty}^{\infty} B_n^0 \frac{i}{\rho^0} \left(\dot{F} k_{1n} - k_{2n}^{0+} \right) \exp \left\{ i \left[k_{1n} x_1 + k_{2n}^{0+} f \right] \right\} -$$
$$\sum_{n=-\infty}^{\infty} A_n^1 \frac{i}{\rho^1} \left(\dot{F} k_{1n} + k_{2n}^{1+} \right) \exp \left\{ i \left[k_{1n} x_1 + k_{2n}^{1+} f \right] \right\} = 0 \; ; \; \forall x_1 \in \mathbb{R} \; . \tag{6.5.24}$$

Eq. (6.5.23) is multiplied by $\exp \left\{ -i \left[k_{1m} x_1 + k_{20}^{0+} f \right] \right\} \frac{dx_1}{d}$, (6.5.24) by $\exp \left\{ -i \left[k_{1m} x_1 - k_2^{1+} f \right] \right\} \frac{dx_1}{d}$ (for $\forall m \in \mathbb{Z}$), and both are integrated over one period:

$$A^i \int_0^d \exp \left[i \left(-\frac{2\pi m}{d} x_1 - 2 k_2^{i+} F \right) \right] \frac{dx_1}{d} +$$
$$\sum_{n=-\infty}^{\infty} B_n^0 \int_0^d \exp \left\{ i \left[\frac{2\pi (n-m)}{d} x_1 + (k_{2n}^{0+} - k_{20}^{0+}) F \right] \right\} \frac{dx_1}{d} -$$
$$\sum_{n=-\infty}^{\infty} A_n^1 \int_0^d \exp \left\{ i \left[\frac{2\pi (n-m)}{d} x_1 - (k_{2n}^{1+} + k_{20}^{0+}) F \right] \right\} \frac{dx_1}{d} = 0 \; ;$$
$$\forall m \in \mathbb{Z} \; , \tag{6.5.25}$$

$$
\begin{aligned}
A^i \frac{i}{\rho^0} \int_0^a \left(\dot{F} k_1^i + k_2^{i+}\right) \times \\
\exp\left[i\left(-\frac{2\pi m}{d} x_1 - (k_2^{i+} - k_{20}^{1+})F\right)\right] \frac{dx_1}{d} + \\
\sum_{n=-\infty}^{\infty} B_n^0 \frac{i}{\rho^0} \int_0^d \left(\dot{F} k_{1n} - k_{2n}^{0+}\right) \times \\
\exp\left\{i\left[\frac{2\pi(n-m)}{d} x_1 + (k_{2n}^{0+} + k_{20}^{1+})F\right]\right\} \frac{dx_1}{d} - \\
\sum_{n=-\infty}^{\infty} A_n^1 \frac{i}{\rho_1} \int_0^d \left(\dot{F} k_{1n} + k_{2n}^{1+}\right) \times \\
\exp\left\{i\left[\frac{2\pi(n-m)}{d} x_1 - (k_{2n}^{1+} - k_{20}^{1+})F\right]\right\} \frac{dx_1}{d} = 0 \ ; \ \forall m \in \mathbb{Z} \ .
\end{aligned}
\tag{6.5.26}
$$

□ These two linear systems of coupled algebraic equations in an infinite number of unknowns can only be resolved numerically, so that analysis ends here unless more restrictions are made.

6.6 Perturbation analysis for high frequency approximation of plane wave coefficients

■ Thus, as of now, we place ourselves in a high-frequency context, i.e., it is assumed that *period d is large compared to wavelength in medium* M_0, i.e.,

$$\xi \equiv \frac{2\pi}{k_0 d} << 1 \ . \tag{6.6.27}$$

☐ Suggests change of variables:

$$\varsigma = \frac{x_1}{d} \ , \tag{6.6.28}$$

whence

$$F(x_1) = F\left(\frac{x_1}{d}d\right) = F(\varsigma d) \equiv H(\varsigma) = H \ , \tag{6.6.29}$$

$$\dot{F}(x_1) = \frac{dF(x_1)}{dx_1} = \frac{1}{d}\frac{dH(\varsigma)}{d\varsigma} \equiv \frac{1}{d}\dot{H}(\varsigma) = \frac{1}{d}\dot{H} \ , \tag{6.6.30}$$

$$k_{2n}^{j+} = \sqrt{\left(k^{(j)}\right)^2 - \left(k_1^i + 2n\pi/d\right)^2} = k^0\sqrt{\left(\frac{k^j}{k^0}\right)^2 - \left(\frac{k_1^i}{k^0} + n\xi\right)^2} \ , \tag{6.6.31}$$

☐ Two systems of equations become:

$$A^i \int_0^1 \exp\left[i\left(-2\pi m\varsigma - 2k_2^{i+}g\right)\right] d\varsigma +$$
$$\sum_{n=-\infty}^{\infty} B_n^0 \int_0^1 \exp\left\{i\left[2\pi(n-m)\varsigma + (k_{2n}^{0+} - k_{20}^{0+})H\right]\right\} d\varsigma -$$
$$\sum_{n=-\infty}^{\infty} A_n^1 \int_0^1 \exp\left\{i\left[2\pi(n-m)\varsigma - (k_{2n}^{1+} + k_{20}^{0+})H\right]\right\} d\varsigma = 0 \; ;$$
$$\forall m \in \mathbb{Z} \; , \quad (6.6.32)$$

$$A^i \frac{1}{\rho^0} \int_0^1 \left(\dot{H} k_1^i \frac{k^0 \xi}{2\pi} + k_2^{i+}\right) \exp\left[i\left(-2\pi m\varsigma - (k_2^{i+} - k_{20}^{1+})H\right)\right] d\varsigma +$$
$$\sum_{n=-\infty}^{\infty} B_n^0 \frac{1}{\rho^0} \int_0^1 \left(\dot{H} k_{1n} \frac{k^0 \xi}{2\pi} - k_{2n}^0\right) \times$$
$$\exp\left\{i\left[2\pi(n-m)\varsigma + (k_{2n}^{0+} + k_{20}^{1+})H\right]\right\} d\varsigma -$$
$$\sum_{n=-\infty}^{\infty} A_n^1 \frac{1}{\rho_1} \int_0^1 \left(\dot{H} k_{1n} \frac{k^0 \xi}{2\pi} + k_{2n}^{1+}\right) \times$$
$$\exp\left\{i\left[2\pi(n-m)\varsigma - (k_{2n}^{1+} - k_{20}^{1+})H\right]\right\} d\varsigma = 0$$
$$; \; \forall m \in \mathbb{Z} \; . \quad (6.6.33)$$

■ The *perturbation method* consists in expanding all quantities in these two systems of equations which depend on small parameter ξ in series of powers of ξ.

□ To *zeroth order in* ξ, this gives rise to:

$$k_{2n}^{(j)+} \approx k_{2n}^{(j)+}|_{\xi=0} = \sqrt{(k^j)^2 - (k_1^i)^2} = k_{20}^{j+} \equiv k_2^{ji+} \ , \qquad (6.6.34)$$

$$B_n^0 \approx B_n^0|_{\xi=0} \equiv B_n^{0[0]} \ \ , A_n^1 \approx A_n^1|_{\xi=0} \equiv A_n^{1[0]} \ , \qquad (6.6.35)$$

$$\begin{aligned} A^i \int_0^1 \exp\left[i\left(-2\pi m\varsigma - 2k_{20}^{0+}H\right)\right] d\varsigma + \\ \sum_{n=-\infty}^{\infty} B_n^{0[0]} \int_0^1 \exp\left\{i2\pi(n-m)\varsigma\right\} d\varsigma - \\ \sum_{n=-\infty}^{\infty} A_n^{0[0]} \int_0^1 \exp\left\{i\left[2\pi(n-m)\varsigma - (k_{20}^{1+}+k_{20}^{0+})H\right]\right\} d\varsigma = 0 \ ; \\ \forall m \in \mathbb{Z} \ , \end{aligned} \qquad (6.6.36)$$

$$\begin{aligned} A^i \frac{1}{\rho^0} \int_0^1 k_{20}^{0+} \exp\left[i\left(-2\pi m\varsigma - (k_{20}^{0+}-k_{20}^{1+})H\right)\right] d\varsigma + \\ \sum_{n=-\infty}^{\infty} B_n^{0[0]} \frac{1}{\rho^0} \int_0^1 (-k_{20}^{0+}) \times \\ \exp\left\{i\left[2\pi(n-m)\varsigma + (k_{20}^{0+}+k_{20}^{1+})H\right]\right\} d\varsigma - \\ \sum_{n=-\infty}^{\infty} A_n^{0[0]} \frac{1}{\rho^1} \int_0^1 k_{20}^{1+} \exp\left\{i2\pi(n-m)\varsigma\right\} d\varsigma = 0 \ ; \ \forall m \in \mathbb{Z} \ . \end{aligned} \qquad (6.6.37)$$

□ Identity

$$\int_0^1 \exp\left\{i2\pi(n-m)\varsigma\right\} d\varsigma = \delta_{nm} \qquad \Rightarrow \tag{6.6.38}$$

$$B_m^{0[0]} = -A^i \int_0^1 \exp\left[i\left(-2\pi m\varsigma - 2k_{20}^{0+}H\right)\right] d\varsigma + \sum_{n=-\infty}^{\infty} A_n^{1[0]} \int_0^1 \exp\left\{i\left[2\pi(n-m)\varsigma - (k_{20}^{1+}+k_{20}^{0+})H\right]\right\} d\varsigma = 0\ ; \quad \forall m \in \mathbb{Z}\ , \tag{6.6.39}$$

$$A_m^{0[0]} = -\frac{\rho^1 k_{20}^{0+}}{\rho^0 k_{20}^{1+}} A^i \int_0^1 \exp\left[i\left(-2\pi m\varsigma - (k_{20}^{0+}-k_{20}^{1+})H\right)\right] d\varsigma - \sum_{n=-\infty}^{\infty} B_n^{1[0]} \frac{\rho^1 k_{20}^{0+}}{\rho^0 k_{20}^{1+}} \int_0^1 \exp\left\{i\left[2\pi(n-m)\varsigma + (k_{20}^{0+}+k_{20}^{1+})H\right]\right\} d\varsigma = 0\,; \quad \forall m \in \mathbb{Z}\ . \tag{6.6.40}$$

□ Introduction of second of these relations into first yields:

$$B_m^{0)[0]} = -A^i \int_0^1 \exp\left[i\left(-2\pi m\varsigma - 2k_{20}^{0+}H\right)\right] d\varsigma + \frac{\rho^1 k_{20}^{0+}}{\rho^0 k_{20}^{1+}} A^i \int_0^1 \exp\left[i\left(-2\pi m\varsigma - 2k_{20}^{0+}H\right)\right] d\varsigma - \frac{\rho^1 k_{20}^{0+}}{\rho^0 k_{20}^{1+}} \sum_{l=-\infty}^{\infty} B_l^{1[0]} \int_0^1 \exp\left\{i2\pi(l-m)\varsigma\right\} d\varsigma = 0 \ ; \ \forall m \in \mathbb{Z} \ , \tag{6.6.41}$$

where use has been made of

$$\sum_{n=-\infty}^{\infty} \exp\left[i2\pi n(\varsigma - \zeta)\right] = \delta(\varsigma - \zeta) \ \ ; \ \ \varsigma, \zeta \in [0,1] \ . \tag{6.6.42}$$

□ Re-use of (6.6.38) ⇒

$$B_m^{0[0]} = A^i \left(\frac{\rho^1 k_{20}^{0+} - \rho^0 k_{20}^{1+}}{\rho^1 k_{20}^{0+} + \rho^0 k_{20}^{1+}}\right) \int_0^1 \exp\left[i\left(-2\pi m\varsigma - 2k_{20}^{0+}H\right)\right] d\varsigma \ ; \quad \forall m \in \mathbb{Z} \ , \tag{6.6.43}$$

and, after introduction of this result into (6.6.40) and re-use of (6.6.42):

$$A_m^{0[0]} = A^i \left(\frac{2\rho^1 k_{20}^{0+}}{\rho^1 k_{20}^{0+} + \rho^0 k_{20}^{1+}}\right) \times \int_0^1 \exp\left[i\left(-2\pi m\varsigma - (k_{20}^{0+} - k_{20}^{1+})H\right)\right] d\varsigma \ ; \ \forall m \in \mathbb{Z} \ . \tag{6.6.44}$$

■ Employment of (6.6.34) and (6.6.35) ⇒

$$B_m^0 \approx B_m^{0[0]} = A^i \left(\frac{\rho^1 k_2^{i+} - \rho^0 k_2^{1i+}}{\rho^1 k_2^{i+} + \rho^0 k_2^{1i+}} \right) \times \int_0^1 \exp\left[i \left(-2\pi m \varsigma - 2 k_2^{i+} H \right) \right] d\varsigma \ ; \ \forall m \in \mathbb{Z} \ , \quad (6.6.45)$$

$$A_m^0 \approx A_m^{0[0]} = A^i \left(\frac{2\rho^1 k_2^{i+}}{\rho^1 k_2^{i+} + \rho^0 k_2^{1i+}} \right) \times \int_0^1 \exp\left[i \left(-2\pi m \varsigma - (k_2^{i+} - k_2^{1i+}) H \right) \right] d\varsigma \ ; \ \forall m \in \mathbb{Z} \ . \quad (6.6.46)$$

□ To understand meaning of these expressions, consider case in which interface is a horizontal plane located at

$$x_2 = D_b = \text{constant} \ . \quad (6.6.47)$$

□ Then (6.6.45),(6.6.46), and (6.6.38) give rise to:

$$B_m^0 = A^i \left(\frac{\rho^1 k_2^{i+} - \rho^0 k_2^{1i+}}{\rho^1 k_2^{i+} + \rho^0 k_2^{1i+}} \right) \exp\left[-i 2 k_2^{i+} D_b \right] \delta_{m0} \ ; \ \forall m \in \mathbb{Z} \ , \quad (6.6.48)$$

$$A_m^0 = A^i \left(\frac{2\rho^1 k_2^{i+}}{\rho^1 k_2^{i+} + \rho^0 k_2^{1i+}} \right) \exp\left[-i(k_2^{i+} - k_2^{1i+}) D_b \right] \delta_{m0} \, ; \, \forall m \in \mathbb{Z} \, , \tag{6.6.49}$$

wherein δ_{m0} is Kronecker symbol and $\approx$ sign has been replaced by $=$ sign to underline fact that these results are *exact* .

$\square$ Introduction of the last two expressions into (6.4.16) and (6.4.17) gives

$$p^0(\mathbf{x}) = p^i(\mathbf{x}) + A^i R(D_b) \exp\left[i \left(k_1^i x_1 + k_2^{i+} x_2 \right) \right] \;\; ; \;\; x_2 \geq D_b \;\; , \;\; x_1 \in \mathbb{R} \, , \tag{6.6.50}$$

$$p^1(\mathbf{x}) = A^i T(D_b) \exp\left[i \left(k_1^i x_1 - k_2^{1i+} x_2 \right) \right] \;\; ; \;\; x_2 \leq D_b \;\; , \;\; x_1 \in \mathbb{R} \, , \tag{6.6.51}$$

wherein

$$R(D_b) = \left(\frac{\rho^1 k_2^{i+} - \rho^0 k_2^{1i+}}{\rho^1 k_2^{i+} + \rho^0 k_2^{1i+}} \right) \exp\left[-i 2 k_2^{i+} D_b \right] \;\; , \tag{6.6.52}$$

$$T(D_b) = \left(\frac{2\rho^1 k_2^{i+}}{\rho^1 k_2^{i+} + \rho^0 k_2^{1i+}} \right) \exp\left[-i(k_2^{i+} - k_2^{1i+}) D_b \right] \;\; . \tag{6.6.53}$$

$\square$ Eqs. (6.6.50)-(6.6.51) indicate that:

1. field in Ω_0 is expressed as sum of incident plane wave and a

specularly-reflected plane wave whose amplitude (R), with respect to that of incident wave, denotes *reflection coefficient* , and

2. field in Ω_1 is expressed as a transmitted (or refracted) plane wave whose amplitude (T), with respect to that of incident wave, denotes *transmission coefficient* .

□ Important to note that usually R and T do not contain phase terms; the reason for this is that (in demonstrations of Fresnel formulae) one generally locates the (flat) interface at $x_2 = 0$, which is equivalent to $D_b = 0$ and therefore leads to disappearance of phase terms in (6.6.52)-(6.6.53).

6.7 Perturbation analysis for high frequency approximation of field leading to ICBA

□ Opportune to address problem of determination of *field* for case of an *uneven interface*.

□ Point of departure is Rayleigh plane wave representations (6.4.16)-(6.4.17), which, after invocation of Rayleigh hypothesis, division by $\exp(ik_1^i x_1)$, and change of variables $x_1 = \zeta d$, gives rise to:

$$w^0(\zeta, x_2) \equiv p^0(\mathbf{x}) \exp(-ik_1^i x_1) = p^i(\mathbf{x}) \exp(-ik_1^i x_1) + \sum_{n=-\infty}^{\infty} b_n^0 \exp\left[i\left(2\pi n\zeta + k_{2n}^{0+} x_2\right)\right] \ ; \ x_2 \geq f(x_1) \ , \ x_1 \in \mathbb{R} \ , \quad (6.7.54)$$

$$w^0(\zeta, x_2) \equiv p^0(\mathbf{x}) \exp(-ik_1^i x_1) =$$
$$\sum_{n=-\infty}^{\infty} a_n^0 \exp\left[i\left(2\pi n\zeta - k_{2n}^{0+} x_2\right)\right] \ ; \ x_2 \leq f(x_1) \ , \ x_1 \in \mathbb{R} \ . \quad (6.7.55)$$

□ Perturbation analysis is again brought into play under hypothesis $\xi << 1$.

□ To zeroth order in ξ:

$$w^0(\zeta, x_2) \approx w^{0[0]}(\mathbf{x}) = p^i(\mathbf{x}) \exp(-ik_1^i x_1) +$$
$$\sum_{n=-\infty}^{\infty} B_n^{0[0]} \exp\left[i\left(2\pi n\zeta + k_2^{i+} x_2\right)\right] \ ; \ x_2 \geq F(x_1) \ , \ x_1 \in \mathbb{R} \ , \quad (6.7.56)$$

$$w^1(\varsigma, x_2) \approx w^{1[0]}(\mathbf{x}) =$$
$$\sum_{n=-\infty}^{\infty} A_n^{1[0]} \exp\left[i\left(2\pi n\zeta - k_2^{0i+} x_2\right)\right] \ ; \ x_2 \leq F(x_1) \ , \ x_1 \in \mathbb{R} \ , \quad (6.7.57)$$

which, on account of (6.6.45)-(6.6.46), become

$$w^{0[0]}(\mathbf{x}) = p^i(\mathbf{x}) \exp(-ik_1^i x_1) + A^i \left(\frac{\rho^1 k_2^{i+} - \rho^0 k_2^{1i+}}{\rho^1 k_2^{i+} + \rho^0 k_2^{1i+}} \right) \exp\left(ik_2^{i+} x_2\right) \times \int_0^1 \exp\left(-2ik_2^{i+} g(\varsigma)\right) \sum_{n=-\infty}^{\infty} \exp\left[i(2\pi n(\zeta - \varsigma)\right] \; ; \; x_2 \geq F(x_1) \; , \; x_1 \in \mathbb{R} \; , \quad (6.7.58)$$

$$w^{1[0]}(\mathbf{x}) = A^i \left(\frac{2\rho^1 k_2^{i+}}{\rho^1 k_2^{i+} + \rho^0 k_2^{1i+}} \right) \exp\left(-ik_2^{0i+} x_2\right) \times \int_0^1 \exp\left[-i(k_2^{i+} - k_2^{1i+}) g(\varsigma)\right] \sum_{n=-\infty}^{\infty} \exp\left[i(2\pi n(\zeta - \varsigma)\right] \; ; \; x_2 \leq F(x_1) \; , \; x_1 \in \mathbb{R} \; . \quad (6.7.59)$$

□ Making use, once again, of (6.6.42), as well as of (6.6.52)-(6.6.53) ⇒

$$w^{0[0]}(\mathbf{x}) = p^i(\mathbf{x}) \exp(-ik_1^i x_1) + A^i R(H(\zeta)) \exp\left(ik_2^{i+} x_2\right) \; ; \; x_2 \geq F(x_1) \; , \; x_1 \in \mathbb{R} \; , \quad (6.7.60)$$

$$w^{1[0]}(\mathbf{x}) = A^i R(H(\zeta)) \exp\left(-ik_2^{1i+} x_2\right) \; ; \; x_2 \leq F(x_1) \; , \; x_1 \in \mathbb{R} \; . \quad (6.7.61)$$

■ Product of these relations with $\exp(ik_1^i)$ and change of variables $\zeta = x_1/a$, lead to:

$$p^0(\mathbf{x}) \approx p^{0[0]}(\mathbf{x}) = p^i(\mathbf{x}) + A^i R(F(x_1)) \exp\left[i(k_1^i x_1 + k_2^{i+} x_2)\right] \ ; \\ x_2 \geq F(x_1) \ , \ x_1 \in \mathbb{R} \ , \quad (6.7.62)$$

$$p^1(\mathbf{x}) \approx p^{1[0]}(\mathbf{x}) = A^i T(F(x_1)) \exp\left[i(k_1^i x_1 - k_2^{1i+} x_2)\right] \ ; \\ x_2 \leq F(x_1) \ , \ x_1 \in \mathbb{R} \ . \quad (6.7.63)$$

□ These two formulae express fact, made apparent by comparison with (6.6.50)-(6.6.53), that, when parameter ξ, related to ratio between characteristic lateral dimension of uneveness of interface and wavelength in Ω_0 is very small, scattered field, constituting response of interface to incident plane wave p^i, is approximately (i.e., to zeroth order in ξ) identical, on a vertical line passing through abscissa x_1, to field reflected and transmitted (constituting response to same incident wave) by a *flat, horizontal interface* located at ordinate $x_2 = F(x_1)$, media above and below interfaces being same in two (even and uneven) configurations.

■ The 'body' occupying semi-infinite domain opposite one in which incident plane wave propagates and whose boundary is a flat, horizontal plane, is called *intersecting canonical body at abscissa* x_1 because solution of problem of scattering by such a 'body' is known analytically (i.e., Fresnel formulae; (6.6.50)-(6.6.53)).

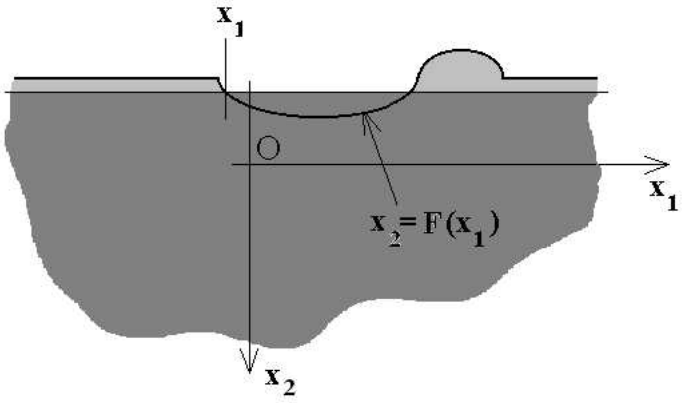

Figure 6.7.1: Cross section view of configuration for scattering from an rough interface. Dark grey region denotes canonical body (a flat plane separating same two media as original rough surface) located at height $F(x_1)$ corresponding to a given abscissa x_1. When this abscissa is changed, canonical body changes (is displaced vertically; compare this subfigure with next one).

■ Height of intersecting canonical body varies with abscissa, which means that to a given uneven interface corresponds not one, but many intersecting canonical bodies (see figs. 6.7.1, 6.7.2).

■ All-important feature of perturbation analysis (carried out to zeroth order in perturbation parameter ξ) is that ξ, and therefore d, are absent from final result, so that *this intersecting canonical body approximation (ICBA) applies just as well to a non-periodically as to a periodically uneven interface* .

■ It has thus been shown that in a high-frequency context involving an interface with rather gentle uneveness (in mean flat and horizontal), scattered field takes a form, locally, as if interface were flat and horizontal. Contrary to what occurs in reflection and refraction by a flat horizontal interface, reflection and transmission coefficients

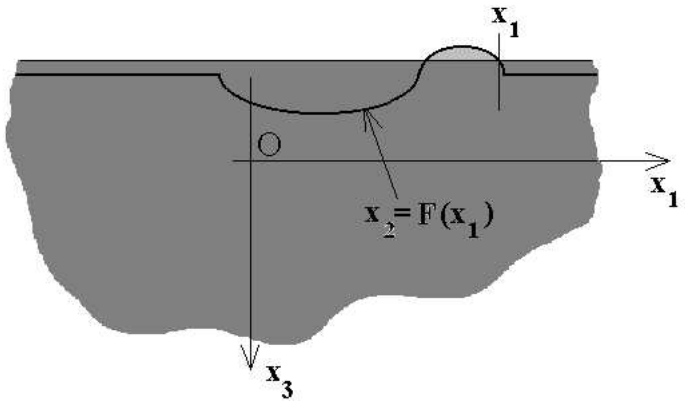

Figure 6.7.2: Cross section view of configuration for scattering from an rough interface. The dark grey region denotes canonical body (a flat plane separating same two media as original rough surface) located at height $F(x_1)$ corresponding to a given abscissa x_1. When this abscissa is changed, canonical body changes (is displaced vertically; compare this subfigure with preceding one).

for uneven interface are not constants with respect to coordinates. However, these coefficients, at abscissa x_1, are obtained in closed-form and are, in fact, Fresnel coefficients for a local, canonical body consisting of half space whose flat, horizontal boundary, intersects uneven boundary at point $(x_1, f(x_1))$.

Chapter 7

Boundary integral formulation employing the free-space Green's function for the description of scattering of a plane wave by an acoustically-soft rough boundary of infinite extent

7.1 Statement of problem of scattering of sound by an irregular, in the mean flat, horizontal, pressure-release boundary overlying a homogeneous, inviscid fluid

☐ Problem at hand is typically that of scattering from sea surface (see fig. 7.1.1).

☐ $Ox_1x_2x_3$ is a cartesian coordinate system. Assume initially that a flat interface between two media M^0 and M^1 occupies entire $x_2 = 0$ plane.

☐ Interface is then deformed in such manner that departure from flatness is independent of x_3 coordinate (fig. 7.1.1), i.e., interface is

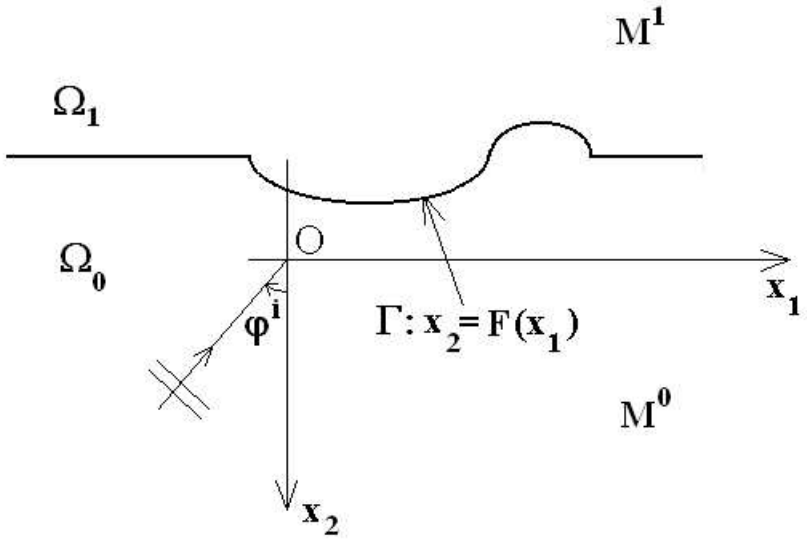

Figure 7.1.1: Cross section view of configuration for scattering of a plane wave from an acoustically-soft or acoustically-hard irregular surface overlying a fluid. Incident wave is assumed to propagate in lower fluid medium.

cylindrical surface.

□ Treat so-called acoustically-soft or Dirichlet boundary condition problem. Medium M^0 is assumed to be inviscid fluid wherein sound is sent towards interface in form of plane pressure wave whose propagation vector $\mathbf{k}^i$ lies in $x_1 - x_2$ plane, i.e., has no component along x_3 axis. Other medium (i.e., M^1) is assumed to be of such feeble density (e.g., air) that sound field cannot penetrate therein and results in vanishing pressure field on interface. The latter is termed 'boundary' and attached to adjective 'pressure-release' in language of marine acoustics.

□ Symbol p^0 (hereafter termed 'field') designates pressure field. Symmetry arguments entail that diffracted and total (i.e., incident plus diffracted) fields in half-space above and below uneven interface do not depend on x_3 coordinate.

■ Problem is to predict scattered sound field from knowledge of incident sound field and shape of cylindrical interface (forward scattering problem).

□ Two-dimensional nature of problem means that entire analysis takes place in $x_1 - x_2$ plane (see fig. 7.1.1). The two semi-infinite portions of latter are designated by Ω_0 and Ω_1 and trace of interface in $x_1 - x_2$ plane by Γ.

■ It is assumed that Γ can be described by parametric equation

$$x_2 = F(x_1) \; ; \; \forall x_1 \in \mathbb{R} \; , \tag{7.1.1}$$

wherein $F(x_1)$ is a continuous, single-valued function of x_1 for all $x_1 \in \mathbb{R}$.

☐ Scattering boundary is submitted to a *monochromatic* plane wave whose angular frequency is ω. Actually, the restriction to an incident plane wave is not necessary.

☐ $\mathbf{x}$ is vector connecting origin O to a generic point (x_1, x_2), and let $p^i(\mathbf{x}, \omega)$, $p^{0d}(\mathbf{x}, \omega)$, $p^0(\mathbf{x}, \omega)$ designate incident, diffracted, and total pressure fields in Ω_0.

7.2 Governing equations for field

☐ Dirichlet problem is formulated as follows. Pressure field p^0 satisfies:

$$p^0(\mathbf{x}, \omega) = p^i(\mathbf{x}, \omega) + p^{0d}(\mathbf{x}, \omega) \; , \tag{7.2.2}$$

$$p^i(\mathbf{x}, \omega) = A^i \exp(i\mathbf{k}^i \cdot \mathbf{x}) \; , \tag{7.2.3}$$

$$\left(\nabla^2 + \left(k^0\right)^2\right) p^0(\mathbf{x}, \omega) = 0 \; ; \; \forall \mathbf{x} \in \Omega_0 \; , \tag{7.2.4}$$

$$p^0(\mathbf{x},\omega) = 0 \ ; \ \forall \mathbf{x} \in \Gamma \ , \tag{7.2.5}$$

and radiation (outgoing wave) condition

$$p^{0d}(\mathbf{x},\omega) \sim \text{outgoing plane waves} \ ; \ \forall \frac{\mathbf{x}}{\|\mathbf{x}\|} \ ; \ \|k^0\mathbf{x}\| \to \infty \ , \ \mathbf{x} \in \Omega_0 \ , \tag{7.2.6}$$

wherein A^i is amplitude of incident wave, $\mathbf{k}^i = (k_1^i, k_2^i) = (k^0 \sin\varphi^i, -k^0 \cos\varphi^i)$ the incident wave vector such that φ^i is incident angle with respect to $+x_2$ axis, $k^0 = \omega/c^0 = \omega/\sqrt{\lambda^0/\rho^0}$ the wavenumber and c^0 the (real) speed of sound (assumed constant in M^0), ρ^0 the density (assumed constant in M^0), and $\boldsymbol{\nu} = \boldsymbol{\nu}(\mathbf{x})$ the unit vector normal to Γ pointing into Ω_1.

□ Henceforth, we drop ω dependence on all field quantities and consider it to be implicit.

7.3 Governing equations of 2D free-space Green's function

□ 2D free-space Green's function satisfies:

$$\left[\nabla^2 + \left(k^0\right)^2\right] G^0(\|\mathbf{x}-\mathbf{y}\|) = -\delta(\mathbf{x}-\mathbf{y}) \ ; \ \forall \mathbf{x} \in \mathbb{R}^2 \ , \tag{7.3.7}$$

and radiation condition.

7.4 The boundary integral formulation employing 2D free-space Green's function

☐ Applying Green's theorem to $G^0(\|\mathbf{x}-\mathbf{y}\|)$ and $p^0(\mathbf{x})$ in Ω_0, and making use of relations governing G^0 and $p^0 \Rightarrow$

$$\mathcal{H}_{\Omega_0}(\mathbf{y})p^0(\mathbf{y}) = p^i(\mathbf{y}) + \int_\Gamma \left[G^0(\|\mathbf{x}-\mathbf{y}\|)\partial_\nu p^0(\mathbf{x}) - p^0(\mathbf{x})\partial_\nu G^0(\|\mathbf{x}-\mathbf{y}\|)\right] d\gamma(\mathbf{x}) \ , \quad (7.4.8)$$

wherein $\partial_\nu := \boldsymbol{\nu}\cdot\bigtriangledown$, $d\gamma(\mathbf{x})$ infinitesimal arc length along Γ and

$$\mathcal{H}_{\Omega_0}(\mathbf{y}) = \begin{cases} 1 & ;\ \mathbf{y}\in\Omega_0 \\ 0 & ;\ \mathbf{y}\in\mathbb{R}^2\setminus\overline{\Omega}_0 \\ 1/2 & ;\ \mathbf{y}\in\Gamma \end{cases} \ , \quad (7.4.9)$$

it being understood that to value $1/2$ corresponds a Cauchy principal value (designated hereafter by pv) in any integral involving normal derviative of Green's function (7.4.8) in neighborhood of its singularity at $\mathbf{y}=\mathbf{x}$.

☐ The free-space Green's function is given by:

$$G^0(\|\mathbf{x}-\mathbf{y}\|) = \frac{i}{4}H_0^{(1)}(k^0\|\mathbf{y}-\mathbf{x}\|) \ , \quad (7.4.10)$$

with $H_0^{(1)}(.)$ the Hankel function of first kind and order 0.

☐ It follows from (7.4.8) and (7.4.9) that *boundary integral representation* of field in lower half space is:

$$p^0(\mathbf{y}) = p^i(\mathbf{y}) + \int_\Gamma \left[G^0(\|\mathbf{x}-\mathbf{y}\|)\partial_\nu p^0(\mathbf{x}) - p^0(\mathbf{x})\partial_\nu G^0(\|\mathbf{x}-\mathbf{y}\|)\right] d\gamma(\mathbf{x}) \; ; \; \forall \mathbf{y} \in \Omega_0 \; . \tag{7.4.11}$$

□ This is only a *representation* of field, not solution to the problem, since integral contains two unknown functions constituted by pressure and normal derivative of pressure on Γ.

□ The first of these vanishes due to pressure-release boundary condition, so that

$$\mathcal{H}_{\Omega_0}(\mathbf{y})p^0(\mathbf{y}) = p^i(\mathbf{y}) + \int_\Gamma G^0(\|\mathbf{x}-\mathbf{y}\|)\partial_\nu p^0(\mathbf{x}) d\gamma(\mathbf{x}) \; ; \; \forall \mathbf{y} \in \Omega_0 \; . \tag{7.4.12}$$

7.5 Boundary integral equations

□ To get normal derivative of pressure on boundary, one can reapply boundary condition outside of integral to obtain

$$0 = p^i(\mathbf{y}) + \int_\Gamma G^0(\|\mathbf{x}-\mathbf{y}\|)\partial_\nu p^0(\mathbf{x}) d\gamma(\mathbf{x}) \; ; \; \forall \mathbf{y} \in \Gamma \; . \tag{7.5.13}$$

which is a singular integral equation of first kind for $\partial_\nu p^0$ on Γ.

□ Two difficulties in connection with this equation:

1. its first-kind nature which means that equation is often badly ill-conditioned (i.e., small numerical errors lead to large discrepancy in solutions),
2. fact that support of the unknown is not compact.

☐ To resolve at least first difficulty, take normal derivative of (7.4.12) and then restrict $\mathbf{y}$ to $\Gamma \Rightarrow$

$$\frac{1}{2}\partial_{\nu(\mathbf{y})}p^0(\mathbf{y}) = \partial_{\nu(\mathbf{y})}p^i(\mathbf{y}) + pv\int_\Gamma \partial_{\nu(\mathbf{y})}G^0(\|\mathbf{x}-\mathbf{y}\|)\partial_{\nu(\mathbf{x})}p^0(\mathbf{x})d\gamma(\mathbf{x}) \ ; \ \forall \mathbf{y} \in \Gamma \ . \quad (7.5.14)$$

which is a singular integral equation of second kind, that usually does not suffer from ill-conditioning of its first kind counterpart.

☐ Difficulty concerning unbounded support of the unknown cannot be resolved unless irregularity of surface is of bounded support, and outside of this interval surface is flat, in which case a suitable approximation of field can be introduced on flat portions, or a *specific Green's function* can be employed that vanishes on flat portions to eliminate unknown function at these locations.

7.6 Computation of field in fluid

☐ Should be remembered that problem was to predict field in fluid underneath irregular boundary. To do this, introduce function $\partial_{\nu(\mathbf{x})}p^0(\mathbf{x})$, obtained from resolution of integral equation, into (7.4.12) and numerically evaluate integral therein.

□ Hypothesis of plane-wave solicitation is not essential in above analysis. For excitation by wave radiated from cylindrical sources s of bounded support $\Omega_s \subset \mathbb{R}^2$, replace (7.2.3) by

$$p^i(\mathbf{y}) = \int_{\Omega_s} G^0(\|\mathbf{x}-\mathbf{y}\|)s(\mathbf{x})dv(\mathbf{x}) \ . \tag{7.6.15}$$

7.7 Iterative solution of second-kind integral equation

□ Return to second-kind integral equation

$$\begin{aligned}\partial_{\nu(\mathbf{y})}p^0(\mathbf{y}) &= 2\partial_{\nu(\mathbf{y})}p^i(\mathbf{y}) + \\ &pv\int_\Gamma \partial_{\nu(\mathbf{y})}G^0(\|\mathbf{x}-\mathbf{y}\|)2\partial_{\nu(\mathbf{x})}p^0(\mathbf{x})d\gamma(\mathbf{x}) \ ; \ \forall \mathbf{y}\in\Gamma \ .\end{aligned} \tag{7.7.16}$$

□ For moment, discussion takes no account of unbounded support of $\partial_{\nu(\mathbf{x})}p^0$-on-$\Gamma$ difficulty.

□ Assuming can neglect integral ⇒ approximation

$$\partial_{\nu(\mathbf{y})}p^0(\mathbf{y}) \approx \partial_{\nu(\mathbf{y})}p^{0[0]}(\mathbf{y}) := 2\partial_{\nu(\mathbf{y})}p^i(\mathbf{y}) \ . \tag{7.7.17}$$

□ Latter (termed zeroth-order Kirchhoff (ZOK) approximation) can be considered to be initialisation term of iterative scheme (i.e., Neumann series)

$$\partial_{\nu(\mathbf{y})}p^{0[l]}(\mathbf{y}) = 2\partial_{\nu(\mathbf{y})}p^{i}(\mathbf{y}) + pv\int_{\Gamma}\partial_{\nu(\mathbf{y})}G^{0}(\|\mathbf{x}-\mathbf{y}\|)2\partial_{\nu(\mathbf{x})}p^{0[l-1]}(\mathbf{x})d\gamma(\mathbf{x})\ ;\ \forall\mathbf{y}\in\Gamma\ ;\ l=1,2,\ldots. \tag{7.7.18}$$

7.8 Physical optics approximation of pressure in the fluid for a boundary that is non-flat only in a finite x_1-interval

□ Physical optics approximation of pressure in fluid is expressed by replacing $\partial_{\nu(\mathbf{x})}p^0$ by $\partial_{\nu(\mathbf{x})}p^{0[0]}$ within integral defining scattered field, i.e.,

$$p^0(\mathbf{y}) \approx p^{0[POA]}(\mathbf{y}) := p^i(\mathbf{y}) + \int_{\Gamma} G^0(\|\mathbf{x}-\mathbf{y}\|)\partial_{\nu(\mathbf{x})}p^{0[0]}(\mathbf{x})d\gamma(\mathbf{x})\ ;\ \forall\mathbf{y}\in\Omega_0\ , \tag{7.8.19}$$

or

$$p^0(\mathbf{y}) \approx p^{0[POA]}(\mathbf{y}) := p^i(\mathbf{y}) + \int_{\Gamma} G^0(\|\mathbf{x}-\mathbf{y}\|)2\partial_{\nu(\mathbf{x})}p^{i}(\mathbf{x})d\gamma(\mathbf{x})\ ;\ \forall\mathbf{y}\in\Omega_0\ . \tag{7.8.20}$$

□ Recall that $\boldsymbol{\nu}\cdot\nabla p^0(\mathbf{x})|_{\mathbf{x}\in\Gamma} = \frac{(\dot{F}\partial_{x_1}-\partial_{x_2})p^j(x_1,F)}{\sqrt{\dot{F}^2+1}}$, $d\gamma = \sqrt{\dot{F}^2+1}dx_1$, wherein $F := F(x_1)$, $\dot{F} := \frac{dF(x_1)}{dx_1}$, so that

$$p^0(\mathbf{y}) \approx p^{0[POA]}(\mathbf{y}) := p^i(\mathbf{y}) + \int_{-\infty}^{\infty} \frac{i}{2} H_0^{(1)}(k^0 R_\Gamma)(\dot{F}\partial_{x_1} - \partial_{x_2}) p^i(x_1, F) dx_1 \; ; \; \forall \mathbf{y} \in \Omega_0 \; . \quad (7.8.21)$$

wherein $R_\Gamma = |\sqrt{(y_1 - x_1)^2 + (y_2 - F)^2}|$.

■ Restrict attention to case in which

$$F(x_1) = \begin{cases} f(x_1) & ; \quad x_1^g < x_1 < x_1^d \\ 0 & ; \quad -\infty < x_1 \leq x_1^g \\ 0 & ; \quad x_1^d \leq x_1 < \infty \end{cases} \quad , \quad (7.8.22)$$

so that

$$p^{0[POA]}(y_1, y_2) = p^i(y_1, y_2) + \int_{-\infty}^{\infty} \frac{i}{2} H_0^{(1)}\left(k^0 \left|\sqrt{(y_1 - x_1)^2 + y_2^2}\right|\right) A^i ik \sin\varphi^i e^{-ikx_1 \cos\varphi^i} dx_1 - \int_{x_1^g}^{x_1^d} \frac{i}{2} H_0^{(1)}\left(k^0 \left|\sqrt{(y_1 - x_1)^2 + y^2}\right|\right) A^i ik \sin\varphi^i e^{-ikx_1 \cos\varphi^i} dx_1 - \int_{x_1^g}^{x_1^d} \frac{i}{2} H_0^{(1)}\left(k^0 \left|\sqrt{(y_1 - x_1)^2 + (y_2^2 - f(x_1))^2}\right|\right) \times A^i ik \left[g'(x_1)\cos\varphi^i - \sin\varphi^i\right] e^{-ik(x_1 \cos\varphi^i + f(x_1)\sin\varphi^i)} dx_1 \; ; \quad \forall (y_1, y_2) \in \Omega_0 \; . \quad (7.8.23)$$

□ Can easily show:

$$\int_{-\infty}^{\infty} \frac{i}{2} H_0^{(1)} \left(k^0 \left| \sqrt{(y_1 - x_1)^2 + y_2^2} \right| \right) A^i ik \sin\varphi^i e^{-ikx_1 \cos\varphi^i} dx_1 =$$
$$p^r(\mathbf{y}) = -p^i(y_1, -y_2) \; ; \; \forall y_2 \geq 0 \; , \quad (7.8.24)$$

so that (7.8.23) becomes

■

$$p^{0[POA]}(y_1, y_2) = p^i(y_1, y_2) + p^r(y_1, y_2) +$$
$$\int_{x_1^g}^{x_1^d} \frac{i}{2} H_0^{(1)} \left(k^0 \left| \sqrt{(y_1 - x_1)^2 + y^2} \right| \right) A^i ik \sin\varphi^i e^{-ikx_1 \cos\varphi^i} dx_1 -$$
$$\int_{x_1^g}^{x_1^d} \frac{i}{2} H_0^{(1)} \left(k^0 \left| \sqrt{(y_1 - x_1)^2 + (y_2^2 - f(x_1))^2} \right| \right) \times$$
$$A^i ik \left[\dot{f}(x_1) \cos\varphi^i - \sin\varphi^i \right] e^{-ik(x_1 \cos\varphi^i + f(x_1) \sin\varphi^i)} dx_1 \; ;$$
$$\forall (y_1, y_2) \in \Omega_0 \; . \quad (7.8.25)$$

□ Use of (e.g.) Simpson quadrature to compute the two integrals in (8.4.4) completes procedure for predicting field in Ω_0 by means of physical optics approximation.

Chapter 8

Identification of the rough acoustically-soft boundary of a half-space probed by a plane wave

8.1 Introduction

□ On Feb. 9, 2001, submarine USS Greeneville of US Navy, collided with japanese fishing and training vessel Ehime Maru during a routine surfacing operation. Although such submarines are equipped with both modern radar and (passive and active) sonar devices for detecting and locating subsurface and floating (on sea surface) 'targets', information provided by these devices was either insufficient or simply not used by crew of american vessel.

□ An idealized version of such (active) devices is studied herein to investigate type, quality, and quantity of information they may yield. Of particular interest is influence of position of receiver with respect to target, shape of latter, frequency of emitted signal, and existence and possible removal of spurious images (term employed to designate reconstructed shape, size and location of target from analysis of scattered radiation).

☐ More specifically, present investigation addresses problem of reconstruction of boundary (e.g., presumably flat sea surface interrupted by hull of a floating vessel) of a half plane.

☐ Other applications of this work are: rough surface characterization by optical, microwave, or acoustic means, depth sounding in sea by sonar, etc.

☐ Employed method appeals to an estimator (mathematical entity used to account for wavefield scattered by a test target) that is exact for a canonical boundary (i.e., flat mirror) scattering problem and shown to lead to an infinite number of solutions for inverse problem of reconstruction of canonical boundary when probe radiation is a plane monochromatic plane wave.

☐ It is also shown:

1. that employing probe radiation at two frequencies enables to eliminate spurious solutions and

2. how to transpose this method to retrieval of cylindrical boundaries of infinite extent with localized deformations (i.e., bumps or troughs).

8.2 Framework of forward and inverse scattering problems

☐ Let $Ox_1x_2x_3$ be a cartesian coordinate system.

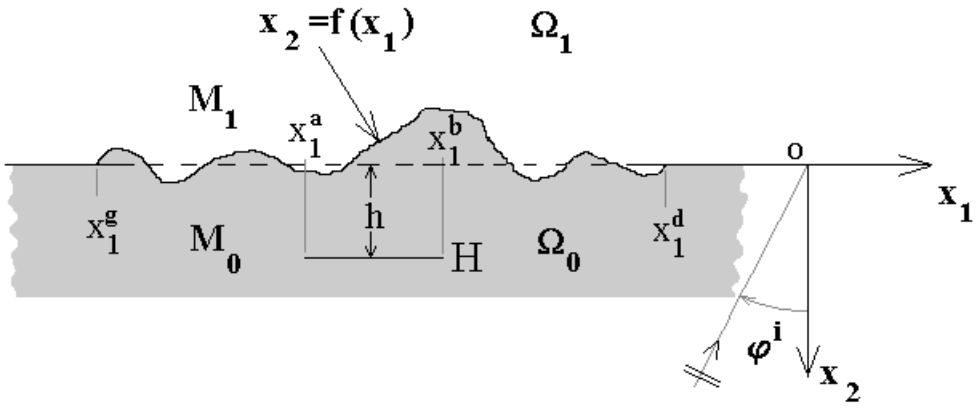

Figure 8.2.1: Scattering configuration in cross-section plane. Measurement segment H is at depth h below reference plane $x_2 = 0$.

☐ Assume initially that a (in acoustic terms) mirror occupies entire $x_2 = 0$ plane. Mirror is then deformed locally in interval $x_1^l < x_1 < x_1^r$ such that departure from flatness is independent of x_3 coordinate (see fig. 8.2.1).

☐ Medium in half-space above 2D mirror is impervious to sound waves.

☐ Lower medium is either a perfect fluid wherein sound is sent towards mirror in form of plane pressure wave whose propagation vector $\mathbf{k}^i$ lies in $x_1 - x_2$ plane, i.e., has no component along x_3 axis.

☐ Let symbol p (hereafter termed 'field') designate pressure field. Symmetry arguments entail that diffracted and total (i.e., incident plus diffracted) fields in half-space above deformed mirror do not depend on x_3 coordinate. Two-dimensional nature of these problems

means that entire analysis takes place in $x_1 - x_2$ plane (see fig. 8.2.1).

■ Investigation is concerned with 2D scattering problem involved in reconstructing shape (i.e., profile function) of boundary from knowledge of incident and scattered fields.

□ Fluid (lower) portion of latter is designated by Ω and trace of boundary by Γ.

■ Assume that Γ can be described by parametric equation

$$x_2 = F(x_1) \; ; \; \forall x_1 \in \mathbb{R} \; , \tag{8.2.1}$$

wherein $f(x_1)$ is a continuous, single-valued function of x_1 for all $x_1 \in \mathbb{R}$, such that

$$F(x_1) = \begin{cases} f(x_1) & ; \quad x_1^g < x_1 < x_1^d \\ 0 & ; \quad -\infty < x_1 \leq x_1^g \\ 0 & ; \quad x_1^d \leq x_1 < \infty \end{cases} \quad , \tag{8.2.2}$$

with $f(x_1)$ a continuous, single-valued function of x_1 for all $x_1 \in]x_1^g, x_1^d[$.

□ One or two probe wave realizations are made to provide data for resolution of inverse problems. These probe waves are *monochromatic* plane waves whose angular frequency is ω, latter changing from one realization to other.

□ Time factor $\exp(-i\omega t)$ is implicit in all that follows.

■ Synthetic data concerning scattered field on strip H is generated via physical optics approximation (POA).

■ Intersecting canonical body approximation (ICBA) is employed in estimator.

8.3 Statement of forward and inverse scattering problems

□ The *forward problem* is: knowing

1. incident wave (i.e., amplitude, frequencies and direction),
2. physical properties (i.e., wavespeed) of fluid or dielectric,
3. height (assumed to be nil) of flat portion (assumed to be horizontal), position, shape and size of deformation of boundary assumed to be acoustically soft,

find diffracted pressure $p^d(\mathbf{x}, \omega)$ in Ω^0.

■ The *inverse problem* is: knowing

1. incident wave (i.e., amplitude, frequencies and direction),
2. physical properties (i.e., wavespeed) of fluid or dielectric,
3. measured or simulated diffracted field $u^d(\mathbf{x}, \omega)$ on a horizontal segment (see fig.8.2.1)

$$H = \left\{ x_2 = h > \max f(x_1),\ x_1 \in [x_1^a, x_1^b] \right\} \tag{8.3.3}$$

below boundary assumed to be acoustically soft,

find latter (i.e., position, shape and size of deformed portion).

■ We solve direct problem in approximate manner (by use of the POA predictor) to generate synthetic data.

■ We employ the ICBA estimator to solve the inverse problem.

8.4 The predictor: an approximate solution of forward problem to simulate measured data

□ Since, in present context, no measured data is available, we replace latter by solutions of forward scattering problem on measurement segment H.

□ To this end, we employ

$$p^{0[POA]}(y_1,h,\omega)=p^i(y_1,h,\omega)+p^r(y_1,h,\omega)+$$
$$\int_{x_1^g}^{x_1^d}\frac{i}{2}H_0^{(1)}\left(k^0\left|\sqrt{(y_1-x_1)^2+h^2}\right|\right)A^iik\sin\varphi^ie^{-ikx_1\cos\varphi^i}dx_1-$$
$$\int_{x_1^g}^{x_1^d}\frac{i}{2}H_0^{(1)}\left(k^0\left|\sqrt{(y_1-x_1)^2+(h^2-f(x_1))^2}\right|\right)\times$$
$$A^iik\left[\dot{f}(x_1)\cos\varphi^i-\sin\varphi^i\right]e^{-ik(x_1\cos\varphi^i+f(x_1)\sin\varphi^i)}dx_1\ ;$$
$$\forall y_1\in[x_1^a,x_1^b)]\ , \quad (8.4.4)$$

(wherein $p^i(y_1,y_2,\omega)=A^i\exp[ik^0(x_1\sin\varphi^i-x_2\cos\varphi^i)]$ and $p^r(y_1,y_2,\omega)=p^i(y_1,-y_2,\omega)$) which is mathematical expression of

POA field on measurement segment.

□ Use of Simpson quadrature to compute two integrals in (8.4.4) completes procedure for simulating measured field.

8.5 ICBA estimator

□ It was previously mentioned that, in absence of any deformation, mirror gives rise, in response to incident plane wave, to (exact) total field

$$p(\mathbf{y},\omega) = p^i(\mathbf{y},\omega) + p^r(\mathbf{y},\omega) \ ; \ \forall \mathbf{y} \in \Omega \ , \tag{8.5.5}$$

so that, in particular,

$$q(y_1,0,\omega) = -2\frac{\partial}{\partial y_2} p^i(y_1,0,\omega) \ ; \ \forall y_1 \in \mathbb{R} \ , \tag{8.5.6}$$

which is equivalent, for flat mirror $\{y_2 = 0 \ ; \ \forall y_1 \in \mathbb{R}\}$, to what zeroth-order Kirchhoff (ZOK) approximation predicts for a deformed mirror. Thus, ZOK is exact for flat mirror $\{y_2 = 0 \ ; \ \forall y_1 \in \mathbb{R}\}$.

□ Another consequence of ZOK is that:

$$q(y_1,\tau,\omega) = 2q^i(y_1,\tau,\omega) \ , \tag{8.5.7}$$

which is exact solution for normal derivative of response (*on boundary*) of perfectly flat mirror $\{y_2 = \tau = const. \ ; \ \forall y_1 \in \mathbb{R}\}$ to plane wave $p^i(\mathbf{y})$.

□ Exact solution for response, *at any point below boundary* of this mirror (corresponding to (8.5.5) for horizontal flat mirror situated at $y_2 = \tau$), is

$$p(\mathbf{y}, \omega) = p^i(\mathbf{y}, \omega) + \mathcal{R}p^r(\mathbf{y}, \omega) \; ; \; \forall y_2 > \tau \; ; \; \forall y_1 \in \mathbb{R} \; , \qquad (8.5.8)$$

with

$$\mathcal{R} \equiv -\exp(-2ik\tau \sin \varphi^i) \; . \qquad (8.5.9)$$

□ *Approach here is to employ (8.5.8) as an approximation of field at any point* (y_1, h) *below a trial deformed mirror* $y_2 = \tau(y_1)$.

■ The *estimator* employed to obtain $\tau(y_1)$ appeals to so-called *intersecting canonical boundary approximation* (this name, designated hereafter by letters ICBA, derives from fact that $(y_1, \tau(y_1))$ is point of intersection of deformed boundary with flat horizontal canonical boundary, i.e., for which boundary value problem is analytically-solvable)(see (8.5.8)-(8.5.9)).

□ There are as many canonical boundaries (each at a different depth $\tau(y_1)$), as number of measurement points (y_1, h) on measurement segment H (see fig. 8.5.1).

■ The ICBA estimator is expressed by

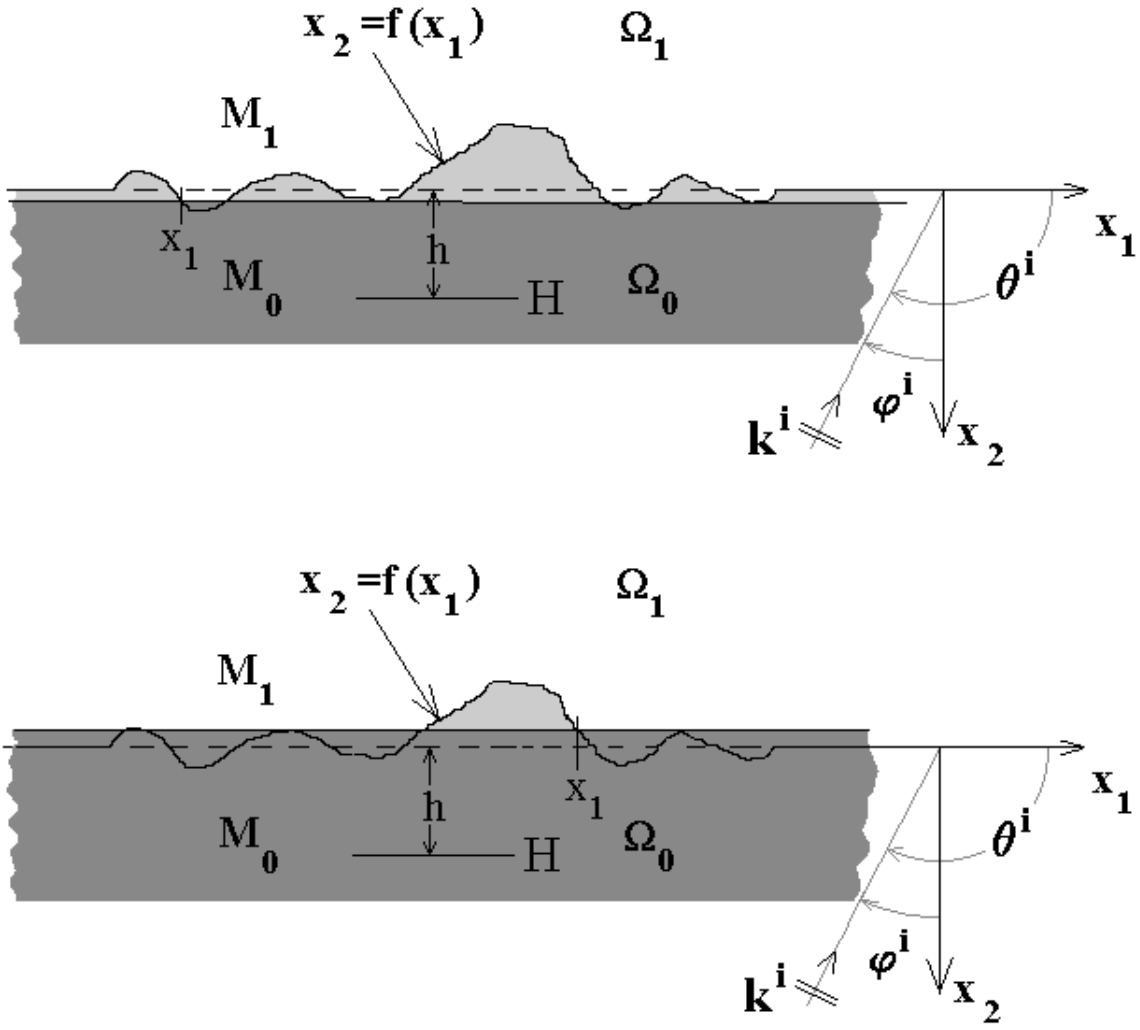

Figure 8.5.1: Examples of intersecting canonical bodies (depicted by dark grey half spaces) at two abscissas x_1.

$$p(y_1, y_2) \approx p^{ICBA}(y_1, y_2) \equiv A^i e^{-ik(y_1 \cos\varphi^i + y_2 \sin\varphi^i)} - A^i e^{-ik(y_1 \cos\varphi^i - [y_2 - 2\tau(y_1)] \sin\varphi^i)} \ . \quad (8.5.10)$$

□ From this relation one finds:

$$p^{ICBA}(y_1, \tau(y_1)) = 0 \ , \quad (8.5.11)$$

and

$$p^{ICBA}(y_1, h) = A^i e^{-ik(y_1 \cos\varphi^i + h \sin\varphi^i)} - A^i e^{-ik(y_1 \cos\varphi^i - [h - 2\tau(y_1)] \sin\varphi^i)} \ . \quad (8.5.12)$$

□ First of these two equations expresses fact that boundary condition is satisfied by ICBA estimator at all points of deformed boundary, and second relation constitutes ICBA estimation of response, on measurement segment, of trial boundary to incident wave.

■ Can be appreciated, by comparison with (8.4.4), that ICBA estimator is quite different, mathematically speaking, from POA predictor, this meaning that there is little risk of committing *inverse crime* when employing this predictor/estimator pair to reconstruct boundary.

8.6 Combining predictor and estimator to reconstruct profile function of deformed boundary

□ As indicated previously, inverse problem is to identify profile function $f(x_1)$ of scattering boundary.

■ Input is simulated data generated by POA *predictor*. Latter is compared to estimated response, provided by ICBA *estimator*, in order to retrieve a trial value of $\tau(y_1)$ of $f(y_1)$ corresponding to each measurement point (y_1, h). Comparison amounts to generating a function expressing *discrepancy* between diffracted fields provided by predictor and estimator, and associating correct solution(s) for profile with that value (or values) of $\tau(y_1)$ for which this function is nil or minimal.

□ Two such functions are employed hereafter.

□ Let $\hat{p}(y_1, h, f(y_1), \omega)$ and $\tilde{p}(y_1, h, \tau(y_1), \omega)$ designate total predicted and estimated total fields respectively at point (y_1, h) of measurement segment H.

□ Note that $f(y_1)$ has been explicitly incorporated in arguments of $\hat{p}$, and $\tau(y_1)$ in arguments of $\tilde{p}$, to signify that predictor is related to true profile function $f(y_1)$ whereas estimator is related to trial profile function $\tau(y_1)$.

□ Aforementioned comparison functions are:

$$I(y_1, h, f(y_1), \tau(y_1), \omega) \equiv \hat{u}(y_1, h, f(y_1)) - \tilde{u}(y_1, h, \tau(y_1), \omega) \tag{8.6.13}$$

and

$$J(y_1, h, f(y_1), \tau(y_1), \omega) \equiv |\hat{p}(y_1, h, f(y_1)) - \tilde{p}(y_1, h, \tau(y_1), \omega)|^2 \ , \tag{8.6.14}$$

it being understood that $\tau(y_1)$ will either be associated with root(s) of *comparison equation*

$$I(y_1, h, f(y_1), \tau(y_1), \omega) = 0 \tag{8.6.15}$$

or with minimum (or minima) of *least-squares cost function* $J(y_1, h, f(y_1), \tau(y_1), \omega)$.

$\square$ If it is assumed that estimated and predicted *incident* fields are identical (this may not always be true) then

$$I(y_1, h, f(y_1), \tau(y_1), \omega) \equiv \hat{p}^d(y_1, h, f(y_1)) - \tilde{p}^d(y_1, h, \tau(y_1), \omega) \tag{8.6.16}$$

and

$$J(y_1, h, f(y_1), \tau(y_1), \omega) \equiv |\hat{p}^d(y_1, h, f(y_1)) - \tilde{p}^d(y_1, h, \tau(y_1), \omega)|^2 \ , \tag{8.6.17}$$

wherein $\hat{p}^d$ and $\tilde{p}^d$ are diffracted fields of predictor and estimator respectively.

■ One of very specific features of use of ICBA predictor in comparison or cost functions should be underlined. Suppose that measurements, or simulations thereof, are carried out at M points on segment H whose abscissas are $y_1^1, y_1^2, ..., y_1^M$. Due to fact that ICBA incorporates a *local* approximation of field on H, *ICBA estimator involves only a single value* of profile function $\tau(y_1)$, i.e., $\tau(y_1^m)$, at each measurement point $(y_1^m, \tau(y_1^m))$.

□ This means that reconstruction proceeds either by solving a *single* comparison equation of form

$$I(y_1^m, h, f(y_1), \tau(y_1), \omega) = 0 \tag{8.6.18}$$

involving a *single* unknown $\tau(y_1^m)$ for each value of $m \in [1, M]$, or by minimizing a *single* cost function $J(y_1^m, h, f(y_1), \tau(y_1^m), \omega)$ involving same *single* unknown for each value of $m \in [1, M]$.

□ Due to fact that POA predictor does not involve a local, but rather a global, approximation of measured field, comparison equation in (8.6.18) and associated cost function involve true profile function $f(y_1)$ at *all points* $y_1 \in \mathbb{R}$,

■ I and J are *nonlinear* functions of $\tau(y_1^m)$ due to fact that ICBA estimator is a nonlinear function of $\tau(y_1^m)$.

□ Latter feature is shared by most of estimators employed in recent inverse scattering studies, but former feature is unique and specific

to use of ICBA estimator.

8.7 The information one can obtain by committing inverse crime

■ Before actually solving boundary reconstruction problem by minimizing cost function J, it is useful to see what happens when POA predictor is replaced by ICBA predictor in comparison equation:

$$I(y_1^m, h, f(y_1), \tau(y_1), \omega) = \hat{p}^d(y_1^m, h, \omega) - \tilde{p}^d(y_1^m, h, \omega) = \\ p^{d\ ICBA}(y_1^m, h, f(y_1^m)\omega) - p^{d\ ICBA}(y_1^m, h, \tau(y_1^m)\omega) = 0\ . \quad (8.7.19)$$

□ In explicit terms (see (8.5.12)) this amounts to:

$$I(y_1^m, h, f(y_1), \tau(y_1), \omega) = \\ A^i e^{-ik(y_1^m \cos\varphi^i + [h-2f(y_1^m)]\sin\varphi^i)} - A^i e^{-ik(y_1^m \cos\varphi^i - [h-2\tau(y_1^m)]\sin\varphi^i)} = 0\ , \quad (8.7.20)$$

from which is obtained:

$$\sin\left\{k[f(y_1^m) - \tau(y_1^m)]\sin\varphi^i\right\} = 0\ , \quad (8.7.21)$$

■ The solutions of this equation are:

$$\tau(y_1^m) = f(y_1^m) + \frac{n\pi}{k\sin\varphi^i}\ ;\ n = 0, \pm 1, ... \quad (8.7.22)$$

■ This (explicit inversion) result, which is an outcome of committing *inverse crime* (i.e., employing a predictor and estimator that are functionally equivalent), expresses:

i) fact (qualified by Colton and Kress as "trivial") that one recovers true profile (for $n = 0$) ordinate $\tau(y_1^m) = f(y_1^m)$ at abscissa y_1^m and

ii) fact (not trivial and not envisaged by Colton Kress) that an *infinite number of spurious profile ordinates* (i.e., for $n \neq 0$) are also obtained by this means.

□ This underlines a common feature of inverse problems: *non-uniqueness* of their solutions.

□ It will be seen in following section how this non-uniqueness manifests itself and in a later section how to eliminate ambiguity.

8.8 Some profile reconstructions arising from a single measurement realization

□ By a *single realization* is meant that data is generated at a single frequency ω and for a single incident angle φ^i chosen to be 0, i.e., normal incidence, in all that follows .

□ Measurement abscissas are equispaced and given by

$$y_1^m = x_1^l + (n-1)\frac{x_1^b - x_1^a}{M-1} \; ; \; m = 1, 2, .., M \; . \tag{8.8.23}$$

☐ Profile functions $F(x_1)$ are chosen to be nil outside of interval $[x_1^g = -(a_1 - a_3), x_1^d = a_1 + a_3]$ and to be sinusoidal in this interval so that:

$$f(x_1) = \frac{a_2}{2}\left\{1 + \cos\left[\frac{\pi}{a_1}(x_1 - a_3)\right]\right\} \ . \tag{8.8.24}$$

☐ In this relation, a_3 is a measure of lateral position of centroid of boundary deformation (e.g., vessel hull) with respect to origin, a_2 a measure of maximal deviation of of (e.g., sea) boundary with respect to reference line $x_2 = 0$, and a_1 a measure of width of boundary deformation.

☐ Reconstruction of other boundary deformation profiles (triangular, rectangular and elliptic) has also been carried out, but corresponding results are not shown herein since they are qualitatively same as for sinusoidal boundary deformation.

☐ A possible approach to reconstructing boundary from cost function J is to employ an off-the-shelf iterative nonlinear least squares minimizing algorithm (such as Levenberg-Marquardt scheme or simplex technique of Nelder and Mead).

☐ This requires, for each y_1^m, a starting value to initiate iterations, and, more often than not, obtained value of $\tau(y_1^m)$ corresponds to location of minimum of J closest to starting value. If starting values are close to true values, one obtains, in this way, a discrete representation of reconstructed profile (i.e., $\tau(y_1^1), \tau(y_1^2), ..., \tau(y_1^M)$) that

can be close to true profile. Moreover, if only one starting value is provided for each abscissa, one may be inclined to conclude that this minimization technique leads to a unique, satisfactory, boundary reconstruction.

□ However, result of previous section, constitutes a warning that *such a conclusion may be erroneous* because of non-uniqueness. Moreover, if starting values in iterative minimization scheme are relatively far from their true values, chances are that scheme will hone in on local rather than global minima, with result that reconstructed profile be very far from true profile.

□ For this reason, *strategy adopted herein* is to compute cost function for all abscissas $y_1^1, y_1^2, ..., y_1^M$ and for a discrete set of trial profile ordinates $\tau_1(y_m^1), \tau_2(y_1^m), ..., \tau_L(y_1^M)$ at each of aforementioned abscissas y_1^m.

□ Every $\tau_l(y_1^m)$ is chosen to be within reasonable limits, i.e.,

$$b_1 \leq \tau_l(y_1^m) \leq b_2 \ , \tag{8.8.25}$$

wherein b_2 can be taken to be of order or equal to h since measurement segment is assumed to be *below* lowest excursion of boundary deformation.

■ This procedure, involving computation of $L \times M$ cost functions (whose graphical representation is hereafter termed $J - map$) may appear to have a high price, but it possesses virtue of avoiding elimi-

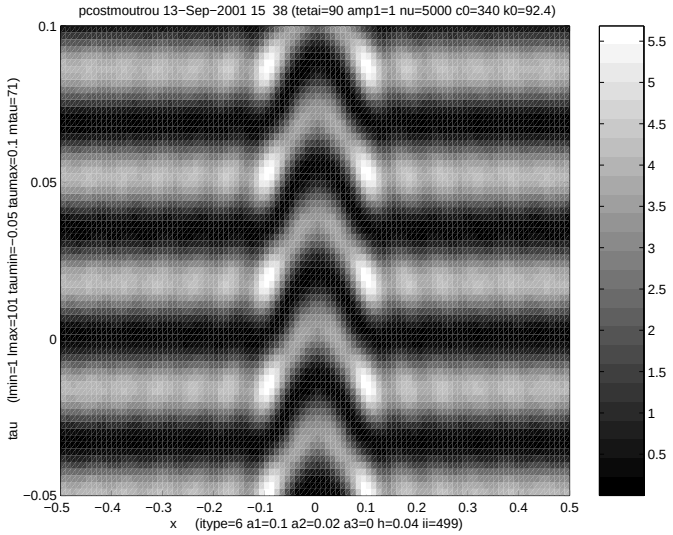

Figure 8.8.1: J map for sinusoidal boundary deformation: $a_1 = 20m,\ a_2 = 4m,\ a_3 = 0m,\ h = 8m,\ c = 340m/s,\ \omega/2\pi = 25Hz$. This figure, as well as all subsequent figures has to be put upside down to be consistent with sea surface detection problem (i.e., probe radiation coming from bottom, sea surface, including hull of floating vessel, on top).

nation (by accident or design) of acceptable candidate solutions corresponding to either global or local minima of cost function.

■ Fig. 8.8.1 illustrates what J-map looks like for a sinusoidal boundary deformation (representative of intrusive portion of hull of a light floating vessel.

□ It is apparent that cost function (J) map exhibits many minima for each abscissa, in conformity with analysis of previous section, and that an iterative minimization technique employing one starting value per abscissa would provide only one boundary reconstruction, which could be far from true boundary if starting values were relatively far from true boundary.

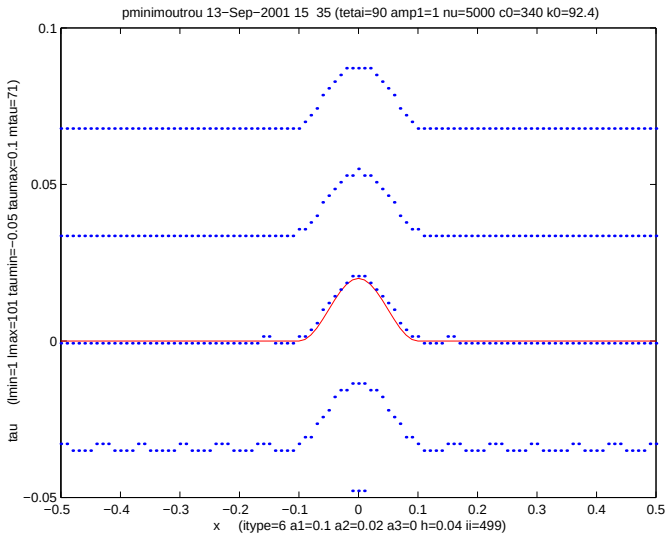

Figure 8.8.2: W-map for same configuration and same parameters as in fig.8.8.1. Dots refer to reconstructed boundaries whereas continuous thin line refers to actual boundary in present and all subsequent figures. This figure has to be put upside down to be consistent with sea surface detection problem.

☐ Previous figure is difficult to exploit quantitatively, so that next step should involve *finding all minima* (local and global) of J-map. This is done by a simple scanning technique and results in a graph (called the W-map) such as Fig. 8.8.2 for same sinusoidal boundary deformation wherein it can be appreciated that different solutions follow, very closely, inverse crime prediction of previous section.

☐ There remains problem of eliminating spurious solutions.

8.9 Removal of spurious solutions

☐ Relation (8.7.22), resulting from inverse crime, indicates that only solution that does not depend on wavenumber and incident angle is one corresponding to $n = 0$, latter being correct solution, and spurious solutions corresponding to $n \neq 0$.

■ This suggests that *a way of eliminating spurious solutions is to vary either wavenumber (i.e., frequency ω, since two are related by $k = \omega/c$) or incident angle φ^i.*

□ Thus, suppose that *two measurement realizations are carried out at two frequencies ω_1 and ω_2.*

□ Eq. (8.7.22) indicates that all but one of dark horizontal 'fringes' in system of 'fringes' (corresponding to minima of cost function) in J-map (see e.g., fig. 8.8.1) are displaced when ω changes, so that it suffices to isolate single static dark fringe in order to spot correct profile.

■ A more *quantitative* method is to assign a weight of 1 to each pixel in J-map corresponding to position of a minimum (global or local) and a weight of 0 to each pixel corresponding to positions at which there are no minima, this being done for two J-maps at two frequencies. Thus, two new graphs (for two frequencies) are generated, called $X - maps$, containing a series of ones and zeros (positions occupied by ones are indicated by a dark point, others being left blank in graphs of W-maps).

□ Two maps are then added, resulting in a new graph ($Y - map$) containing a series of zeros, ones and twos.

□ Pixels occupied by zeros indicate positions $(y^1, \tau(y^1))$ for which there are no minima at either frequency.

□ Pixels occupied by ones indicate positions $(y^1, \tau(y^1))$ for which there is a minimum at one frequency, but not at other frequency, these being (according to (8.7.22)) spurious solutions.

□ Pixels occupied by twos indicate positions $(y^1, \tau(y^1))$ for which there is a minimum at both frequencies, these being (according to (8.7.22)) correct solutions.

■ Thus, by eliminating all positions corresponding to weights less than two (a process termed 'filtering'), one generates so-called $Z - map$ which, normally speaking, should constitute graph of discretized form of correct profile function.

■ Graphical form of Z-map is such that dark points indicate positions with weight two, all other positions being left blank.

□ Degree of success of this procedure is illustrated in W-maps of fig. 8.8.2 (for $\omega_1/2\pi = 25Hz$), fig. 8.9.1 (for $\omega_1/2\pi = 27.5Hz$) and Z-map of fig. 8.9.2.

□ A similar procedure could be adopted by changing incident angle instead of frequency, but owing to fact that accuracy of POA predictor is sensitive to incident angle due to shadowing and multiple scattering, filtering process based on incident angle changes may be less successful than that based on frequency changes (moreover, it may not be easy for a submarine to change angle of incidence of its sonar or radar beam).

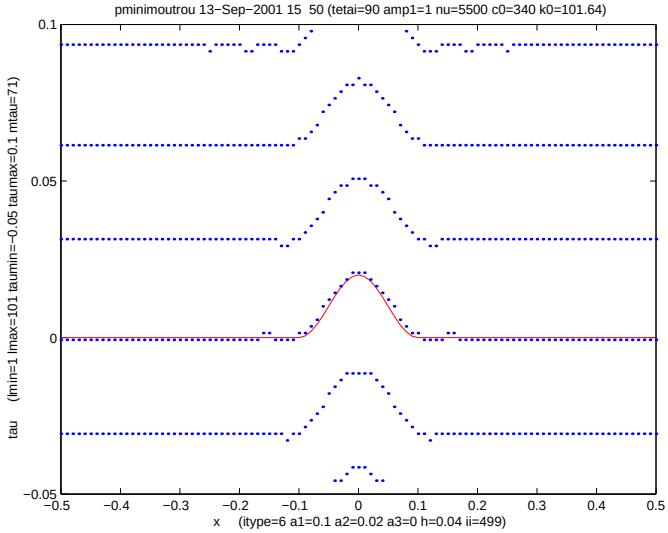

Figure 8.9.1: W-map for same configuration and same parameters as in fig. 8.8.2, except that $\omega/2\pi = 27.5Hz$. This figure has to be put upside down to be consistent with sea surface detection problem.

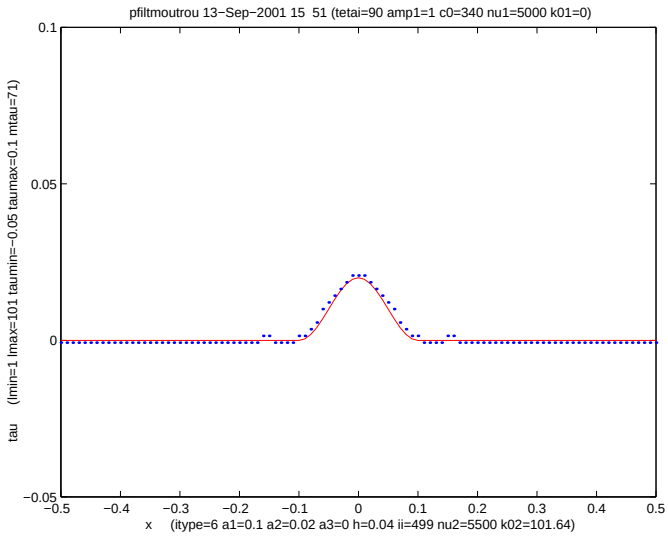

Figure 8.9.2: Z-map obtained by filtering W-maps for realizations at $\omega/2\pi = 25Hz$ and $\omega/2\pi = 27.5Hz$ corresponding to configurations in figs. 8.8.2 and 8.9.1. This figure has to be put upside down to be consistent with sea surface detection problem.

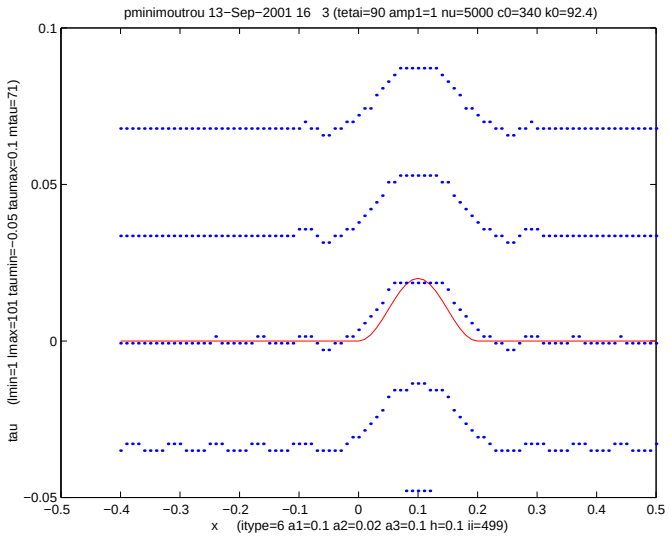

Figure 8.10.1: W-map for sinusoidal boundary deformation. $a_1 = 20m,\ a_2 = 4m,\ a_3 = 20m,\ h = 20m,\ c = 340m/s,\ \omega/2\pi = 25Hz$. This figure has to be put upside down to be consistent with sea surface detection problem.

☐ Note that frequency should be sufficiently large for fringes in J-map to be separated, but not so large as to change significantly accuracy of POA prediction when going from one frequency to other.

8.10 More results

☐ Performance of filtering procedure is further illustrated in figs. 8.10.1-8.10.11 for sinuoidal boundary deformation having different slopes, with detection at different depths and at different frequencies.

☐ Figs. 8.10.1- 8.10.3 apply to same boundary deformation (although displaced laterally by $20m$) as in figs. 8.8.1- 8.9.2, that is *detected on a strip at depth* $h = 20m$ *instead of previous* $h = 8m$.

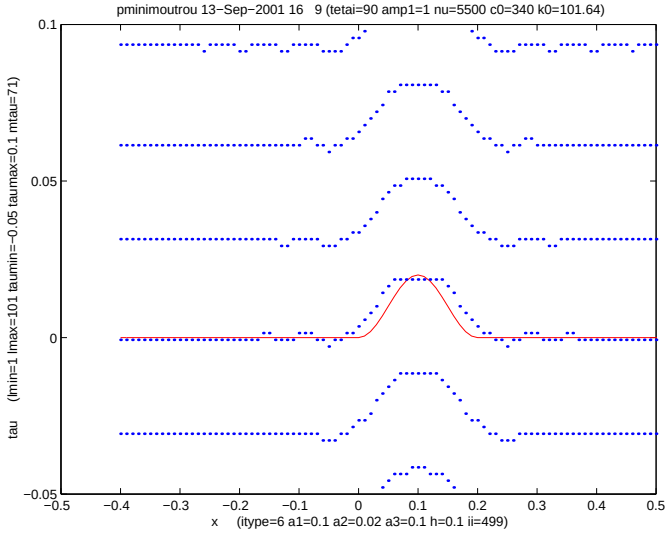

Figure 8.10.2: W-map for same configuration and same parameters as in fig.8.10.1, except that $\omega/2\pi = 27.5Hz$. This figure has to be put upside down to be consistent with sea surface detection problem.

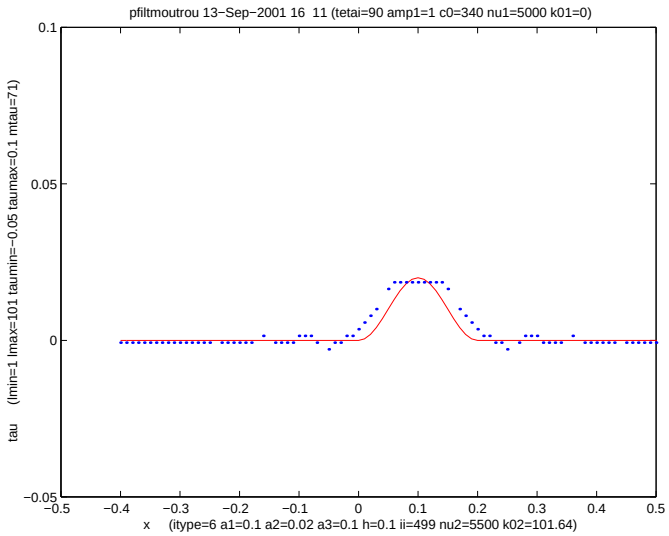

Figure 8.10.3: Z-map obtained by filtering W-maps for realizations at $\omega/2\pi = 25Hz$ and $\omega/2\pi = 27.5Hz$. corresponding to configurations in figs. 8.10.1 and 8.10.2. This figure has to be put upside down to be consistent with sea surface detection problem.

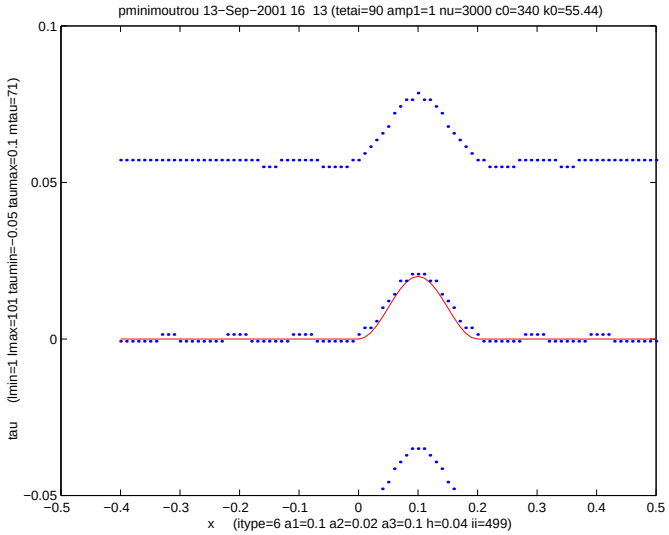

Figure 8.10.4: W map for sinusoidal boundary deformation. $a_1 = 20m,\ a_2 = 4m,\ a_3 = 20m,\ h = 8m,\ c = 340m/s,\ \omega/2\pi = 15Hz$. This figure has to be put upside down to be consistent with sea surface detection problem.

□ This results in somewhat of a degradation of quality of reconstruction of shape of hull, but lateral position ($a_3 = 20m$) of hull is correctly predicted, just as in previous example ($a_3 = 0m$). Despite this, fig. 8.10.3 shows that *filtering procedure is still effective.*

□ Figs. 8.10.4- 8.10.7 deal essentially with effect of *reducing frequency* of probe radiation.

□ This effect is such as to degrade quality of reconstructed shape, all more so than measurement strip is farther from boundary.

■ Nevertheless lateral position of boundary deformation is correctly recovered in all these examples.

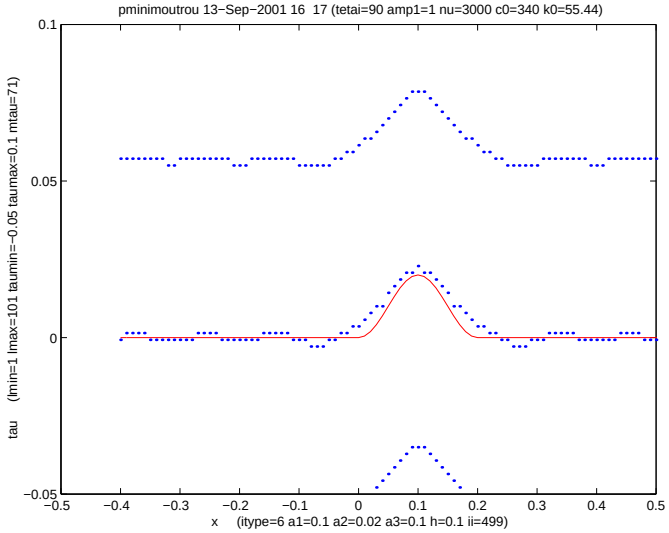

Figure 8.10.5: W-map for same configuration and same parameters as in fig.8.10.4, except that $h = 20m$. This figure has to be put upside down to be consistent with sea surface detection problem.

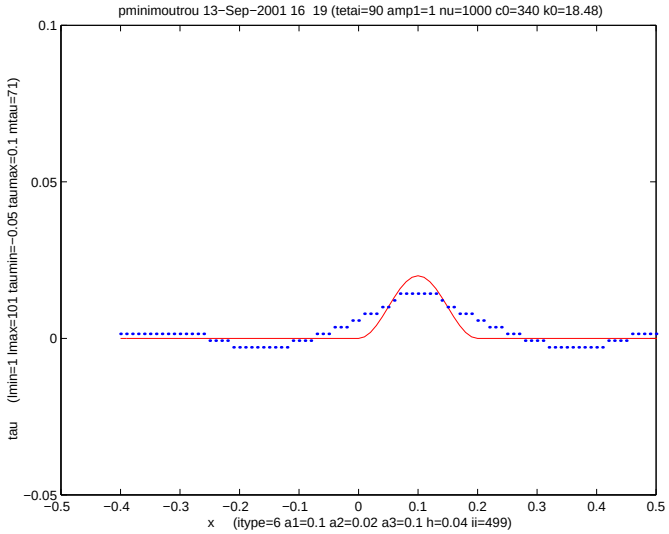

Figure 8.10.6: W map for sinusoidal boundary deformation. $a_1 = 20m,\ a_2 = 4m,\ a_3 = 20m,\ h = 8m,\ c = 340m/s,\ \omega/2\pi = 5Hz$. This figure has to be put upside down to be consistent with sea surface detection problem.

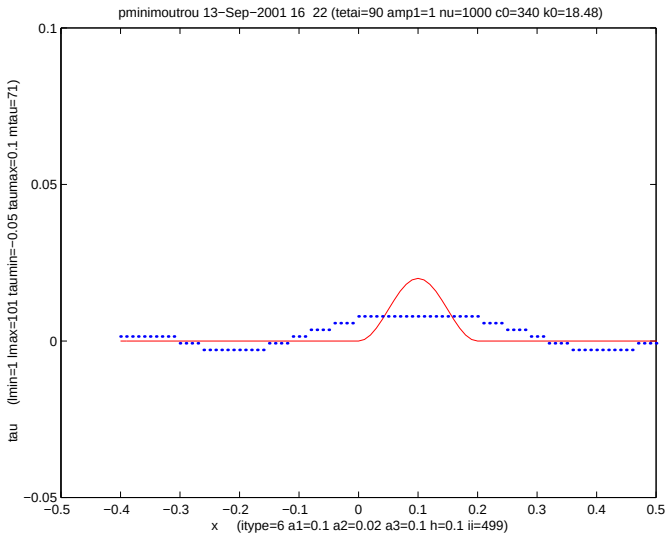

Figure 8.10.7: W-map for same configuration and same parameters as in fig. 8.10.6, except that $h = 20m$. This figure has to be put upside down to be consistent with sea surface detection problem.

■ An *interesting feature* of figs. 8.10.6 and 8.10.7, relative to lowest frequency probe radiation, is that W-maps contain *only one reconstructed profile* in a search interval $[b_1, b_2]$ that is same as at higher frequencies.

■ This may explain why investigations dealing with inverse scattering often give impression that solution is unique.

□ This would not be true in results of figs. 8.10.6 and 8.10.7 if search interval were chosen to be larger (in alluded-to investigations it is often quite small), and results of other figures show that solutions are certainly not unique at higher frequencies.

□ Figs. 8.10.8-8.10.11 deal essentially with effect of *increasing slope of boundary deformation* (by increasing amplitude parameter a_2).

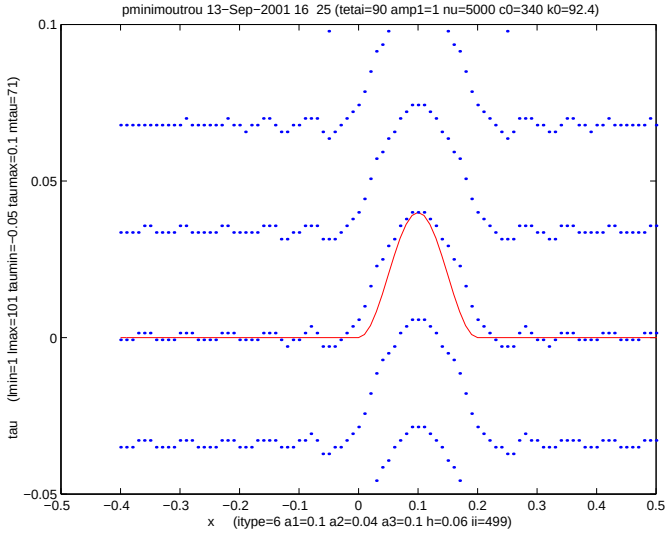

Figure 8.10.8: W map for sinusoidal boundary deformation. $a_1 = 20m,\ a_2 = 8m,\ a_3 = 20m,\ h = 12m,\ c = 340m/s,\ \omega/2\pi = 25Hz$. This figure has to be put upside down to be consistent with sea surface detection problem.

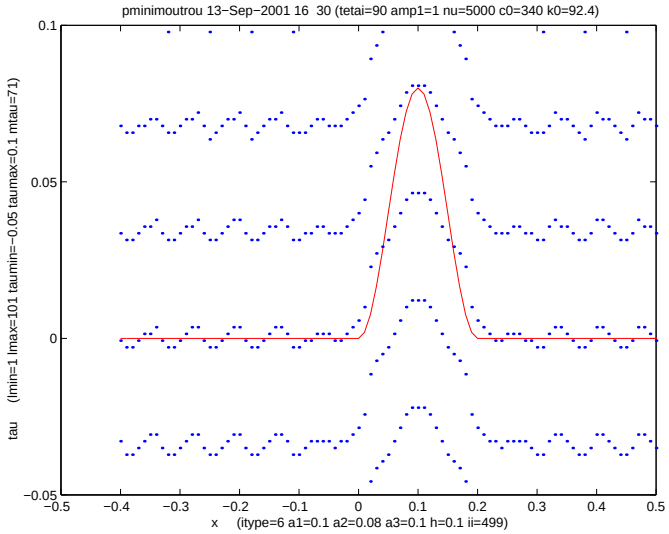

Figure 8.10.9: W map for sinusoidal boundary deformation. $a_1 = 20m,\ a_2 = 16m,\ a_3 = 20m,\ h = 20m,\ c = 340m/s,\ \omega/2\pi = 25Hz$. This figure has to be put upside down to be consistent with sea surface detection problem.

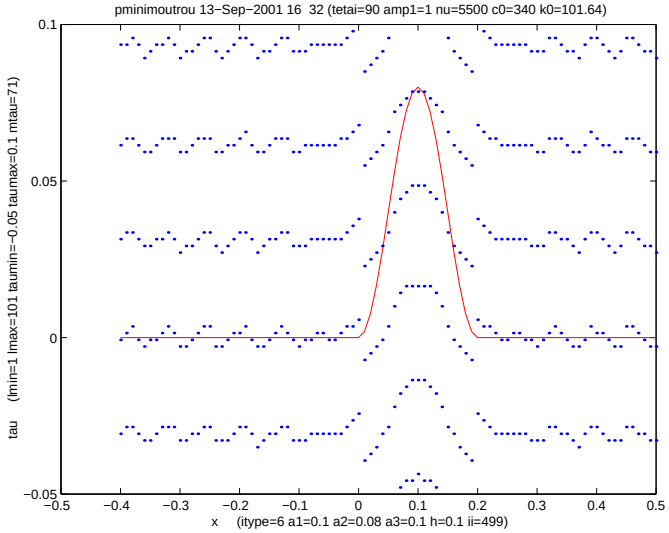

Figure 8.10.10: W-map for same configuration and same parameters as in fig. 8.10.9, except that $\omega/2\pi = 27.5Hz$. This figure has to be put upside down to be consistent with sea surface detection problem.

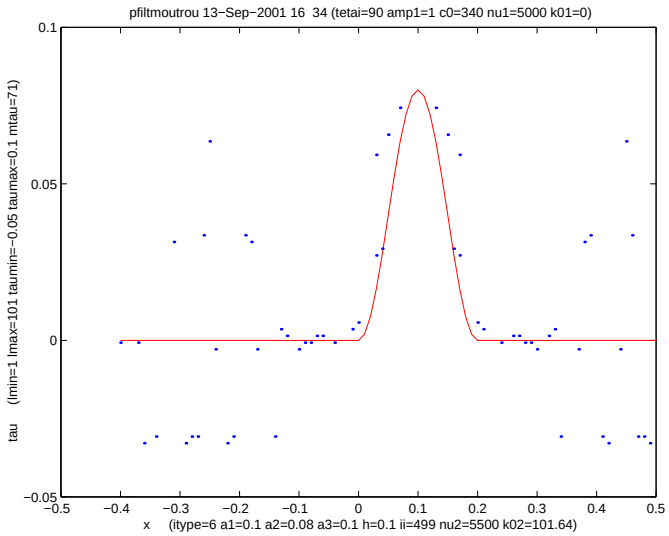

Figure 8.10.11: Z-map obtained by filtering W-maps for realizations at $\omega/2\pi = 25Hz$ and $\omega/2\pi = 27.5Hz$ corresponding to configurations in figs. 8.10.9 and 8.10.10. This figure has to be put upside down to be consistent with sea surface detection problem.

☐ This effect is such as to produce a degradation of quality of reconstructed shape of boundary deformation, with no effect on accuracy of recovered lateral position.

☐ Fig. 8.10.11 shows that *filtering technique is much less effective for relatively large slope boundary deformations*, probably because ICBA estimator is very different from PO predictor for such boundaries.

8.11 Discussion

☐ Previous results seem to indicate that parameters h and a_2/a_1 control similarity between predictor and estimator: when h is small (i.e., measurement segment nearly touches reference plane), or $a_2/a_1 << 1$ (i.e., boundary is almost a flat mirror), ICBA and POA give rise to essentially same diffracted fields, which is why reconstructions are very accurate, i.e., something similar to *inverse crime* is being committed.

☐ Fact that frequency controls resolution is a classical issue in all forms of (e.g., optical) imaging: increasing frequency increases resolution. Here this rule is verified, probably because increasing frequency doesn't produce an increase in discrepancy between ICBA and POA descriptions of diffracted field.

☐ On whole, proposed filtering procedure accomplishes what it is designed for: eliminating spurious solutions for boundaries with small to moderate slopes . This technique is an outcome of a deliber-

ate effort to commit inverse crime, which could (contrary to what is advised in Colton & Kress 1992) be applied to help resolve non-uniqueness issue in other inverse problems.

☐ More generally, successful boundary reconstructions hinge on functional similarity (even for real data as latter can be represented by a function) between predictor and estimator. Herein this is obtained for small h and/or small a_2/a_1; for other predictor/estimator pairs it will be obtained at low frequencies, high frequencies, etc.

☐ When data is real (i.e., obtained by experiment) instead of simulated, best strategy is to employ a predictor that matches as nearly as possible data (accurate for accurate data, less accurate for error-ridden data).

☐ Considering that POA is accurate only for near-normal incidence and at relatively high frequencies ($ka >> 1$, with a a characteristic dimension of boundary deformation), one can advocate use of ICBA as interaction model for predictor only under these conditions.

☐ Fortunately, latter are favorable for obtaining high resolution, and, due to simplicity of ICBA predictor, reconstructions are obtained extremely rapidly.

☐ Thus, proposed method is fast and gives rise to high resolution images of boundary when employed at high frequencies.

☐ Method of present investigation, appealing to ICBA estimator,

is faster, computationally speaking, and gives rise to reconstructions of about same accuracy, as compared to so-called 'generalized dual space indicator' (or 'linear sampling') method. However, latter presents advantage (substantial in many applications) of not requiring a priori knowledge of nature of boundary condition (as long as it is of Dirichlet (acoustically soft), Neumann (acoustically rigid) or Robin (impedance) type). In this sense, two methods are complementary and results obtained with one can be confirmed by other.

□ A final issue to be considered, related to problem alluded to in introduction, is whether a reconstruction procedure of type described herein enables detection of a floating vessel from within sea, especially if sea surface is perturbed by gravity waves. As long as these waves do not have slopes that are too steep, rough sea surface with deformation due to presence of vessel can be reconstructed by proposed method. If several realizations were made of reconstruction at several instants (separated by a very short time interval), and various reconstructions were averaged, hopefully a more or less inclined (because vessel rocks in a rough sea) image of hull could be obtained, flanked by a horizontal mirror (because sea surface is, on average, mirror-like and horizontal). Further work has to be done to verify truth of this expectation, which would depend on whether average amplitude of gravity waves is smaller than that of average intrusion of vessel into sea water.

Chapter 9

Identification of an acoustically-soft rough boundary of infinite extent by low-frequency probe radiation

9.1 Features of forward and inverse scattering problem

□ Object: 2D fluid acoustical inverse problem illustrated in fig. 9.1.1.

□ In absence of roughness, configuration is that of an impenetrable half space domain $\overline{\Omega}_1$ separated by flat, horizontal interface $\overline{\Gamma} = \Gamma^g \cup \Gamma^0 \cup \Gamma^d$ (wherein $\Gamma^g,\ \Gamma^0,\ \Gamma^d$ are flat, horizontal segments) from half-infinite domain $\overline{\Omega}_0$ filled with a known homogeneous fluid M^0 with (spatially-constant) acoustic parameters (k^0, ρ^0).

□ *In presence of roughness*, localized in domain Γ^c described by parametric equation $x_2 = f(x_1)$, interface is $\Gamma = \Gamma^g \cup \Gamma^c \cup \Gamma^d$.

■ Problem is to identify Γ^c from measurements of pressure field in subdomains of Ω_0^{d1}, Ω_0^{d2},..., $\Omega_0^{dM_0}$ of Ω_0 when configuration is probed by cylindrical waves radiated by cylindrical sources having supports Ω_0^{s1}, Ω_0^{s2},..., $\Omega_0^{sN_0}$ in Ω_0. Γ separates half-infinite domain $\Omega_0 \supset \overline{\Omega}_0$

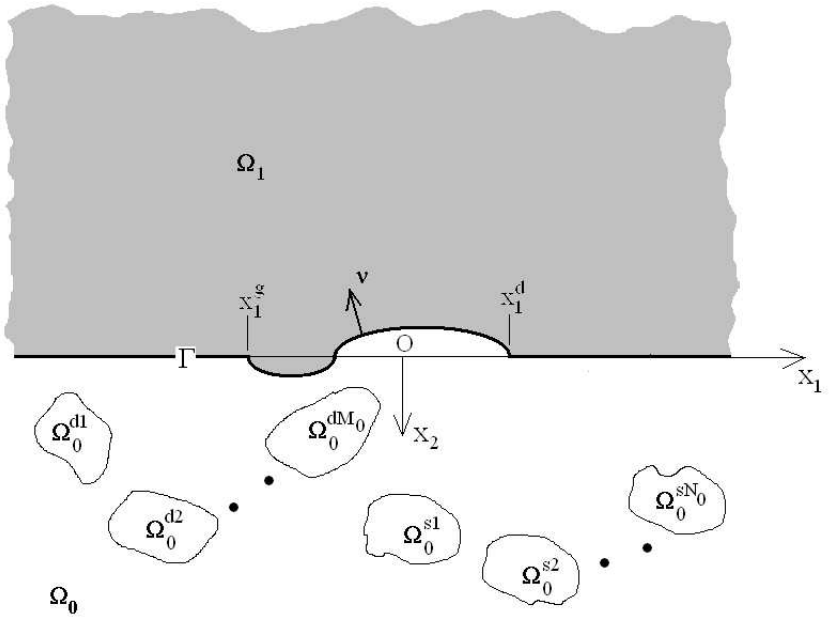

Figure 9.1.1: Configuration, in cross-section plane, corresponding to inverse problem of identification of rough interface between two homogeneous fluid-like half spaces, probed by the waves radiated by a set of cylindrical sources located in lower half space.

filled with a known homogeneous fluid M^0 with (spatially-constant) acoustic parameters (k^0, ρ^0) from half-infinite impenetrable domain $\Omega_1 \supset \overline{\Omega}_1$.

□ Note that each experimental realization is conducted with only one source radiating at a time and measurements of pressure field are made in any or all of subdomains Ω_0^{d1}, Ω_0^{d2},..., $\Omega_0^{dM_0}$ of Ω_0 for n_0-th incident-wave-in-Ω_0 realization.

9.2 Governing equations for scattering from a rough interface separating a homogeneous half space separated from an impenetrable half space, probed by a cylindrical wave radiated by a cylindrical source whose support is $\Omega_0^{sn_0}$

□ Governing equations for pressure field:

$$\left[\triangle + \left(k^0\right)^2\right] p^{0n}(\mathbf{x}, \omega) = -s^{0n}(\mathbf{x}) \;\; ; \;\; \mathbf{x} \in \Omega_0 \; , \tag{9.2.1}$$

$$p^{0n}(\mathbf{x}, \omega) = 0 \;\; ; \;\; \mathbf{x} \in \Gamma \; , \tag{9.2.2}$$

$$p^{0n}(\mathbf{x}, \omega) \sim \text{outgoing waves} \; , \; \mathbf{x} \in \Omega_0 \; , \; \|\mathbf{x}\| \to \infty \; , \tag{9.2.3}$$

(wherein $n = n_0$), and $\boldsymbol{\nu}$ is unit vector normal to Γ). Note that there are N_0 of these sets of equations for realizations $n_0 = 1, 2, ..., N_0$.

9.3 Governing equations for specific Green's function

☐ Governing equations:

$$\left[\triangle + \left(k^0\right)^2\right] g^0(\mathbf{x}, \mathbf{z}, \omega) = -\delta(\mathbf{x} - \mathbf{z}) \ \ ; \ \ \mathbf{x} \in \overline{\Omega_0} \ , \ \mathbf{z} \in \overline{\Omega_0} \ , \quad (9.3.4)$$

$$g^0(\mathbf{x}, \mathbf{z}, \omega) = 0 \ \ ; \ \ \mathbf{x} \in \overline{\Gamma} \ , \quad (9.3.5)$$

$$g^0(\mathbf{x}, \mathbf{z}, \omega) \sim \text{outgoing waves} \ , \ \mathbf{x} \in \overline{\Omega}_0 \ , \ \|\mathbf{x}\| \to \infty \ . \quad (9.3.6)$$

☐ Henceforth we drop ω dependence of various field quantites.

9.4 Integral representation of pressure field in Ω_0 for n-th realization

☐ In obvious short-hand notation, we obtain from previous governing equations:

$$g^0 \left[\Delta + \left(k^0\right)^2\right] p^{0n} = -g^0 s^{0n} \ \ ; \ \ \text{in } \Omega_0 \ , \quad (9.4.7)$$

$$p^{0n} \left[\Delta + \left(k^0\right)^2\right] g^0 = -p^{0n} \delta \ \ ; \ \ \text{in } \Omega_0 \ , \quad (9.4.8)$$

so that after use of Green's theorem and sifting property of δ function:

$$\int_\Gamma (g^0 \partial_\nu p^{0n} - p^{0n} \partial_\nu g^0) d\gamma + \int_{\Omega_0} g^0 s^{0n} d\varpi = \mathcal{H}_{\Omega_0}(\mathbf{z}) p^{0n}(\mathbf{z}) \ , \quad (9.4.9)$$

wherein $\partial_\nu \mathcal{F} := \boldsymbol{\nu}(\mathbf{x}) \cdot \nabla \mathcal{F}(\mathbf{x})$, $d\gamma$ is differential element of arc length, and $d\varpi$ differential element of area.

□ Employing boundary condition (9.2.2) gives

$$\int_\Gamma g^0 \partial_\nu p^{0n} d\gamma + \int_{\Omega_0} g^0 s^{0n} d\varpi = \mathcal{H}_{\Omega_0}(\mathbf{z}) p^{0n}(\mathbf{z}) \ , \tag{9.4.10}$$

□ From fact that Γ is composite,

$$\int_{\Gamma^g + \Gamma^d} g^0 \partial_\nu p^{0n} d\gamma + \int_{\Gamma^c} g^0 \partial_\nu p^{0n} d\gamma + \int_{\Omega_0} g^0 s^{0n} d\varpi = \mathcal{H}_{\Omega_0}(\mathbf{z}) p^{0n}(\mathbf{z}) \ , \tag{9.4.11}$$

which takes form, after use of boundary condition (9.3.5):

$$\int_{\Gamma^c} g^0 \partial_\nu p^{0n} d\gamma + \int_{\Omega_0} g^0 s^{0n} d\varpi = \mathcal{H}_{\Omega_0}(\mathbf{z}) p^{0n}(\mathbf{z}) \ , \tag{9.4.12}$$

whence following expression of field in Ω_0:

$$p^{0n}(\mathbf{z}) = \int_{\Omega_0} g^0(\mathbf{z}, \mathbf{x}) s^{0n}(\mathbf{x}) d\varpi(\mathbf{x}) + \int_{\Gamma^c} g^0(\mathbf{z}, \mathbf{x}) \partial_{\nu_x} p^{0n}(\mathbf{x}) d\gamma(\mathbf{x}) \ . \tag{9.4.13}$$

9.5 Specific Green's function

□ We make ansatz

$$g^0(\mathbf{z}, \mathbf{x}) = G^0(\mathbf{z}, \mathbf{x}) - G^0(\mathbf{z}, \mathbf{x}') \ , \tag{9.5.14}$$

wherein

$$G^0(\mathbf{z},\mathbf{x}) = \frac{i}{4} H_0^{(1)}(k^0\|\mathbf{z}-\mathbf{x}\|) \ , \tag{9.5.15}$$

$$\mathbf{x} = (x_1, x_2) \ \ , \ \ \mathbf{x}' = (x_1, -x_2) \ . \tag{9.5.16}$$

□ Since free-space Green's function $G^0(\mathbf{z},\mathbf{x})$ satisfies inhomogeneous Helmholtz equation (9.3.4) and radiation condition (9.3.6), we conclude that our ansatz for $g^0(\mathbf{z},\mathbf{x})$ also satisfies (9.3.4) and (9.3.6).

□ Recall that $\overline{\Gamma} = \{x_2 = 0 \ ; \ \forall x_1 \in \mathbb{R}\}$. From fact that $\mathbf{x} = \mathbf{x}'$ for $x_2 = 0$ and that $x_2 = 0 \Longleftrightarrow \mathbf{x} \in \overline{\Gamma}$, we find

$$g(\mathbf{z},\mathbf{x}) = 0 \ \ ; \ \ \mathbf{x} \in \overline{\Gamma} \ , \tag{9.5.17}$$

which shows that our ansatz satisfies boundary condition (9.3.5) as it should.

■ Since our ansatz satisfies all required condtions for specific Green's function, it is correct specific Green's function for our problem.

9.6 Another form of pressure field

□ On account of (9.5.14) we can cast (9.4.13) into form

$$p^{0n}(\mathbf{z}) = p^{in}(\mathbf{z}) + p^{rn}(\mathbf{z}) + p^{sn}(\mathbf{z}) \ \ ; \ \ \mathbf{z} \in \Omega_0 \ , \tag{9.6.18}$$

wherein

$$p^{in}(\mathbf{z}) = \int_{\Omega_0} G^0(\mathbf{z},\mathbf{x}) s^{0n}(\mathbf{x}) d\varpi(\mathbf{x}) \ , \tag{9.6.19}$$

is incident field,

$$p^{rn}(\mathbf{z}) = -\int_{\Omega_0} G^0(\mathbf{z},\mathbf{x}') s^{0n}(\mathbf{x}) d\varpi(\mathbf{x}) \ , \tag{9.6.20}$$

specularly-reflected field, and

$$p^{sn}(\mathbf{z}) = \int_{\Gamma^c} g^0(\mathbf{z},\mathbf{x}') \partial_{\nu_x} p^{0n}(\mathbf{x}) d\gamma(\mathbf{x}) \ . \tag{9.6.21}$$

scattered field.

□ This subdivision stems from fact that $p^{sn}(\mathbf{z}) = 0$ when $\Gamma^c = \Gamma^0$, and $p^{0n}(\mathbf{z}) = p^{in}(\mathbf{z}) + p^{rn}(\mathbf{z})$ is indeed solution of problem of a pressure wave incident on a flat, soft interface (i.e., incident wave is specularly-reflected by interface).

9.7 Sum-of-plane-waves form of scattered pressure field below lowest point of scattering boundary

□ Cartesian coordinate integral representation of free-space Green's function is

$$G^0(\mathbf{z},\mathbf{x}) = G^0(\mathbf{x},\mathbf{z}) = \frac{i}{4\pi} \int_{-\infty}^{\infty} \exp\{i[k_1(x_1-z_1)+k_2^{0+}|x_2-z_2|]\} \frac{dk_1}{k_2^{0+}} \ , \tag{9.7.22}$$

wherein $k_2^{0\pm} = \pm\sqrt{(k^0)^2 - (k_1)^2}$, $\Re k_2^{0+} \geq 0$ and $\Im k_2^{0+} \geq 0$.

■ In same cartesian coordinate system, we assume that boundary curve Γ is sufficiently regular for it to be representable by parametric equation

$$x_2 = F(x_1) = \begin{cases} f(x_1) & ; \quad x_1^g < x_1 < x_1^d \\ 0 & ; \quad -\infty < x_1 \leq x_1^g \ , \ x_1^d \leq x_1 < \infty \end{cases} . \tag{9.7.23}$$

wherein f is a continuous, differentiable, single-valued function of x_1.

□ Then

$$\partial_{\nu_x} p^{0n}(\mathbf{x})\Big|_{\Gamma^c} = \boldsymbol{\nu}_x \cdot \nabla p^{0n}(\mathbf{x})\Big|_{\Gamma^c} = \frac{\left(\dot{f}(x_1)\partial_{x_1} - \partial_{x_2}\right)}{\sqrt{\left(\dot{f}(x_1)\right)^2 + 1}} p^{0n}(x_1, f(x_1) \ , \tag{9.7.24}$$

$$\dot{f}(x_1) := \frac{df(x_1)}{dx_1} \quad , \quad d\gamma(\mathbf{x}) = \sqrt{\left(\dot{f}(x_1)\right)^2 + 1}\ dx_1 \ , \tag{9.7.25}$$

so that

$$p^{sn}(\mathbf{z}) = \frac{i}{4\pi}\int_{-\infty}^{\infty}\frac{dk_1}{k_2^{0+}}e^{ik_1z_1}\int_{x_1^g}^{x_1^d}dx_1\Big[e^{i(-k_1x_1+k_2|z_2-f(x_1)|)}\_ \\ e^{i(-k_1x_1+k_2|z_2+f(x_1)|)}\Big]\times\Big(\dot{f}(x_1)\partial_{x_1}-\partial_{x_2}\Big)p^{0n}(x_1,f(x_1))\ . \quad (9.7.26)$$

□ Let

$$f_{min}=\min_{x\in[x_1^g,x_1^d]}\ ,\ f_{max}=\max_{x\in[x_1^g,x_1^d]}\ ,\ \Omega_0^+=\{x_2>f_{max}\ ;\ \forall x_1\in\mathbb{R}\} \\ \Rightarrow \quad (9.7.27)$$

■

$$p^{sn}(\mathbf{z})=\int_{-\infty}^{\infty}B^{0n}(k_1)e^{i[k_1z_1+k_2z_2]}dk_1\ \ ;\ \ \mathbf{z}\in\Omega_0^+\ , \quad (9.7.28)$$

wherein

$$B^{0n}(k_1)=\frac{i}{4\pi k_2^{0+}}\int_{-\infty}^{\infty}\Big[e^{-i[k_1z_1+k_2f(x_1)]}\_ \\ e^{-i[k_1z_1-k_2f(x_1)]}\Big]\Big(\dot{f}(x_1)\partial_{x_1}-\partial_{x_2}\Big)p^{0n}(x_1,f(x_1))dx_1\ . \quad (9.7.29)$$

9.8 Scattered pressure field in far-field zone

☐ Starting point is (9.6.21)

$$p^{sn}(\mathbf{z}) = \int_{\Gamma^c} g^0(\mathbf{z},\mathbf{x}')\partial_{\nu_x} p^{0n}(\mathbf{x}) d\gamma(\mathbf{x}) = \\ \frac{i}{4}\int_{\Gamma^c}\left[H_0^{(1)}(k^0\|\mathbf{z}-\mathbf{x}\|) - H_0^{(1)}(k^0\|\mathbf{z}-\mathbf{x}'\|)\right]\partial_{\nu_x} p^{0n}(\mathbf{x}) d\gamma(\mathbf{x}) \ . \tag{9.8.30}$$

☐ We employ polar coordinates $r_x,\ \theta_x,\ r_z,\ \theta_z$ related to cartesian coordinates of $\mathbf{x},\ \mathbf{z}$ by:

$$x_1 = r_x\cos\theta_x \quad , \quad x_2 = r_x\sin\theta_x \quad , \quad z_1 = r_z\cos\theta_z \quad , \quad z_2 = r_z\sin\theta_z \ , \tag{9.8.31}$$

to obtain

$$\|\mathbf{z}-\mathbf{x}\| = \left|\sqrt{r_x^2 + r_z^2 - 2r_x r_z\cos(\theta_z-\theta_x)}\right| \quad , \\ \|\mathbf{z}-\mathbf{x}'\| = \left|\sqrt{r_x^2 + r_z^2 - 2r_x r_z\cos(\theta_z+\theta_x)}\right| \ , \tag{9.8.32}$$

or

$$\|\mathbf{z}-\mathbf{x}\| = r_z\left|\sqrt{1+\varepsilon^2 - 2\varepsilon\cos(\theta_z-\theta_x)}\right| \quad , \\ \|\mathbf{z}-\mathbf{x}'\| = r_z\left|\sqrt{1+\varepsilon^2 - 2\varepsilon\cos(\theta_z+\theta_x)}\right| \ , \tag{9.8.33}$$

with

$$\varepsilon := \frac{r_x}{r_z} \ . \tag{9.8.34}$$

□ In integral in (9.8.30), x_2 varies between f_{min} and f_{max}, and x_1 varies betweeen x_1^g and x_1^d, which means that r_x varies between $\sqrt{(x_1^g)^2 + (f_{min})^2}$ and $\sqrt{(x_1^d)^2 + (f_{max})^2}$, both of which are finite values.

□ Let us now suppose that point of observation is far from Γ^c, which means that

$$\varepsilon := \frac{r_x}{r_z} << 1 \quad ; \quad \mathbf{x} \in \Gamma^c \ . \tag{9.8.35}$$

□ Then, by Taylor series expansions in terms of ε,

$$\begin{aligned} \|\mathbf{z} - \mathbf{x}\| &= |r_z - r_x \cos(\theta_z - \theta_x)| = r_z - r_x \cos(\theta_z - \theta_x) \quad , \\ \|\mathbf{z} - \mathbf{x}'\| &= |r_z - r_x \cos(\theta_z + \theta_x)| = r_z - r_x \cos(\theta_z + \theta_x) \ , \end{aligned} \tag{9.8.36}$$

so that

$$\begin{aligned} p^{sn}(\mathbf{z}) \sim -\frac{i}{4} \int_{\Gamma^c} \Big[& H_0^{(1)}(k^0(r_z - r_x \cos(\theta_z - \theta_x)) - \\ & H_0^{(1)}(k^0(r_z - r_x \cos(\theta_z + \theta_x)) \Big] \partial_{\nu_x} p^{0n}(\mathbf{x}) d\gamma(\mathbf{x}) \quad ; \quad k^0 \|\mathbf{z}\| \to \infty \ . \end{aligned} \tag{9.8.37}$$

□ We make use of asymptotic form of Hankel function

$$H_0^{(1)}(\zeta) \sim \left(\frac{2}{\pi|\zeta|}\right)^{\frac{1}{2}} e^{i\left[|\zeta|-\frac{\pi}{4}\right]} \;\; ; \;\; |\zeta| \to \infty \quad \Rightarrow \tag{9.8.38}$$

■

$$p^{sn}(\mathbf{z}) \sim \hat{p}^{sn}(k^0,\theta_z)\left(\frac{2}{\pi k^0 r_z}\right)^{\frac{1}{2}} e^{i\left[k^0 r_z-\frac{\pi}{4}\right]} \;\; ; \;\; k^0\|\mathbf{z}\| \to \infty \; . \tag{9.8.39}$$

wherein

$$\hat{p}^{sn}(k^0,\theta_z) := \frac{i}{4}\int_{\Gamma^c}\Big[e^{-ik^0 r_x\cos(\theta_z-\theta_x)} - e^{-ik^0 r_x\cos(\theta_z+\theta_x)}\Big]\partial_{\nu_x}p^{0n}(\mathbf{x})d\gamma(\mathbf{x}) \;\; ; \;\; k^0\|\mathbf{z}\| \to \infty \; . \tag{9.8.40}$$

is *far-field complex scattering function.*

□ Let $k_1 = k^0\cos\theta_z,\ k_2^{0+} = k^0\sin\theta_z$; then

$$k^0 r_x\cos(\theta_z \pm \theta_x) = x_1 k^0\cos\theta_z \pm x_2 k^0\sin\theta_z = k_1 x_1 \pm k_2^{0+}x_2 \; , \tag{9.8.41}$$

or

$$k^0 r_x\cos(\theta_z \pm \theta_x)\Big|_{\mathbf{x}\in\Gamma^c} = k_1 x_1 \pm k_2^{0+} f(x_1) \; , \tag{9.8.42}$$

so that recalling that

$$d\gamma(\mathbf{x})\partial_{\nu_x}p^{0n}(\mathbf{x})\Big|_{\Gamma^c} = dx_1\left(\dot{f}(x_1)\partial_{x_1} - \partial_{x_2}\right)p^{0n}(x_1,f(x_1)) \quad \Rightarrow \tag{9.8.43}$$

■

$$\hat{p}^{sn}(\theta_z) := \frac{i}{4}\int_{x_1^g}^{x_1^d}\left[e^{-i(k_1x_1+k_2f(x_1))} - e^{-i(k_1x_1-f(x_1))}\right]\times$$
$$\left(\dot{f}(x_1)\partial_{x_1} - \partial_{x_2}\right)p^{0n}(x_1, f(x_1))dx_1 \;\; ; \;\; k^0\|\mathbf{z}\| \to \infty \; . \quad (9.8.44)$$

■ By comparing this result with that in (9.7.29), we obtain

$$B^{0n}(k^0\cos\theta_z) = \frac{1}{\pi k^0 \sin\theta_z}\hat{p}^{sn}(k^0, \theta_z) \;\; ; \;\; |k_1| \leq k^0 \; . \quad (9.8.45)$$

■ This formula establishes connection of plane wave amplitude B^{0n} (for propagating plane waves, i.e., for $|k_1| \leq k^0$) with *measurable* far-field scattering function $\hat{p}^{sn}$.

9.9 Rayleigh hypothesis method for solving forward- scattering problem

□ The Rayleigh hypothesis is one of most useful devices for simplifying analysis of forward (and even inverse) scattering problems.

□ In some cases, it is a rigorous consequence of governing equations, but more often than not it furnishes only an approximation to sought-for solution.

□ Quality of this approximation is all greater closer obstacle is to one having a boundary with simple canonical shape.

☐ In cartesian coordinates, latter is planar, in polar coordinates it is circular, in cylindrical coordinates it is circular cylindrical, in spherical coordinates it is spherical, etc. However, there exist extensions of technique to more complicated geometries.

☐ Rayleigh's original intention was merely to develop a simple method for solving problems of scattering of plane waves by opaque and penetrable 2D *periodic* in-the-mean-flat surfaces and it is probable that he did not realize that what has become to be known as Rayleigh hypothesis rests, in most cases, on shaky mathematical grounds.

☐ However, under circumstances in which he employed his hypothesis, i.e., for periodic boundaries with small vertical deviations of planeity from a horizontal mean plane compared to wavelength, or with large profile periods compared to wavelength and/or small maximal profile slopes, his analysis turns out to be sound.

☐ We treat a problem that is slightly different from previous one in that *solicitation is now that of a homogeneous plane wave* instead of previous cylindrical wave (radiated by a cylindrical source) for each realization. Such a plane wave is of form

$$p^{in}(\mathbf{x}) = A^{in} \exp[i(k_1^{in} x_1 + k_2^{in-} x_2)] \ . \tag{9.9.46}$$

wherein

$$k_1^{in} = k^0 \sin \vartheta^{in} \quad , \quad k_2^{in\pm} = \pm k^0 \cos \vartheta^{in} \ , \tag{9.9.47}$$

and ϑ^{in} is angle of incidence with respect to $+x_2$ axis (note that θ_x and θ_z were measured from $+x_1$ and $+z_1$ axes respectively).

□ It is easy to show that, as previously,

$$p^{0n}(\mathbf{z}) = p^{in}(\mathbf{z}) + p^{rn}(\mathbf{z}) + p^{sn}(\mathbf{z}) \;\; ; \;\; \mathbf{z} \in \Omega_0 \; , \tag{9.9.48}$$

wherein

$$p^{rn}(\mathbf{z}) = -p^{in}(\mathbf{z}') = -A^{in} \exp[i(k_1^{in} x_1 - k_2^{in-} x_2)] \; , \tag{9.9.49}$$

specularly-reflected field, and

$$p^{sn}(\mathbf{z}) = \int_{\Gamma^c} g^0(\mathbf{z}, \mathbf{x}') \partial_{\nu_x} p^{0n}(\mathbf{x}) d\gamma(\mathbf{x}) \; . \tag{9.9.50}$$

scattered field.

□ As previously, we find

$$p^{sn}(\mathbf{z}) = \int_{-\infty}^{\infty} B^{0n}(k_1) e^{i[k_1 z_1 + k_2 z_2]} dk_1 \;\; ; \;\; \mathbf{z} \in \Omega_0^+ \; , \tag{9.9.51}$$

□ It should be stressed that up to this point, so-called *Rayleigh plane-wave representation of scattered field* (9.9.51) has been shown to hold only in subdomain Ω_0^+ of Ω_0, and there is no apparent reason why it should hold in remainder of Ω_0.

■ Notwithstanding this remark, Rayleigh made hypothesis (albeit,

for a *periodic* quasi-planar boundary) that (9.9.51) is a valid representation of field even in $\Omega_0 - \Omega_0^+$ and on Γ, with same set of coefficients $\{B^{0n}(k_1)\}$ applying throughout $\Omega_0 \cup \Gamma$, i.e.,

$$p^{0n}(\mathbf{x}) = p^{in}(\mathbf{x}) + p^{rn}(\mathbf{x}) + \int_{-\infty}^{\infty} B^{0n}(k_1) \exp\left\{i\left[k_1 x_1 + k_{F2}^{0+} x_2\right]\right\} dk_1 \ ; \ \mathbf{x} \in \Omega_0 \cup \Gamma \ . \quad (9.9.52)$$

□ This authorizes introduction of (9.9.51) into boundary condition ((9.2.2))

$$p^{0n}(\mathbf{x}, \omega) = 0 \ \ ; \ \ \mathbf{x} \in \Gamma \ , \quad (9.9.53)$$

so as to obtain

$$0 = p^{in}(x_1, F(x_1)) + p^{rn}(x_1, F(x_1)) + \int_{-\infty}^{\infty} B^{0n}(k_1) \exp\left\{i\left[k_1 x_1 + k_2^{0+} F(x_1)\right]\right\} dk_1 \ ; \ \forall x_1 \in \mathbb{R} \ , \quad (9.9.54)$$

which, should enable determination of set $\{B^{0n}(k_1) \ ; \ \forall k_1 \in \mathbb{R}\}$.

□ A way (not employed by Rayleigh) of doing this is to construct a cost function which is a measure of discrepancy between $p^{sn} = \int_{-\infty}^{\infty} B^{0n}(k_1) \exp\left\{i\left[k_1 x_1 + k_2^{0+} F(x_1)\right]\right\} dk_1$ and $-p^{in} - p^{rn}$, i.e.,

$$\mathcal{J}(\{B^{0n}(k_1)\}) = \int_{-\infty}^{\infty} \|p^{in}(x_1, F(x_1)) + p^{rn}(x_1, F(x_1)) + p^{sn}(x_1, F(x_1))\|^2 dx_1 \ , \tag{9.9.55}$$

and to define solution of problem as one which minimizes $\mathcal{J}$.

□ By taking partial derivatives of $\mathcal{J}$ with respect to $B^{0n}(k_1)$ it can be shown that minimum of $\mathcal{J}$ occurs for those $B^{0n}(k_1)$ which are solution of integral equation

$$\int_{-\infty}^{\infty} \mathcal{C}(K_1, k_1)\mathcal{B}(k_1)dk_1 = \mathcal{D}(K_1) \ \ ; \ \ \forall K_1 \in \mathbb{R} \ , \tag{9.9.56}$$

wherein

$$\mathcal{C}(K_1, k_1) = \frac{1}{2\pi}\int_{-\infty}^{\infty} \exp\{i[(k_1 - K_1)x_1 + (k_2^{0+} - K_2^{0+*})F(x_1)]\}dx_1 \ , \tag{9.9.57}$$

$$\mathcal{B}(k_1) = B^{0n}(k_1) \ , \tag{9.9.58}$$

$$\mathcal{D}(K_1) = \frac{1}{2\pi}\int_{-\infty}^{\infty} \big(p^{in}(x_1, F(x_1)) + p^{rn}(x_1, F(x_1))\big) \times \exp\{-i[K_1 x_1 + K_2^{0+*}F(x_1)]\}dx_1) \ , \tag{9.9.59}$$

and

$$K_2^{0\pm} = \pm\sqrt{(k^0)^2 - K_1^2} \;\; ; \;\; \Re(K_2^{0+}) \geq 0 \;\; , \;\; \Im(K_2^{0+}) \geq 0 \; , \; (9.9.60)$$

and symbol $*$ designates conjugate complex operator.

□ Difficulty with this approach is that it requires solving a generally ill-conditioned first-kind integral equation for a function $\mathcal{F}(k_1)$ that is not of compact support.

9.10 A perturbation method for solving forward- scattering problem for small roughess

■ We start by exposing another variant of Rayleigh hypothesis method which will provide framework for a *perturbation scheme* applicable to situation in which the roughness (i.e., maximal excursion of $|f(x_1)|$ with respect to line $x_2 = 0$) of interface is small with respect to wavelength of incident radiation in Ω_0.

□ We found previously that ((9.9.54))

$$0 = p^{in}(x_1, F(x_1)) + p^{rn}(x_1, F(x_1)) + \int_{-\infty}^{\infty} B^{0n}(k_1) \exp\left\{ i \left[k_1 x_1 + k_2^{0+} F(x_1) \right] \right\} dk_1 \; ; \; \forall x_1 \in \mathbb{R} \; , \; (9.10.61)$$

□ We project this integral equation onto Fourier basis $\{(2\pi)^{-1} \exp(-iK_1 x_1 \; ; \; \forall K_1 \in \mathbb{R}\}$ so as to obtain another integral

equation

$$\int_{-\infty}^{\infty} \mathcal{E}(K_1, k_1)\mathcal{F}(k_1)dk_1 = \mathcal{G}(K_1) \;\; ; \;\; \forall K_1 \in \mathbb{R} \; , \qquad (9.10.62)$$

wherein

$$\mathcal{E}(K_1, k_1) = \frac{1}{2\pi}\int_{-\infty}^{\infty} \exp\{i[(k_1 - K_1)x_1 + k_2^{0+}F(x_1)]\}dx_1 \; , \quad (9.10.63)$$

$$\mathcal{F}(k_1) = B^{0n}(k_1) \; , \qquad (9.10.64)$$

$$\mathcal{G}(K_1) = -\frac{1}{2\pi}\int_{-\infty}^{\infty} \Big(p^{in}(x_1, F(x_1)) + p^{rn}(x_1, F(x_1))\Big) \times$$
$$\exp\{-iK_1x_1\}dx_1 = -\frac{A^{in}}{2\pi}\int_{-\infty}^{\infty} \Big[\exp\{i[(k_1^{in} - K_1)x_1 - k_2^{in+}F(x_1)]\} -$$
$$\exp\{i[(k_1^{in} - K_1)x_1 + k_2^{in+}F(x_1)]\}\Big]dx_1 \; . \quad (9.10.65)$$

□ As stated previously, it is not generally easy to solve this type of integral equation by standard methods. However, if roughness is small, a perturbation technique provides a suitable alternative.

□ This technique can be applied when following conditions are filled.

■ In first place, profile function f should be of form

$$F(x_1) = bH(x_1) = \begin{cases} f(x_1) = bh(x_1) & ; \quad x_1^g < x_1 < x_1^d \\ 0 & ; \quad -\infty < x_1 \leq x_1^g \\ 0 & ; \quad x_1^d \leq x_1 < \infty \end{cases} , \tag{9.10.66}$$

with $|H(x_1| \leq 1$, $|h(x_1| \leq 1$ and $b > 0$.

■ In second place, maximal excursion from planeity b should be small compared to wavelength $\Lambda^0 = 2\pi/k^0$, i.e.,

$$\zeta := k^0 b \; << \; 1 \; . \tag{9.10.67}$$

□ This can also be interpreted as a *low-frequency context*.

□ We then express terms of integral equation in terms of ζ and H:

$$\mathcal{E}(K_1, k_1) = \frac{1}{2\pi} \int_{-\infty}^{\infty} \exp\{i[(k_1 - K_1)x_1 + \kappa_2^{0+} \zeta H(x_1)]\} dx_1 \; , \tag{9.10.68}$$

$$\mathcal{G}^n(K_1) = -\frac{A^{in}}{2\pi} \int_{-\infty}^{\infty} \Big[\exp\{i[(k_1^{in} - K_1)x_1 - \kappa_2^{in+} \zeta H(x_1)]\} - \exp\{i[(k_1^{in} - K_1)x_1 + \kappa_2^{in+} \zeta H(x_1)]\} \Big] dx_1 \; , \tag{9.10.69}$$

wherein

$$\kappa_2^{0+} = \frac{k_2^{0+}}{k^0} \quad , \quad \kappa_2^{in+} = \frac{k_2^{in+}}{k^0} \ . \tag{9.10.70}$$

□ We expand $\mathcal{E}$, $\mathcal{G}$ and $\mathcal{F}$ in powers of small quantity ζ:

$$\mathcal{E}(K_1, k_1) = \sum_{p=0}^{\infty} \mathcal{E}^{(p)}(K_1, k_1)\zeta^p \quad ,$$

$$\mathcal{E}^{(p)}(K_1, k_1) := \frac{1}{p!} \frac{\partial^p \mathcal{E}(K_1, k_1)}{\partial \zeta^p}\Big|_{\zeta=0} \ , \tag{9.10.71}$$

$$\mathcal{F}(k_1) = \sum_{q=0}^{\infty} \mathcal{F}^{(q)}(k_1)\zeta^q \ , \tag{9.10.72}$$

$$\mathcal{G}(K_1) = \sum_{l=0}^{\infty} \mathcal{G}^{(l)}(K_1)\zeta^l \quad , \quad \mathcal{G}^{(l)}(K_1) := \frac{1}{l!} \frac{\partial^l \mathcal{G}(K_1)}{\partial \zeta^l}\Big|_{\zeta=0} \ . \tag{9.10.73}$$

□ After introducing these expansions into (9.10.62) and comparing powers of ζ, we finally obtain system of integral equations

$$\sum_{q=0}^{l} \int_{-\infty}^{\infty} \mathcal{E}^{(l-q)}(K_1, k_1)\mathcal{F}^{(q)}(k_1)dk_1 = \mathcal{G}^{(l)}(K_1) \quad ;$$

$$\forall K_1 \in \mathbb{R} \quad ; \quad l = 0, 1, 2, ... \ . \tag{9.10.74}$$

■ For $l = 0$, integral equation is

$$\int_{-\infty}^{\infty} \mathcal{E}^{(0)}(K_1, k_1)\mathcal{F}^{(0)}(k_1)dk_1 = \mathcal{G}^{(0)}(K_1) \;\; ; \;\; \forall K_1 \in \mathbb{R} \; , \quad (9.10.75)$$

wherein:

$$\mathcal{E}^{(0)}(K_1, k_1) = \mathcal{E}(K_1, k_1)\Big|_{\zeta=0} = \int_{-\infty}^{\infty} \exp[i(k_1 - K_1)]\frac{dx_1}{2\pi} = \delta(k_1 - K_1) \; , \quad (9.10.76)$$

$$\mathcal{G}^{(0)}(K_1) = \mathcal{G}(K_1)\Big|_{\zeta=0} = A^{in}\int_{-\infty}^{\infty} \left(\exp[i(k_1^{in} - K_1)] - \exp[i(k_1^{in} - K_1)]\right)\frac{dx_1}{2\pi} = \delta(k_1 - K_1) = 0 \; , \quad (9.10.77)$$

so that

$$\mathcal{F}^{(0)}(K_1) = 0 \;\; ; \;\; \forall K_1 \in \mathbb{R} \; . \quad (9.10.78)$$

■ For $l = 1$, we have

$$\mathcal{F}^{(1)}(K_1) = \mathcal{G}^{(1)}(K_1) - \int_{-\infty}^{\infty} \mathcal{E}^{(1)}(K_1, k_1)\mathcal{F}^{(0)}(k_1)dk_1 \;\; ; \;\; \forall K_1 \in \mathbb{R} \; , \quad (9.10.79)$$

or, on account of $l = 0$ result:

$$\mathcal{F}^{(1)}(K_1) = \mathcal{G}^{(1)}(K_1) \;\; ; \;\; \forall K_1 \in \mathbb{R} \; , \tag{9.10.80}$$

wherein

$$\mathcal{G}^{(1)}(K_1) = -\frac{A^{in}}{2\pi}\frac{\partial}{\partial\zeta}\int_{-\infty}^{\infty}\Big[\exp\{i[(k_1^{in}-K_1)x_1 - \kappa_2^{in+}\zeta H(x_1)]\} - \exp\{i[(k_1^{in}-K_1)x_1 + \kappa_2^{in+}\zeta H(x_1)]\}\Big]dx_1\Big|_{\zeta=0} =$$
$$-\frac{A^{in}}{2\pi}\int_{-\infty}^{\infty}\exp[i(k_1^{in}-K_1)x_1)]\Big[-i\kappa_2^{in+}\exp\{-i\kappa_2^{in+}\zeta H(x_1)\} - i\kappa_2^{in+}\exp\{i\kappa_2^{in+}\zeta H(x_1)]\}\Big]dx_1\Big|_{\zeta=0} =$$
$$2A^{in}i\kappa_2^{in+}\int_{-\infty}^{\infty}H(x_1)\exp[i(k_1^{in}-K_1)x_1)]\frac{dx_1}{2\pi} \; . \tag{9.10.81}$$

□ Consequently:

$$\mathcal{F}^{(1)}(k_1) = A^{in}2i\kappa_2^{in+}\mathcal{I}(k_1^{in}-k_1) \;\; ; \;\; \forall k_1 \in \mathbb{R} \; , \tag{9.10.82}$$

wherein

$$\mathcal{I}(k_1^{in}-k_1) := \int_{-\infty}^{\infty}H(x_1)\exp[i(k_1^{in}-k_1)x_1)]\frac{dx_1}{2\pi} \; . \tag{9.10.83}$$

■ To *first order in* ζ, diffraction coefficients are approximated by

$$B^{0n}(k_1) = \mathcal{F}(k_1) \approx \mathcal{F}^{[1]}(k_1) = \mathcal{F}^{(0)}(k_1) + \zeta\mathcal{F}^{(1)}(k_1) = A^{in} 2i\kappa_2^{in+} \int_{-\infty}^{\infty} \zeta H(x_1) \exp[i(k_1^{in} - k_1)x_1)] \frac{dx_1}{2\pi} \quad ; \quad \forall k_1 \in \mathbb{R} \, , \tag{9.10.84}$$

or

$$B^{0n}(k_1) \approx A^{in} 2i\kappa_2^{in+} \int_{-\infty}^{\infty} F(x_1) \exp[i(k_1^{in} - k_1)x_1)] \frac{dx_1}{2\pi} \quad ; \quad \forall k_1 \in \mathbb{R} \, . \tag{9.10.85}$$

9.10.1 On possibility of extracting information on boundary roughness directly from some characteristics of plane wave coefficient function

☐ We want to show that it is possible to obtain information on $f(x_1)$ without actually solving fully the inverse problem.

☐ We assume that incident wave(s) characteristics A^{in} and k_1^{in} are known a priori.

☐ Idea is to exploit certain features of *pseudo image*, which at present takes form of functions $B^{0n}(k_1)$ or $\|B^{0n}(k_1)\|$.

☐ Starting point is (9.10.85), which, on account of fact that $F(x_1) = 0$ outside of interval $]x_1^g, x_1^d[$, takes form

$$B^{0n}(k_1) \approx A^{in} 2i\kappa_2^{in+} \int_{x_1^g}^{x_1^d} f(x_1) \exp[i(k_1^{in} - k_1)x_1)] \frac{dx_1}{2\pi} \quad ; \quad \forall k_1 \in \mathbb{R} \, . \tag{9.10.86}$$

☐ We assume henceforth that $\approx$ is replaced by $=$ in this expression.

☐ First we consider *isoceles triangular valley*

$$f(x_1) = f(-x_1) = b\left(1 - \frac{2}{w}x_1\right) \quad ; \quad 0 < x_1 < \frac{w}{2} \ . \tag{9.10.87}$$

(i.e., $x_1^g = -\frac{w}{2}$ and $x_1^d = \frac{w}{2}$). Then

$$B^{0n}(k_1) = -A^{in}\frac{bw}{2\pi}i\kappa^{in+}\mathrm{sinc}^2\left[(k_1^{in} - k_1)\frac{w}{4}\right] \ , \tag{9.10.88}$$

wherein $\mathrm{sinc}(\chi) = \frac{\sin\chi}{\chi}$ and $\mathrm{sinc}(0) = 1$.

☐ From this expression we find:

$$B^{0n}(k_1^{in}) = -A^{in}\frac{bw}{2\pi}i\kappa^{in+} \ , \tag{9.10.89}$$

and

$$B^{0n}(k_1^{in}) = 0 \ , \tag{9.10.90}$$

when

$$(k_1^{in} - k_1)\frac{w}{4} = m\pi \quad ; \quad m \in \mathbb{Z} \cap \{0\} \ . \tag{9.10.91}$$

☐ Thus, by purely *kinematical* means (i.e., locating zeros of plane wave coefficient function via (9.10.91)), we can determine width w of valley.

□ Once w is found, we can determine via (9.10.89) depth b of valley from an evaluation of modulus of $B^{0n}(k_1^{in})$.

■ Since, as was shown previously, $B^{0n}(k_1)$ is related to far-field scattering function $\hat{p}^{sn}$ for $|k_1| \leq |k_1^{in}|$, we see that b and w can be determined from one or several kinematic features (i.e., positions of first zero(s)) and a single dynamical feature (i.e., modulus of maximum) of far-field scattering function $\hat{p}^{sn}$.

■ A corollary of previous remark is that it is not necessary to know $B^{0n}(k_1)$ for $|k_1| > |k_1^{in}|$ in order to be able to determine b and w.

□ However, if we do not know beforehand that roughness takes form of an isosceles triangular valley, then previous remark would not be true, which goes to show that *the less one knows beforehand about target, the more data one needs to solve inverse problem, either fully or partially.*

□ Next consider *isoceles triangular hill*

$$f(x_1) = f(-x_1) = -b\left(1 - \frac{2}{w}x_1\right) \quad ; \quad 0 < x_1 < \frac{w}{2} \; . \qquad (9.10.92)$$

□ Then, we find

$$B^{0n}(k_1) = A^{in}\frac{bw}{2\pi}i\kappa^{in+}\mathrm{sinc}^2\left[(k_1^{in} - k_1)\frac{w}{4}\right] \; , \qquad (9.10.93)$$

so that all that was written concerning corresponding valley applies once again.

■ However, dynamical measurement of *modulus* of maximum of far-field scattering function does not enable to distinguish between hill and corresponding valley.

□ Next consider truncated cosinusoïdal hill

$$f(x_1) = f(-x_1) = -b\cos(\pi x_1) \;\; ; \;\; 0 < x_1 < \frac{w}{2} \, , \qquad (9.10.94)$$

for which

$$B^{0n}(k_1) = -A^{in}\frac{bw}{2\pi} i\kappa^{in+} \Big\{ \mathrm{sinc}\left[\left(\frac{\pi}{w} + k_1^{in} - k_1\right)\frac{w}{2}\right] + \mathrm{sinc}\left[\left(-\frac{\pi}{w} + k_1^{in} - k_1\right)\frac{w}{2}\right] \Big\} \, . \qquad (9.10.95)$$

□ Now, kinematical procedure, based on location of zeros, becomes difficult to apply due to appearance of many zeros in plane wave coefficient function, but hill width w can be obtained by locating position of two principal peaks.

□ Hill height b can then be obtained from moduli of these two peaks.

□ Until now, we considered boundaries with only *one (irregular) feature*.

☐ An example of a boundary with *more than one feature* is cosinusoïdal diffraction grating:

$$f(x_1) = f(-x_1) = \frac{b}{2}\left[1 + \cos\left(\frac{2\pi}{d}\right)\right] \quad ; \quad 0 < x_1 < \frac{w}{2} \ , \tag{9.10.96}$$

(wherein d is grating period) for which

$$B^{0n}(k_1) = \\ - A^{in}\frac{bw}{2\pi} i\kappa^{in+} \left\{ \sum_{j=-1}^{1} \frac{1}{\epsilon_{|j|}} \text{sinc}\left[\left(\frac{2\pi}{w} jL + k_1^{in} - k_1\right)\frac{w}{2}\right]\right\} \ , \tag{9.10.97}$$

wherein $\epsilon_0 = 1$, $\epsilon_{\neq 0} = 2$ and $L = \frac{w}{d}$ indicates number of periods of grating within overall width w of global feature.

☐ From this expression, we find

$$B^{0n}(k_1^{in} + \frac{2m\pi}{d}) = -A^{in}\frac{bw}{2\pi} i\kappa^{in+} \left\{ \delta_{0m} + \frac{1}{2}\left[\delta_{1m} + \delta_{-1m}\right]\right\} \ , \tag{9.10.98}$$

wherein $\delta_{m\ m} = 1$, $\delta_{l\neq m\ m} = 0$.

☐ Thus, period d of grating can be determined from position of either $m = -1$ or $m = 1$ peak, and amplitude b of grating can be determined by modulus of $B^{0n}(k_1^{in})$ provided one knows beforehand relation (i.e., L) between d and w.

■ It therefore appears that, in general, it is difficult to obtain information on number of scattering features from this type of simple inspection of plane wave coefficient function.

□ In preceding examples we saw that there is a recurrent apperance of product $\frac{bw}{2}$, which suggests that there exists a relation between modulus of principal diffraction peak (i.e., specular reflection peak) and area of scattering feature.

□ This statement can be put on a mathematical foundation by first noting that plane wave coefficient function in specular reflection direction takes form

$$B^{0n}(k_1^{in}) = A^{in}\frac{i\kappa_2^{in+}}{\pi}\int_{x_1^g}^{x_1^d} f(x_1)dx_1 \ , \tag{9.10.99}$$

from which we clearly see that area $\left|\int_{x_1^g}^{x_1^d} f(x_1)dx_1\right|$ of scattering feature is proportional to modulus of $B^{0n}(k_1^{in})$.

■ This shows that a useful global parameter (i.e., area) of boundary feature (provided only one such feature is present) can be obtained from a very specific dynamical feature (i.e., modulus of far-field scattering function in specular reflection direction without any a priori knowledge of functional form of boundary irregularity.

□ More specific morphological parameters of boundary feature(s), such as its depth, height and width, require a priori knowledge of

functional form of boundary irregularity.

■ Thus, combination of kinematical and dynamical techniques outlined above have their limits and usually cannot replace more elaborate inversion techniques.

9.11 Use of first-order perturbation solution of forward-scattering problem to solve inverse scattering problem of identification of surface roughness

□ From (9.10.85) we obtain

$$\frac{B^{0n}(k_1)}{A^{in}2i\kappa_2^{in+}} \approx \int_{-\infty}^{\infty} F(x_1)\exp[i(k_1^{in}-k_1)x_1)]\frac{dx_1}{2\pi} \quad ; \quad \forall k_1 \in \mathbb{R}\ , \tag{9.11.100}$$

whence, by Fourier inversion

$$F(x_1) \approx \frac{1}{A^{in}}\int_{-\infty}^{\infty} \frac{B^{0n}(k_1)}{2i\kappa_2^{in+}}\exp[i(k_1-k_1^{in})x_1]dk_1\ . \tag{9.11.101}$$

■ This shows that it is possible to obtain an explicit expression for roughness profile function from first-order perturbation approximation of plane-wave coefficient function $B^{0n}(k_1)$.

□ Question of utmost importance is whether it is possible to link $B^{0n}(k_1)$ to some observable and whether latter can be measured for all $k_1 \in \mathbb{R}$.

9.11.1 Identification of surface roughness from data pertaining to far-field scattering function for fixed frequency and variable observation angle

□ We first note that

$$F(x_1) \approx \frac{1}{A^{in}} \left[\int_{-\infty}^{-k^0} + \int_{-k^0}^{k^0} + \int_{k^0}^{\infty} \right] \frac{B^{0n}(k_1)}{2i\kappa_2^{in+}} \exp[i(k_1 - k_1^{in})x_1] dk_1 \ , \tag{9.11.102}$$

or

$$F(x_1) \approx F^{(1)}(x_1) + F^{(2)}(x_1) \ . \tag{9.11.103}$$

wherein

$$F^{(1)}(x_1) := \frac{k^0}{A^{in}} \int_{-k^0}^{k^0} \frac{B^{0n}(k_1)}{2ik_2^{in+}} \exp[i(k_1 - k_1^{in})x_1] dk_1 \ , \tag{9.11.104}$$

$$F^{(2)}(x_1) := \frac{k^0}{A^{in}} \left[\int_{-\infty}^{-k^0} + \int_{k^0}^{\infty} \right] \frac{B^{0n}(k_1)}{2ik_2^{in+}} \exp[i(k_1 - k_1^{in})x_1] dk_1 \ . \tag{9.11.105}$$

□ We concentrate our attention on $F^{(1)}(x_1)$.

□ Recall that θ_z was polar angle of observation, measured clockwise, from positive x_1 axis.

□ Let φ be another angle of observation, measured counterclockwise, from positive x_2 axis; then

$$\theta_z = \frac{\pi}{2} - \varphi \ . \tag{9.11.106}$$

□ Make change of variables

$$k_1 = k^0 \sin\varphi \ , \tag{9.11.107}$$

with understanding that φ *is variable and* k^0 *is fixed.*

□ Then $dk_1 = k^0 \cos\varphi \ d\varphi$, and $k_2^{0+} = k^0 \cos\varphi \ d\varphi$, so that (recalling that $k_1^{in+} = k^0 \sin\varphi^{in}$ with φ angle of incidence measured clockwise from positive x_2 axis)

$$F^{(1)}(x_1) = \frac{k^0}{A^{in}} \int_{-\frac{\pi}{2}}^{\frac{\pi}{2}} \frac{B^{0n}(k^0 \sin\varphi)}{2ik^0 \cos\varphi} \exp[ik^0(\sin\varphi - \sin\varphi^{in})x_1] k^0 \cos\varphi d\varphi = \frac{k^0}{2iA^{in}} \int_{-\frac{\pi}{2}}^{\frac{\pi}{2}} B^{0n}(k^0 \sin\varphi) \exp[ik^0 x_1(\sin\varphi - \sin\varphi^{in})] d\varphi \ . \tag{9.11.108}$$

□ We recall result (9.8.45)

$$B^{0n}(k^0 \cos\theta_z) = \frac{1}{\pi k^0 \sin\theta_z} \hat{p}^{sn}(k^0, \theta_z) \ \ ; \ \ |k_1| \leq k^0 \ , \tag{9.11.109}$$

(wherein $\hat{p}^{sn}$ is complex far-field scattering function for n-th incident angle realization) from which we find

$$B^{0n}(k^0 \sin\varphi) = \frac{1}{\pi k^0 \cos\varphi} \hat{p}^{sn}(k^0, \varphi) \quad \Rightarrow \tag{9.11.110}$$

■

$$F^{(1)}(x_1) = \frac{1}{2i\pi A^{in} \cos\varphi} \int_{-\frac{\pi}{2}}^{\frac{\pi}{2}} \hat{p}^{sn}(k^0, \varphi) \exp[ik^0 x_1(\sin\varphi - \sin\varphi^{in})] d\varphi \ . \tag{9.11.111}$$

■ Thus, if the only data that is available is the far-field scattering function $\hat{p}^{sn}(k^0, \varphi)$ for fixed frequency and variable frequency, then one can reconstruct $F^{(1)}(x_1)$, but not $F^{(2)}(x_1)$.

■ This goes to show that *only a filtered version of* $F(x_1)$ (i.e., $F^{(1)}(x_1)$) can be reconstructed when sole data that is available is far-field scattering function for fixed frequency and variable scattering angles, the latter necessarily covering whole reflection half-space.

9.11.2 Identification of surface roughness from data pertaining to far-field scattering function for fixed observation angle and variable frequency

□ We had

$$F(x_1) \approx \int_{-\infty}^{\infty} \frac{B^{0n}(k_1)}{B^{in}} \exp(iKx_1) dk_1 \ , \tag{9.11.112}$$

$$B^{in} := 2i\kappa_2^{in+} A^{in} \quad , \quad K := k_1 - k_1^{in} \ . \tag{9.11.113}$$

□ It follows that

$$F(x_1) = \int_0^\infty \Big[\frac{B^{0n}(-K+k_1^{in})}{B^{in}} \exp(-iKx_1) + \frac{B^{0n}(K+k_1^{in})}{B^{in}} \exp(iKx_1)\Big] dk_1 \ , \quad (9.11.114)$$

(wherein $\approx$ sign has been replaced by $=$) so that

$$F(x_1) - F^*(x_1) = \int_0^\infty \Big\{ \Big[\frac{B^{0n}(-K+k_1^{in})}{B^{in}} - \frac{B^{0n*}(K+k_1^{in})}{B^{in*}}\Big] \exp(-iKx_1) + \Big[\frac{B^{0n}(K+k_1^{in})}{B^{in}} - \frac{B^{0n*}(-K+k_1^{in})}{B^{in*}}\Big] \exp(iKx_1)\Big\} dk_1 \ , \quad (9.11.115)$$

(wherein * designates complex conjugate operator), and since profile function F_{x_1} is real, we must conclude that

$$\frac{B^{0n}(-K+k_1^{in})}{B^{in}} = \frac{B^{0n*}(K+k_1^{in})}{B^{in*}} \ , \quad (9.11.116)$$

whence

$$F(x_1) = 2\Re \int_0^\infty \frac{B^{0n}(K+k_1^{in})}{B^{in}} \exp(iKx_1) dk_1 \ , \quad (9.11.117)$$

or

$$F(x_1) = \Re \left(\frac{1}{A^{in}} \int_{k_1^{in}}^\infty \frac{B^{0n}(k_1)}{i\kappa_2^{in+}} \exp[i(k_1 - k_1^{in})x_1] dk_1 \right) \ . \quad (9.11.118)$$

□ We now make change of variables $k_1 = k^0 \sin\varphi$, wherein φ has same meaning as previously, but is now *fixed*, whereas k^0, related to angular frequency ω by $\frac{\omega}{c^0}$, is now *variable*, so that $dk_1 = \sin\varphi\, dk_0$.

□ In same spirit, we have $k_1^{in} = k^0 \sin\varphi^{in}$ and $k_2^{in} = k^0 \cos\varphi^{in}$, so that

$$F(x_1) = \Re\Big(\frac{k^0}{A^{in}} \int_{k^0 \sin\varphi^{in}}^{\infty} \frac{B^{0n}(k^0 \sin\varphi)}{ik^0 \cos\varphi} \times \exp\{i[k^0 x_1(\sin\varphi - \sin\varphi^{in})]\} \sin\varphi dk^0\Big) \ . \quad (9.11.119)$$

■ On account of relation of $B^{0n}(k^0 \sin\varphi)$ to $\hat{p}^{sn}(k^0, \varphi)$:

$$F(x_1) = \Re\Big(\frac{\sin\varphi}{A_{in} i\pi \cos^2\varphi} \int_{k^0 \sin\varphi^{in}}^{\infty} \hat{p}^{sn}(k^0, \varphi) \times \exp\{i[k^0 x_1(\sin\varphi - \sin\varphi^{in})]\} dk^0\Big) \ . \quad (9.11.120)$$

■ This formula shows, for fixed scattering angle φ, that boundary profile function $F_1(x_1)$ can be fully reconstructed from (frequency-diverse) data pertaining to the far- field scattering function $\hat{p}^{sn}(k^0, \varphi)$; $\forall k^0 \in [k^0 \sin\varphi^{in}, \infty[$.

□ Accuracy of reconstruction will depend on availability of this data in full interval $[k^0 \sin\varphi^{in}, \infty[$; usually, data is available only within a finite subset of this interval due to finite bandwith of source.

□ This problem also arises in so-called frequency-diverse version of diffraction tomography method for reconstruction of material properties of a target.

□ In the frequency-diverse, as well as scattering angle-diverse, methods, it is not necessary to employ data for more than one incident angle realization since reconstruction formula is explicit, and of same form, whatever incident angle.

Bibliography

[1] M. Bonnet. *Boundary Integral Equation Methods for Solids and Fluids*. Wiley, Chichester, 1995.

[2] J.L. Buchanan, R.P. Gilbert, A. Wirgin, and Y. Xu. *Marine Acoustics: Direct and Inverse Problems*. SIAM, Philadelphia, 2004.

[3] D. Colton and R. Kress. *Inverse Acoustic and Electromagnetic Scattering Theory*. Springer, Berlin, 1993.

[4] D. Lesselier and A. Wirgin. Identification d'objets ou milieux par inversion de signaux acoustiques ou électromagnétiques. In M. Bonnet, editor, *Problèmes Inverses*, pages 143–176. No. 22 de la série Arago, OFTA/Tec et Doc, Paris, 1999.

[5] E. Ogam and A. Wirgin. Recovery of the location, size, orientation and shape of a rigid cylindrical body from simulated and experimental scattered acoustic field data. *Inverse Probs.Sci.Engrg.*, 12:433–469, 2004.

[6] A. G. Ramm. *Scattering by Obstacles*. D. Reidel, Dordrecht, 1986.

[7] A. G. Ramm. *Multidimensional Inverse Scattering Problems*. Longman, New York, 1992.

[8] A. Wirgin. Some quasi-analytic and numerical methods for acoustical imaging of complex media. In A. Wirgin, editor, *Wavefield Inversion*, pages 241–304. Springer, Wien, 1999.

[9] A. Wirgin. Acoustical imaging: classical and emerging methods for applications in macrophysics. In R. Pike and P. Sabatier, editors, *Scattering*, pages 95–120. Academic Press, San Diego, 2002.